MODELLING AND OPTIMIZATION OF THREE-PHASE SUBMERGED ARC FURNACES (SAF)

by

AMOS AMADI

submitted in accordance with the requirements

for the degree of

MAGISTER OF TECHNOLOGIAE

in the subject

ENGINEERING: ELECTRICAL

at the

UNIVERSITY OF SOUTH AFRICA

SUPERVISOR: PROF Z WANG

JUNE 2012

Abstract

Title: Modelling and Optimization of Three-phase Submerged Arc Furnaces (SAF)
Author: Amos Amadi

Supervisor: Professor Wang Zenghui

College: College of Science, Engineering and Technology

Degree: Master of Technology (MTech.) Engineering (Electrical)

This thesis investigates the modelling and optimization of electro-thermal variable parameters applicable in obtaining an optimal operating point in SAFs. Graphite electrodes that are symmetrically positioned around the furnace are used to convert electrical energy to heat energy via three-phase arcs. The raw materials are fed via conveyor belts from the top of the furnace and are smelted by the arcs produced by the electrodes. The charge constitutes the resistance variable, whilst the heat emitted from the molten charge constitutes the temperature variable. The supply voltage to the furnace constitutes the last variable and it suffers from the network disturbances such as harmonics, dips, surges and others.

Although there are many variables that are involved in submerged arc furnace operations, the scope of this thesis is restricted to three electro-thermal variable parameters namely, resistance, voltage and temperature. The measurement of these parameters need to be done accurately and controlled effectively in order to achieve optimum output power during the furnace operation. An amalgamated variable parameter measurement (AVPM) system is proposed for the accurate measurement of these variables by use of mathematically modeled modules. The verification of this proposed measurement system is not considered in this thesis as it is recommended for future study.

Modelling is difficult using mathematical functions according to the mechanisms of the actual furnace plant system because of its complexity and many disturbances. The neural networks have been chosen because of its easy to use in modelling nonlinear functions such as the furnace plant. In this thesis, the furnace plant is modeled with the neural networks (NN) algorithm to obtain the SAF NN model. The model is then optimized using the particle swarm optimizer (PSO) algorithm. The formulated PSO based SAF NN model's results are also validated using the real SAF plant samples.

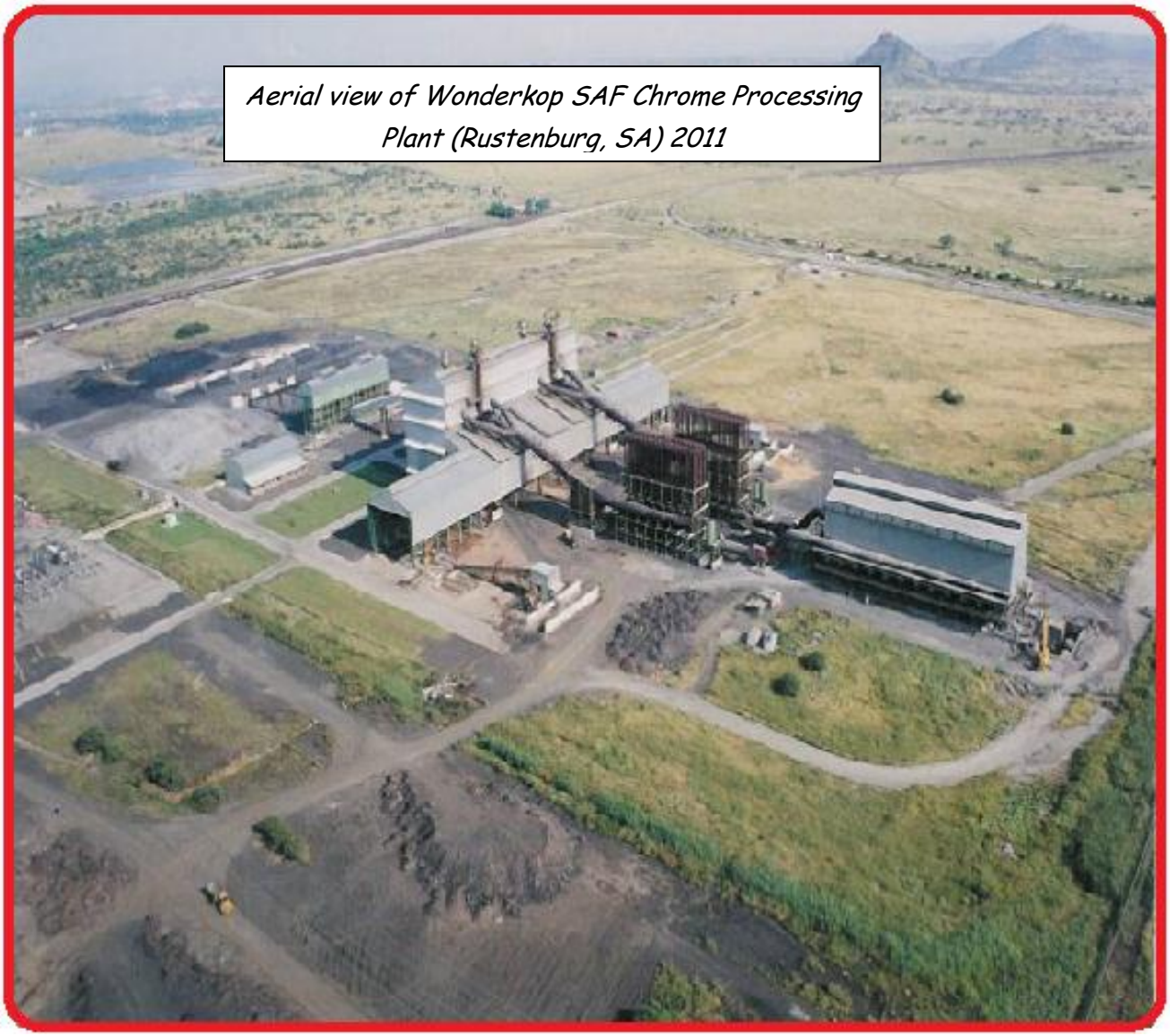

Aerial view of Wonderkop SAF Chrome Processing Plant (Rustenburg, SA) 2011

Acknowledgements

The realization of this thesis was only possible due to several people's collaboration, to which desire to express my gratefulness.

To Professor Zenghui Wang, my supervisor, I am grateful for the trust deposited in my work and for the motivation demonstrated along this ardous course. His support was without doubt, crucial in the discussion and interpretation of some results presented in this thesis.

I would like to thank the UNISA librarian (Engineering) and staff, for providing valuable insights, library information and research papers which were very instrumental in the formulation of the research proposal and the final thesis itself.

To Tong Comprehensive School management and staff, I would like to express my appreciation for their support in granting me permission to attend workshops and seminars regarding my thesis.

I would also express my appreciation to my friends and colleagues that include Mr H.Shoko and others for the mode that gave me enthusiasm and encouragement.

Finally, I would like to thank my parents, sisters, niece, nephews, their love gave me forces to make this work

This thesis is dedicated to my parents and family member for their love, endless support and encouragement.

Declaration and Copyright

I hereby declare that "MODELLING AND OPTIMIZATION OF THREE – PHASE SUBMERGED ARC FURNACES (SAF)" is my own work and all the sources used or quoted have been indicated and acknowledged by means of complete references.

AUTHOR: 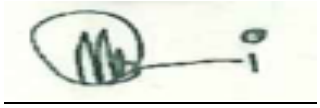 29 February 2012

AMOS AMADI

Table of Contents

CHAPTER THREE

ELECTRO-THERMAL VARIABLE PARAMETERS OF SUBMERGED ARC FURNACES

CHAPTER FOUR

MEASUREMENT OF ELECTRO-THERMAL VARIABLE PARAMETERS IN SUBMERGED ARC FURNACES

LIST OF FIGURES

LIST OF TABLES

Definition of Terms

1. AC	-	Alternating Current
2. ANN	-	Artificial Neural Network
3. AEM	-	Advanced Electrical Module
4. AFM	-	Arc Furnace Module
5. AVPM	-	Amalgamated Variable Parameters Measurement
6. CVCM	-	Current and Voltage Calculation Module
7. BEM	-	Basic Electrical Module
8. DC	-	Direct Current
9. ECM	-	Electrode-to-bath voltage Calculation Module
10. ERICM	-	Electrode resistance and Impedance Calculation
11. EBT	-	Eccentric bottom tap-hole
12. Fe-Cr	-	Ferro-Chrome
13. Fe-Mn	-	Ferro-Manganese
14. FCB	-	Flicker Calculation Block
15. GMVC	-	Generalized minimum variance control
16. HCB	-	Harmonic Calculation Block
17. IR	-	Infrared
18. IRT	-	Infrared Thermometer
19. ITCM	-	IR Temperature Calculation Module
20. KA	-	Kilo-Amperes

21. KW	-	Kilo-watts
22. LV	-	Low Voltage
23. MTech.	-	Masters of Technology
24. MVA	-	Mega Voltage Ampere
25. MW	-	Mega Watts
26. NN	-	Neural Network
27. OLTC	-	On-load tap changers
28. PC	-	Personal Computer
29. PCC	-	Point of common coupling
30. PQA	-	Power Quality Analyzer
31. PSO	-	Particle Swarm Optimization
32. PCM	-	Power Calculation Module
33. PLC	-	Programmable Logic Controllers
34. SAF	-	Submerged Arc Furnaces
35. SLG	-	Single line ground failures
36. THD	-	Total Harmonic Distortion
37. THI	-	Total Harmonic Current
38. THU	-	Total Harmonic Voltage
39. WCM	-	Waveform Calculation Module
40. WCP	-	Wonderkop Chrome Plant

CHAPTER ONE

INTRODUCTION

1.1 Motivation

Over the past decade there has been a drastic increase in the number and size of SAFs constructed for the production of ferro-chromium and ferro-manganese alloys. The economic benefit resulting in the use of larger furnaces has meant that most of those constructed recently are relatively large, e.g. 48 MVA for ferro-chromium, and up to 81 MVA for ferro-manganese, with currents ranging from about 50 to 130KA [1].

Precise modelling and optimization of the electro-thermal variables is importance for optimum operation of SAFs. The measurement of these electro-thermal variables has to combine both the electrical and metallurgical aspects and this can be fully realized by devising a best measurement strategy that incorporates the best selection of these aspects, of which some of their interactions are not fully known [2]. This thesis proposes an amalgamated variable parameter measurement (AVPM) system that introduces a combined different measurement philosophies for the variables, having an improved performance, low workload, low costs and high tolerance.

The increase of the SAFs' power is very important to optimize the energy costs. Before using an optimization algorithm, the defining of the objective function is necessary. Hence, the furnace should be modeled with respect to energy costs. As energy is directly determined by the product of power and time, the objective function can be the power function related to some important variables. The three major electro-thermal variables considered in this thesis include voltage, resistance and temperature and are used for determining the optimum power (energy) of the SAFs.

However, it is difficult using mathematical functions to model SAF according to the mechanisms of the actual furnace plant system, because of its complexity and many disturbances. The neural networks (NN) can be used to model SAFs as it is easy to implement in modeling non-linear functions. Neural networks have been widely used for modeling and have achieved good results [2-3].

The Particle Swarm Optimizer was introduced in 1995 [3], yet very few formal analysis of the behavior of the algorithm have been established. Majority of the published work was

concerned with the empirical results obtained by changing some aspects of the original algorithm. Thus, in this thesis, optimization can be applied based on the neural networks and the particle swarm optimization (PSO) algorithm as it is considered to be one of the most effective optimization algorithms and also easy use. The optimization results of the proposed PSO based SAF NN model will then be validated using real furnace plant samples.

1.2 Research Objectives

The primary objectives of this thesis are summarized as follows:

- To establish the major electro-thermal variable parameters present in SAFs.
- To propose a reliable measurement technique for the electro-thermal variable parameters in SAFs.
- To develop a theoretical Neural Network based model of the Submerged Arc Furnace plant.
- To establish the Particle Swarm Optimization (PSO) algorithm so that it becomes a global optimization technique with guaranteed convergence on global optimal to reduce energy costs in SAFs.

1.3 Thesis Problem Statement

Various papers, articles and conferences have been presented on the measurement of variables in submerged arc furnaces. Majority of them showed that large furnaces have a higher reactance than smaller furnaces, constitute a major problem in the measurement of electro-thermal variables. These difficulties have emerged owing to a number of factors that include errors in the electrode to bath voltages measurements, system connections in hot and harsh furnace environments and power quality problems due to drastic and random operating characteristics of SAFs [4], [5]. Imbalances in electro-thermal may result in no coloration to the output power.

1.4 Contribution

SAFs play an important role in the day to day in the production of ferroalloys (Fe-Cr, Fe-Si, Fe-Mn, Si Metal), thus their viability remains one of the strategic factors of consideration. The thesis's findings are hoped to address one of the most crucial issues that measurement,

modeling and optimization in SAFs. The uniqueness of this research to other researches conducted in the field of modelling and optimization of variables, lies on the fact that it explores the major electro-thermal variables, define the objective function and then utilizes the PSO based SAF NN model algorithm to optimize the power (energy) of SAFs.

1.5 Thesis Approach

The qualitative research design has been adopted in this thesis as it includes quantifying relationships between variables such as voltage, resistance, temperature and others. The thesis involves modeling of the real furnace plant and then optimization of the measured electro-thermal variable parameters. Consultations with related stakeholders that deal with SAFs, such as MINTEK, Chrome production companies (Xtrata Wonderkop, etc.), journals, internet, universities and others, will be done so as to obtain relevant information for the compilation of a more detailed and comprehensive research report.

1.6 Thesis Organization

This section gives a brief outline and short description of the preliminary chapter titles of the proposed thesis. Each chapter are linked to the research objectives, thus the following structure is adopted:

Chapter 1: Introduction

This chapter outlines the introduction motivation and background, contribution, approach and the thesis organization. Reviewed literature is presented with respect to measurement and control topologies of the variables, taking into account both electrical and metallurgical aspects in SAFs.

Chapter 2: Submerged Arc Furnaces (SAF) and their properties

This chapter gives an overview of the SAF operation, different types, its physical construction and their associated equipment.

Chapter 3: Electro-thermal variables parameters of Submerged Arc Furnaces (SAF)

This chapter explores the properties of the various variable parameters present in SAFs and their effects, which include voltage, resistance, current, temperature and power.

Chapter 4: Measurement of electro-thermal variable parameters in the Submerged Arc Furnaces (SAF)

This chapter focuses on how the variable parameters are measured by use of the various measurement techniques so as to obtain accurate and reliable quantities. A multifunctional measurement system (amalgamated variable parameter measurement (AVPM)) that combines different philosophies is proposed to mitigate the measurement constraints.

Chapter 5: Modeling of Submerged Arc Furnace electro-thermal variables based on the neural networks (NN)

This chapter gives an overview of the neural model, architecture, and transfer functions and modelling of the submerged arc furnace plant. The electro-thermal variable parameters are used in the implementation of the training function of the Neural Network Fitting Tool GUI to model the SAF. The simulation plots, testing of the designed SAF NN model output against real furnace data samples will be shown to verify it performance.

Chapter 6: Energy Optimization of Three - Phase submerged arc furnaces (SAF)

This chapter presents a brief introduction of the general concept of the particle swarm optimization and their paradigms. Secondly, the PSO based SAF NN optimization method is proposed and this method comprises the SAF NN model and the particle swarm optimizer. Neural network model of the SAF plant is used as the objective function as it is impossible to use the real SAF Plant. Finally, the optimization results will be tested using the real samples as the objective function is not the real plant.

Chapter 7: Conclusions and Future Works

This chapter will draw up the conclusions of the theses and the future works that can be done in the field of neural networks and particle swarm optimization with regard to SAFs operations. Recommendations are also proposed for further studies and researches in the optimization of energy in SAFs.

CHAPTER TWO

SUBMERGED ARC FURNACES AND THEIR PROPERTIES

2.1 Introduction

This chapter gives an overview of the SAF construction and their properties in the production of ferro-chrome, ferro-silicon and others. The associated equipment that constitutes the SAFs will also be discussed, that include the furnace transformers, knapsack connection, bus tubes, flexible cables, furnace electrodes, electrodes columns, contact shoes, shell lining, and the neutral connections. The cooling systems of both the furnace transformers and the furnace shells will also be discussed, with more emphasis on maintaining the desired temperatures for the furnace operations.

2.2 Submerged Arc Furnace

2.2.1 Construction

Arc furnaces are classified according to their methods of heating such as the direct and indirect furnaces and also the furnaces with a submerged arc. Direct arc furnaces produce electric arcs that burn between the electrodes and the body being heated. In indirect arc furnaces, the arcs burn between the electrodes at a certain distance from the materials being heated. The arcs are also categorized according to their supply, as either AC or DC furnaces. SAFs used for ferrochromium or ferrosilicon consists of a refractory-lined vessel, usually water-cooled in larger sizes, covered with a retractable roof, and through which one or more graphite electrodes enter the furnace [7]. A submerged arc furnace is primarily split into three sections namely:

- the shell, which consists of the sidewalls and lower steel 'bowl'.
- the hearth, which consists of the refractory that lines the lower bowl.
- the roof, which may be refractory-lined or water-cooled, being spherical or frustum (conical section).

The hearth may be hemispherical, halved egg in shape, or having an eccentric bottom tapping furnace as shown in *Fig. 2.1*. Modern furnaces are often raised off the ground floor, so that ladles, crucible or slag pots can easily be maneuvered under the furnace.

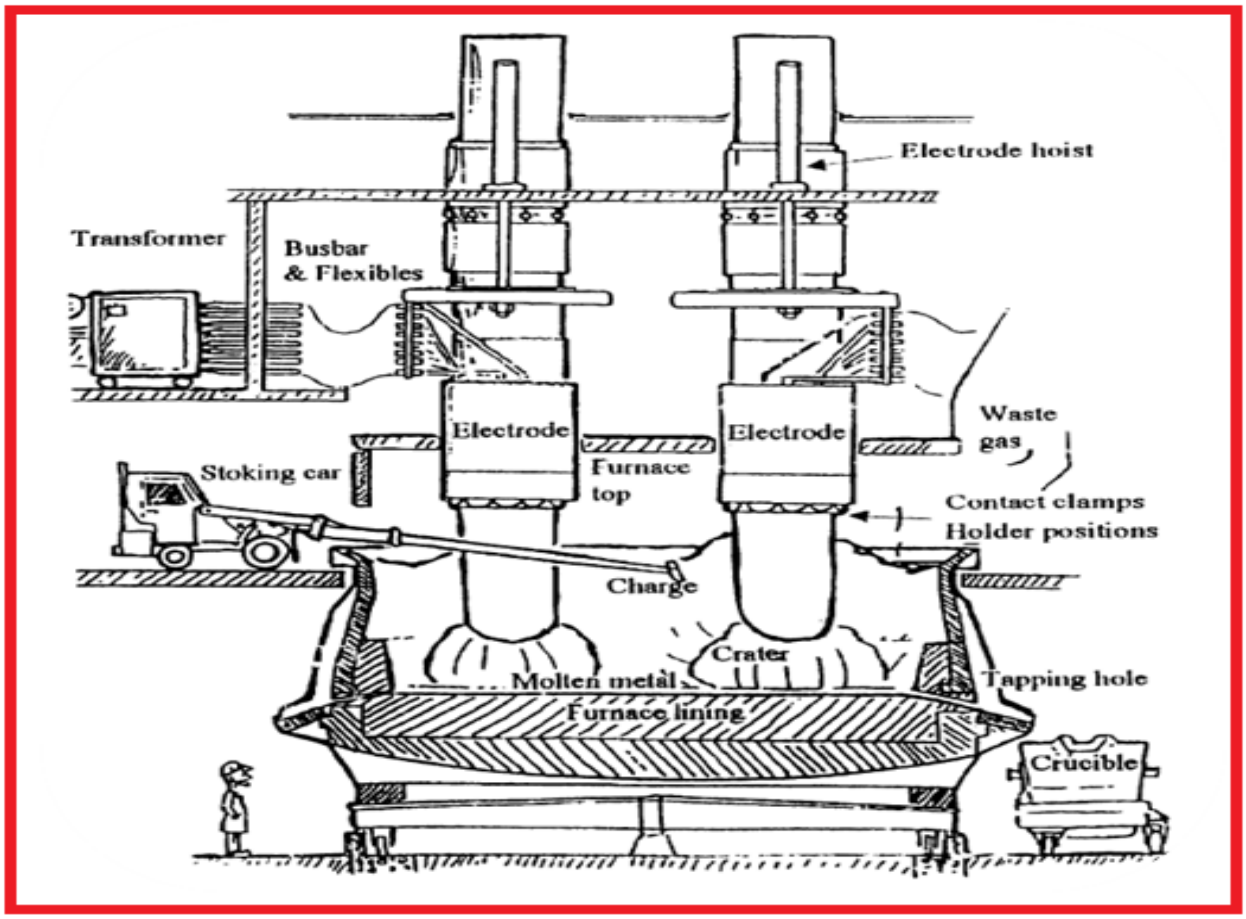

Figure 2.1: Schematic diagram of a Submerged Arc Furnace [7].

2.2.2 Operation

The three electrode circular furnace is shown in the *Fig. 2.1,* is the most common type of SAF used for ferrosilicon or ferrochromium production. In this arrangement, the circular bath is fixed, whilst the three electrodes are submerged in the charge of the raw materials. The charge is composed of proportioned mixture of ore, reductant and fluxes that are transported to the furnace by use of conveyor belt systems, to the holding bins that are situated above the furnace.

A combination of the resistance and arc heating occurs below the three electrodes and provides enough energy for the heating and reduction of the charge into molten metal [8]. The slag, which is lighter in weight than metal, is produced and forms a pool above it and both of them are tapped periodically from the bottom side of the furnace. During the taping process, the molten bath lowers resulting in the fresh raw materials being feed into the reaction zone from the holding bins above the furnace by the force of gravity.

This can be achieved manually or automatically. The electrical power is fed to the electrodes through fixed bus bars and flexible connections from the furnace transformers that will be situated close to the furnace. The transformers convert high voltage (33KV) from the supply authorities (such as ESKOM) to a low voltage (220V), high current (KA) for delivering the power to the furnace. The power control to the furnace is achieved by either adjusting the transformer secondary voltage through voltage tap changers, or by circuit impedance variation under each electrode, by adjusting the vertical position of the electrodes.

The power versus current characteristics shown in *Fig.2.2* is based on the assumption that the supply voltage and the reactance are constant. The operation of the SAF involves trying to maintain the maximum real power input to the furnace within the constraints or limits of the associated equipment of the furnace [9]. A reduction in the secondary voltage, results in the slope of the apparent power curve being reduced concurrently, allowing the current to be increased until either the electrode current limit or the maximum real power point for that particular voltage is reached.

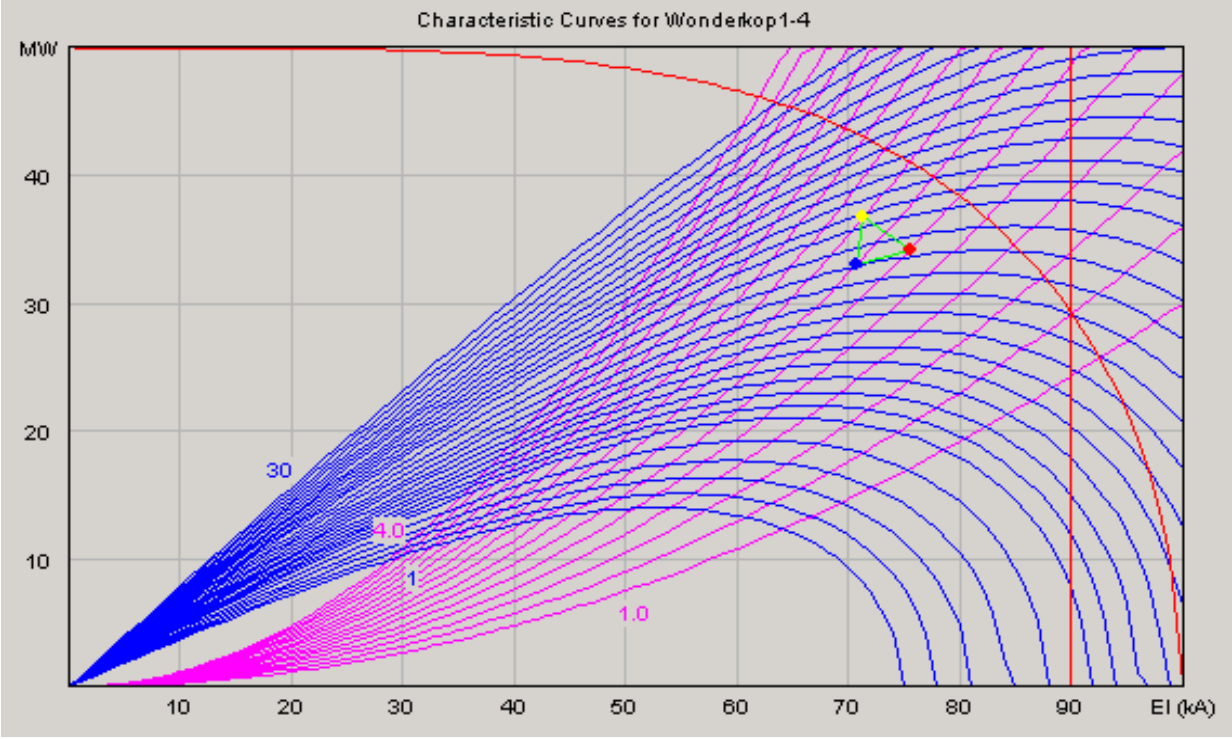

Figure 2.2: Power vs Current Characteristic curves for the 45MW SAF at WCP, Rustenburg.

Careful control of the proportioning and sizing of the raw materials is a prerequisite for good furnace operation. The reduction reaction results in the production of large volumes of

gaseous products such as CO, CO_2 and CR_6 and others that can cause problems if the porosity of the raw material burden is not maintained. A decrease in the porosity of the burden is usually caused by the sintering of fine material before they are fed into the furnace. Another technique, briquetting, which involves mixing the fine ore with a binder and compressing it into briquettes, can be employed to minimize the effect of gaseous products being emitted into the atmosphere [10].

Gas cleaning equipment can also be installed on the furnaces to control air pollution, where, closing the top of the furnace helps in reducing the quantity of air to be cleaned, such that only the gas generated by the process is cleaned [18].

2.3 Submerged Arc Furnace Associated Equipment

2.3.1 Furnace Transformer

The furnace transformers are constructed in a core-type arrangement in accordance with modern high voltage transformer practice, irrespective of the fact that the shell type arrangement has inherently lower reactance owing to reduced leakage paths. The core-type windings are mostly favoured because of their robustness, and also that they can effectively braced to withstand the forces resulting from high currents [11]. The windings are wound in ASEA arrangement, where the parallel circuits connect together on alternate ‘go’ and ‘return’ vertical bus bars so as to reduce the reactance.

Furnace transformers are used to step down high voltages between 11KV and 33 kV to levels of several hundred volts (220V) only. This results in massive secondary currents in the magnitude of kilo – amperes flowing in the secondary circuit. The loading of furnace transformers is essential during the production process. These transformers are associated with open arc furnaces and are subjected to a number of short circuits per melt as the material being melted collapses across the electrodes. The bus-bar flashovers are also a fact of life on most furnace installations they are required to have a lower than normal impedance, to give rise to higher over-current factors.

The furnace transformers’ design need to be robust in terms of their ability to withstand the dynamic effects of repeated short circuits. The minimum impedance values for these furnace transformers of the core type are in the order of 4 – 5 %. These lower values can be achieved

by utilising shell type transformer so as to achieve an upper level of impedance in the range 10 to 24 % depending on the configuration and tapping range [11].

Figure 2.3: Three – phase furnace transformer [11].

2.3.1.1 Knapsack Connection

The Knapsack connection is a connection arrangement that is common to virtually all circular SAF, and it originated from Knapsack, West Germany. The typical arrangement in *Fig. 2.4* shows three separate single-phase transformers, with three secondary circuits being brought out separately from each transformer and a delta connection being made at the electrodes using flexible conductors so as to allow vertical movement of the electrodes.

The reactance of the bus bars are kept to a minimum by interleaving the 'go' and 'return' paths for each phase right up to the flexible connection point close to the electrodes. The electrodes form a star circuit carrying current down to the molten bath which is $\sqrt{3}$ times the current in the delta and transformer circuit, which is the most effective utilization of the transformer's secondary current rating [12].

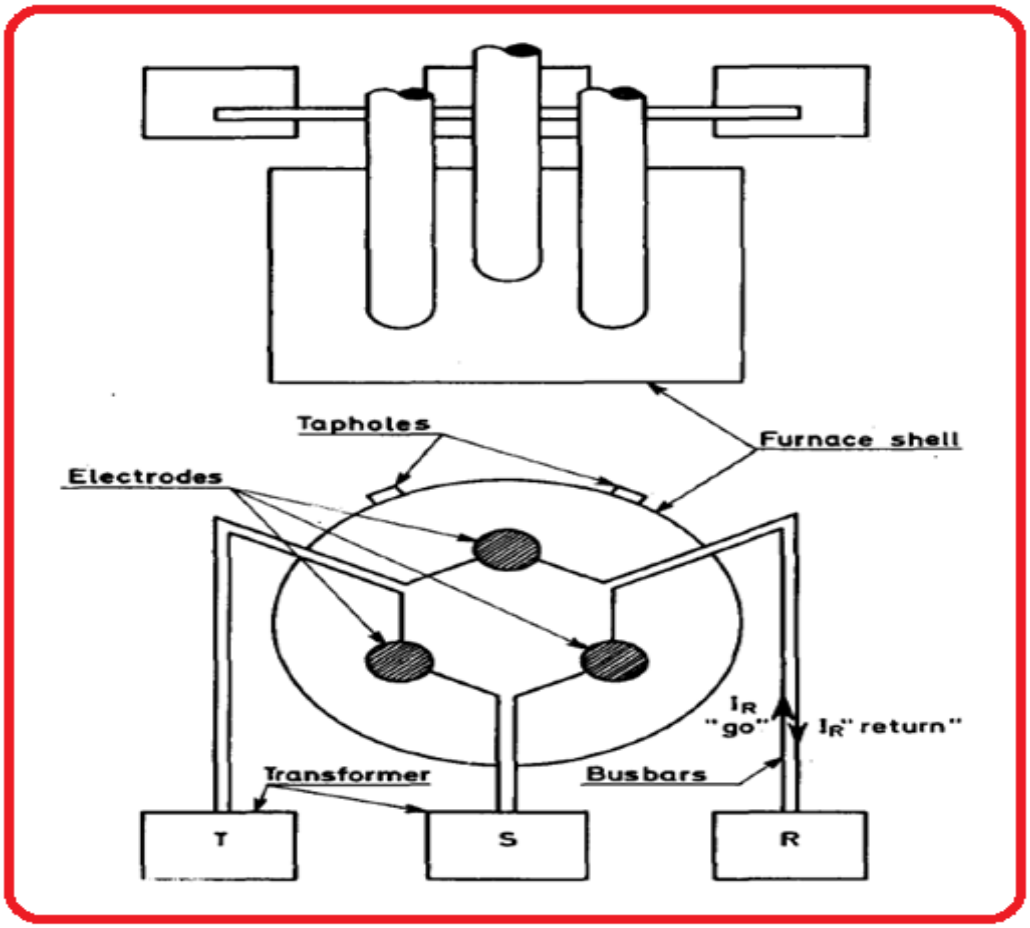

Figure 2.4: The Knapsack AC connection of a large SAF [18].

2.3.1.2 Cooling Systems

The cooling of the transformers is achieved by Oil Forced Air Forced (OFAF) or Oil Forced Water Forced (OFWF). In OFAF, the cooler are situated at the side of the building to facilitate cool air intake. The water coolers that consist of a double membrane tube system are placed in close proximity to the transformers. Leakage detection equipment is placed between the oil and the water tubes to prevent water from getting into the transformer oil [13]. The water is usually at a lower pressure as compared to oil. Coolers are often over-designed so that they will be able to cool the transformers sufficiently even with the loss of some cooler capacity due to failure. The furnace shell is cooled to maintain the desired temperature by use of large fans mounted at the bottom of the furnace housing and also the continuous pump back water system. Detection devices are specified to assist the operator to detect cooling problems at an early stage.

2.3.2 Bus Tubes

The bus tubes are defined as a high current, water-cooled electrical copper conductors utilized to convey electrical current from the final step down transformer to the contact units of the electrode [8]. They are water-cooled so as to prevent the conductor from gaining excessive heat which may cause severe damage, since high currents means high amounts of heat generated. *Fig. 2.5* shows the researcher's proposed cross-section of a bus tube.

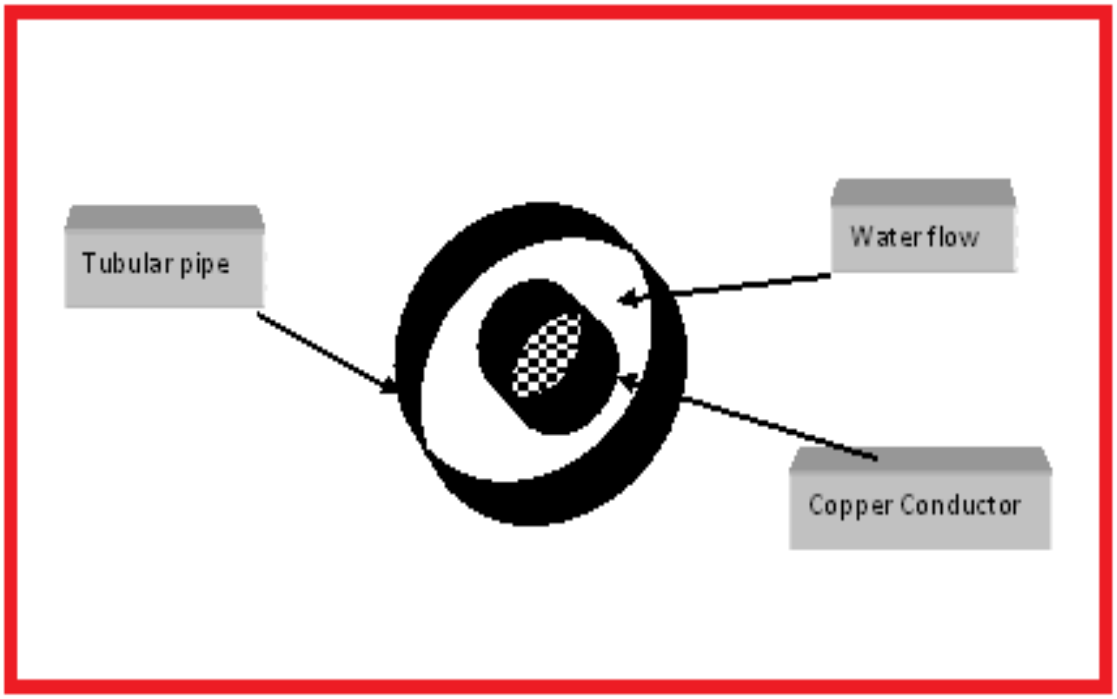

Figure 2.5: Cross- section of a Bus tube.

The bus tubes are not interconnected to each other, but each bus tube is connected to two contact units. This arrangement gives a better current distribution to the electrode casing, resulting in better conductivity through the electrode as well as a better baking profile on the electrode tip.

There are two types of bus tubes namely, static and flexible. The flexible bus tubes comply with the moving electrode column by flexing as the column move according to the furnace operator's control. The diagram in *Fig. 2.6* illustrates how the static bus tubes running from one side are connected to the flexible cables on either side.

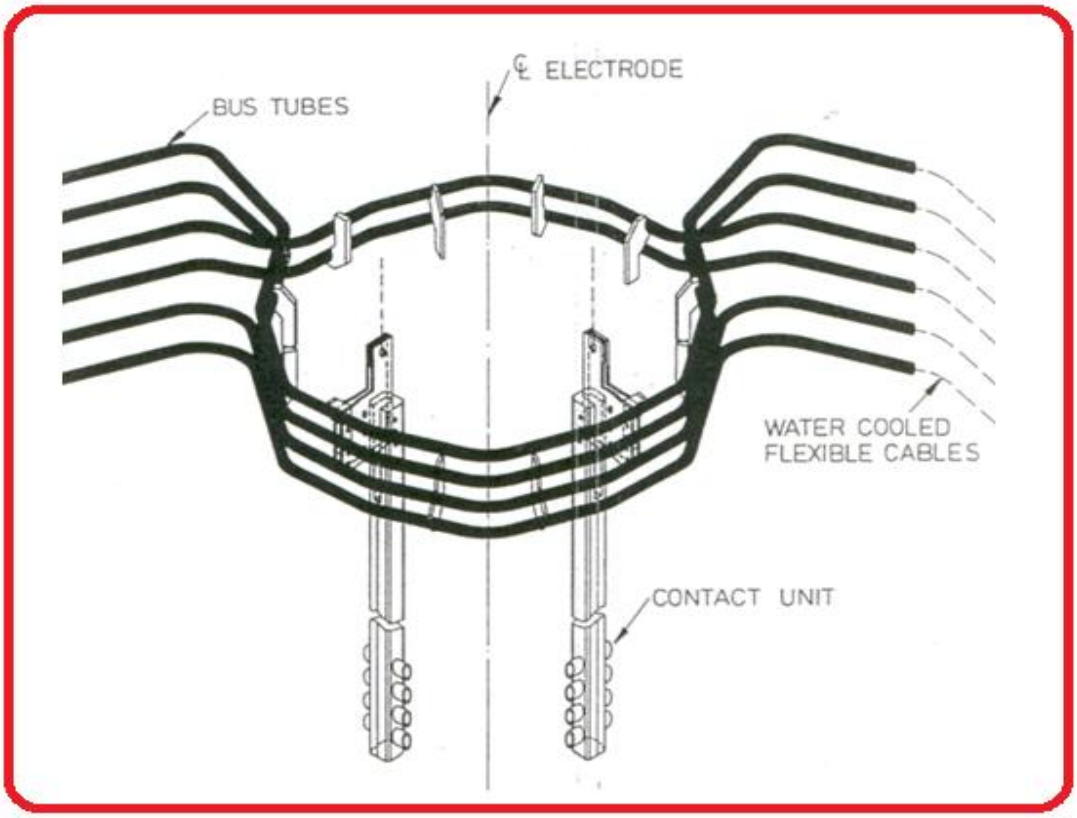

Figure 2.6: Bus tube arrangement [8].

2.3.3 Flexible Cables

The flexible cables facilitate the link between the bus bars and also permit the vertical movement of the column, which is usually 1 – 2m [8]. These flexible cables are made from woven copper wire so as to sustain maximum flexibility. They are made as short as possible, with openings being maintained lower down and as close as possible to the electrode to minimize the magnitude of reactance.

2.3.4 Furnace Electrodes

The electrodes that are made from carbon or graphite provide the electrical link between the bus-bar supply and the hot reaction zone of the furnace. They carry high currents and are able to withstand the very high temperatures generated by the electric arcs. The Söderberg – self baking- electrode, invented by C.W. Söderberg, is a continuous electrode that is built-up and renewed as it is consumed during the production of either ferrochrome or ferrosilicon in a SAF [14]. The primary objective of the electrode is to induce heat to the furnace for the smelting operation.

There are three Söderberg electrodes per furnace to form a three-phase power circuit. The diagram in *Fig. 2.7* shows the three electrodes that are situated in the form of a triangle and separated by wooden boards to prevent any accidental connection of the two phases that can cause serious damage to the casing due to arcing.

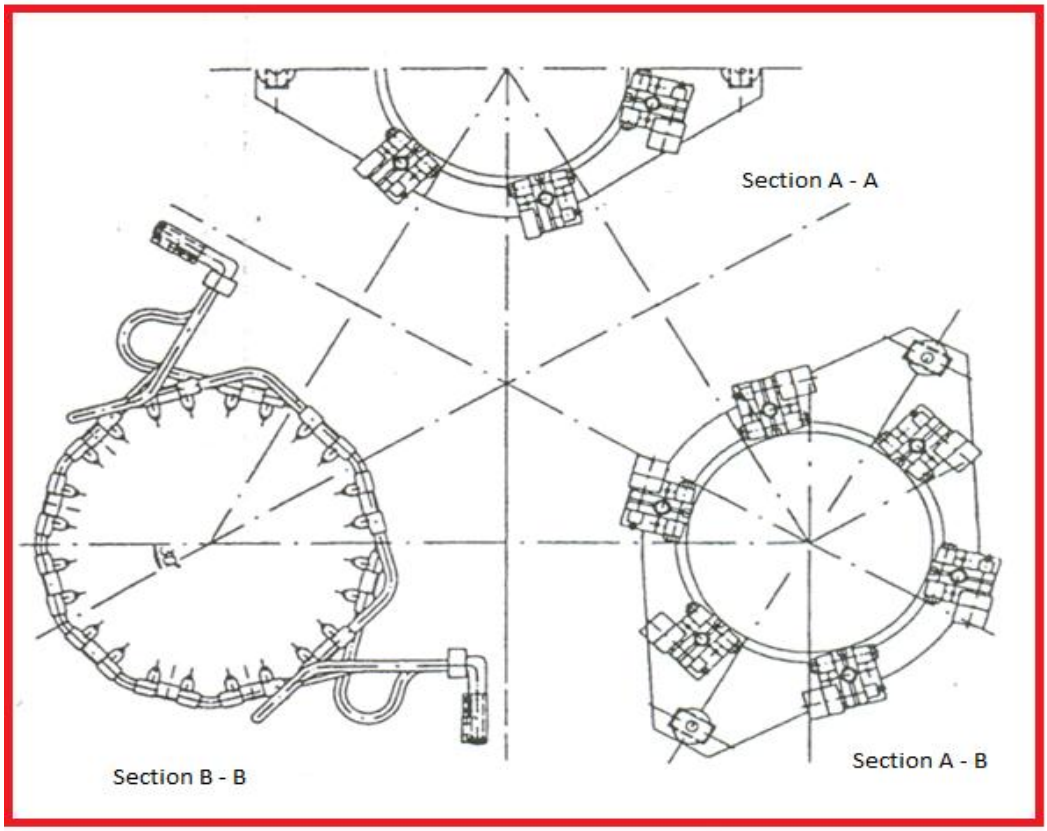

Figure 2.7: Electrode layout in the furnace [14].

Each electrode is approximately 19 meters high from the electrode tip to the top pointer at the casing top [15]. The electrodes' cooling mechanisms protect them from overheating due to the prevailing high temperature of the furnace. The contacts shoes are used for transferring electrical current accompany each moving electrode.

2.3.5 Electrode Column

The electrode column consists of the supporting structure for the electrode, the electrode itself (which weighs approx. 20 tons) and a connection system for transferring current from the flexible into the electrode [16]. The electrode is surrounded by a steel casing filled with carbon-based electrode paste blocks or cylinders as shown in *Fig. 2.8a* and *b.*

Figure 2.8a: Electrode casings.

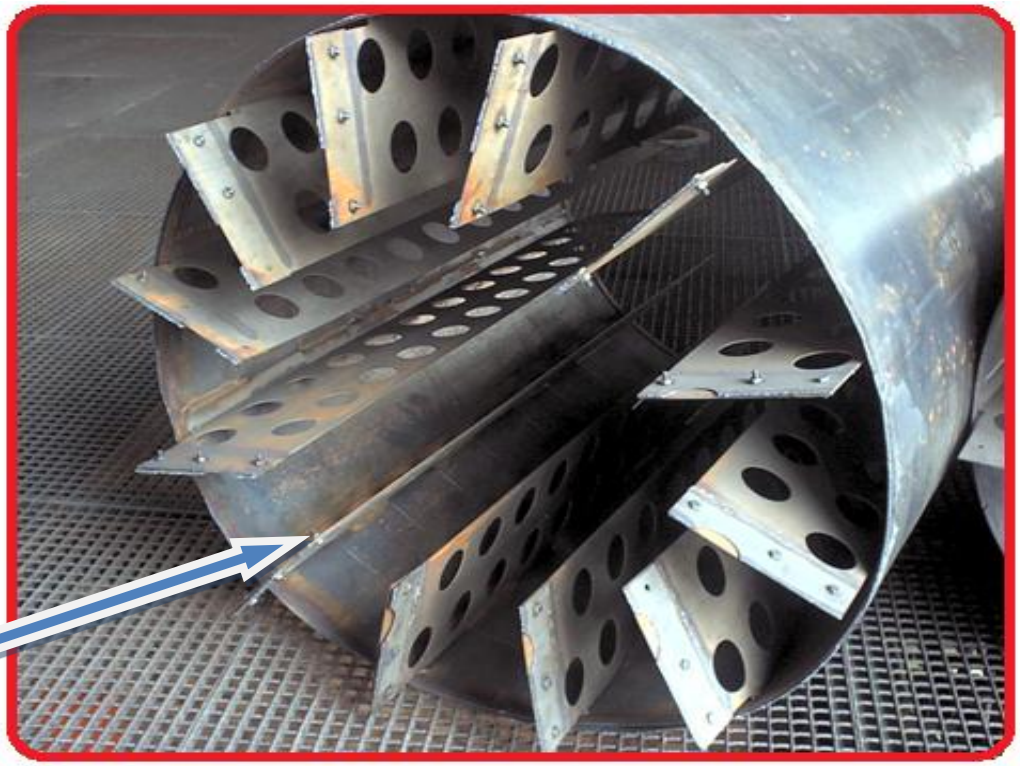

Figure 2.8b: Interior of electrode casing.

The electrode casing is covered with a steel lid that is removable on top of the casing column to prevent dust, steel parts or any unwanted objects from falling into the casing. The lid also prevents the electrode paste from being contaminated that may result in a weak baked electrode. The lid also consists of inspection holes with cover plates that swing opens to facilitate the paste measuring purposes as shown in *Fig. 2.9*. A bended pipe on the lid serves to position air pipes into the casing to prevent electrode paste volatiles, from settling in the casing column.

Figure 2.9: Electrode casing and lid.

The electrode system can either be supported by a hydraulically operated (large furnaces) or motor-driven cable supported with a reduction gear box (small furnace).

The diagram in *Fig. 2.10* shows a presentation of a Söderberg electrodes (Pressure ring system), with inside details. For large furnaces, the electrode column is supported from the upper floor (3) by two hydraulic hoists (2) which are connected to a hoist platform (4). Two hydraulically operated clamping rings (5) and (6), one of which (5) is rigidly connected to the host platform (4), are used to support each the electrode of the furnace.

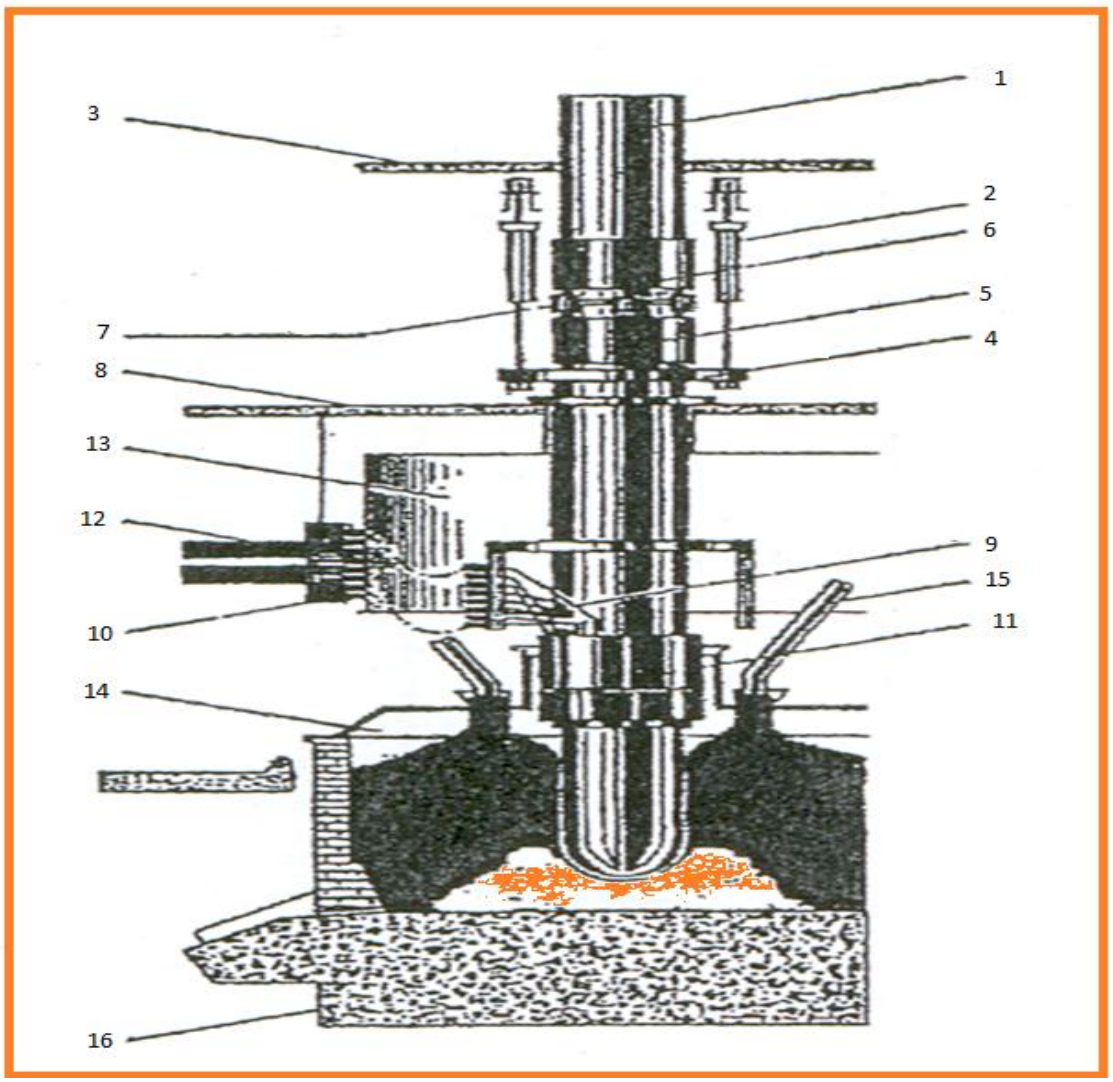

Figure 2.10: Söderberg electrode layout in the furnace [8].

1. *Electrode casing*
2. *Hydraulic hoists*
3. *Upper-level floor*
4. *Hoist platform*
5. *Bottom clamping ring*
6. *Top clamping ring*
7. *Hydraulic actuators*
8. *Middle-level floor*
9. *Water-cooled bus tubes*
10. *Flexibles connecting plate*
11. *Housing for contact shoes*
12. *Bus bar*
13. *Smoke hood*
14. *Furnace cover*
15. *Raw materials charging chute*
16. *Furnace body*

These clamp rings are connected together by a number of hydraulic actuators which when activated, push them apart as shown in *Fig. 2.11*.

Figure 2.11: Hydraulically - operated actuators of a large furnace electrode.

The hydraulic hoists provide the adjustment means of the electrode's position by allowing for changes in the operating conditions of the furnace. The tip of the electrode slowly erodes and has to be replaced periodically by slipping the electrode through the clamp rings. Slip is achieved by releasing the pressure in the top-clamp ring (6) and then applies pressure to the hydraulic actuator (7), so as to separate the two clamp rings, thereby clamping (6), and releasing (5) and then releasing the pressure in the hydraulic actuators, allowing the electrode to slip down as shown in *Fig. 2.11*. The repeated movements of about 1 to 2 cm slip result in the required amount of slipping of the electrode.

The electrical current is supplied to the electrode on the floor below the support structure through a flexible connection plate (10), which is connected by water-cooled bus tubes (9) to brass or copper contact shoes placed through the circumference of the electrode (11).The clamping of the contact shoes is achieved by means of either a rubber membrane that is activated by water or by mechanical spring pressure, and is maintained throughout the slipping operations. Non-magnetic couplings are used to reduce the eddy current problems on the segmented contact shoes and the contact shoes housing (11) is supported from the hoist platform (4).

2.3.6 Contact Shoes

The contact shoes, also known as the contact unit, of the electrode are the part that transfers electrical current from the current source to the electrode and into the furnace, as shown in *Fig. 2.12*. There is a contact shoe on each of the twelve ribs of the casing and electrical current flows through each rib into the electrode paste. Baking of electrode paste takes place in between the contact shoe unit, thus going from liquid phase to solid phase.

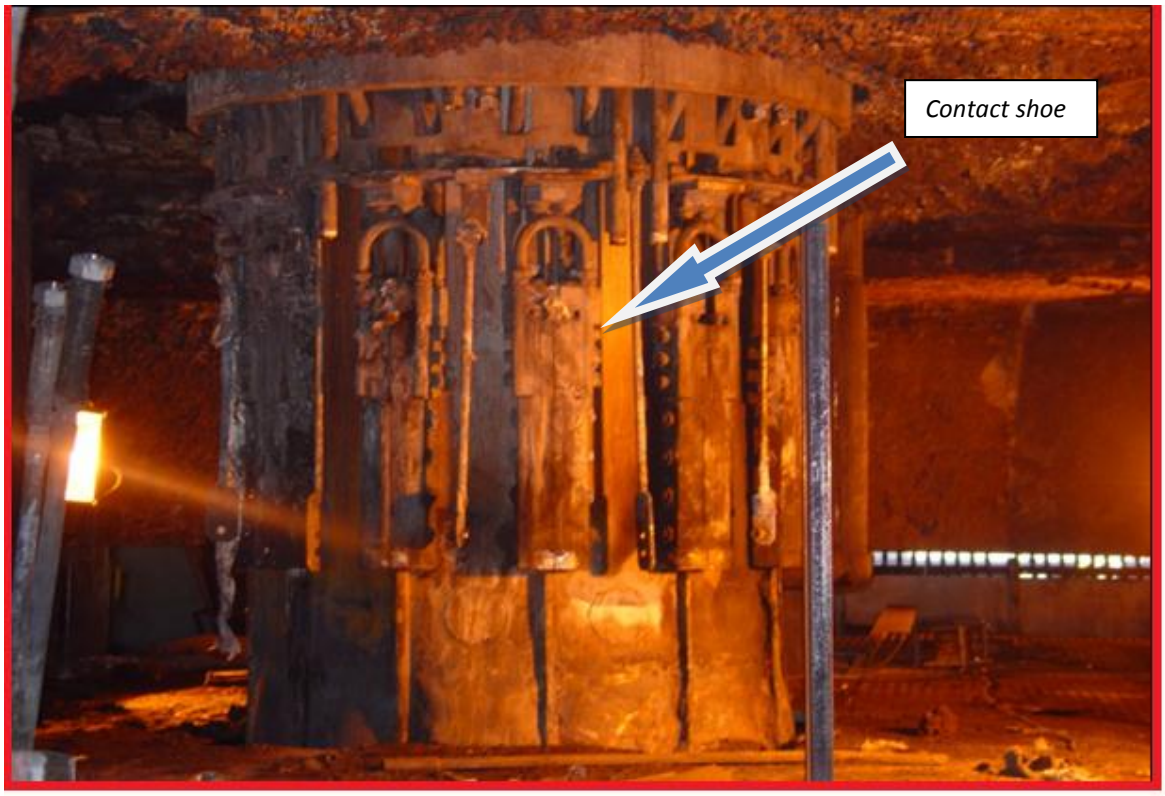

Figure 2.12: Position of contact shoes around an electrode.

The contact element of a contact shoe is made firm by disc springs to ensure that no arcing occurs between the contact unit and the external casing fin (arcing can cause holes in the casing, like a welding effect) [12]. The contact unit operates in very high temperature surroundings and is therefore protected by a water-cooled shield. The arrangement of the contact shoes and the position of the water-cooled shield are shown in *Fig. 2.13*.

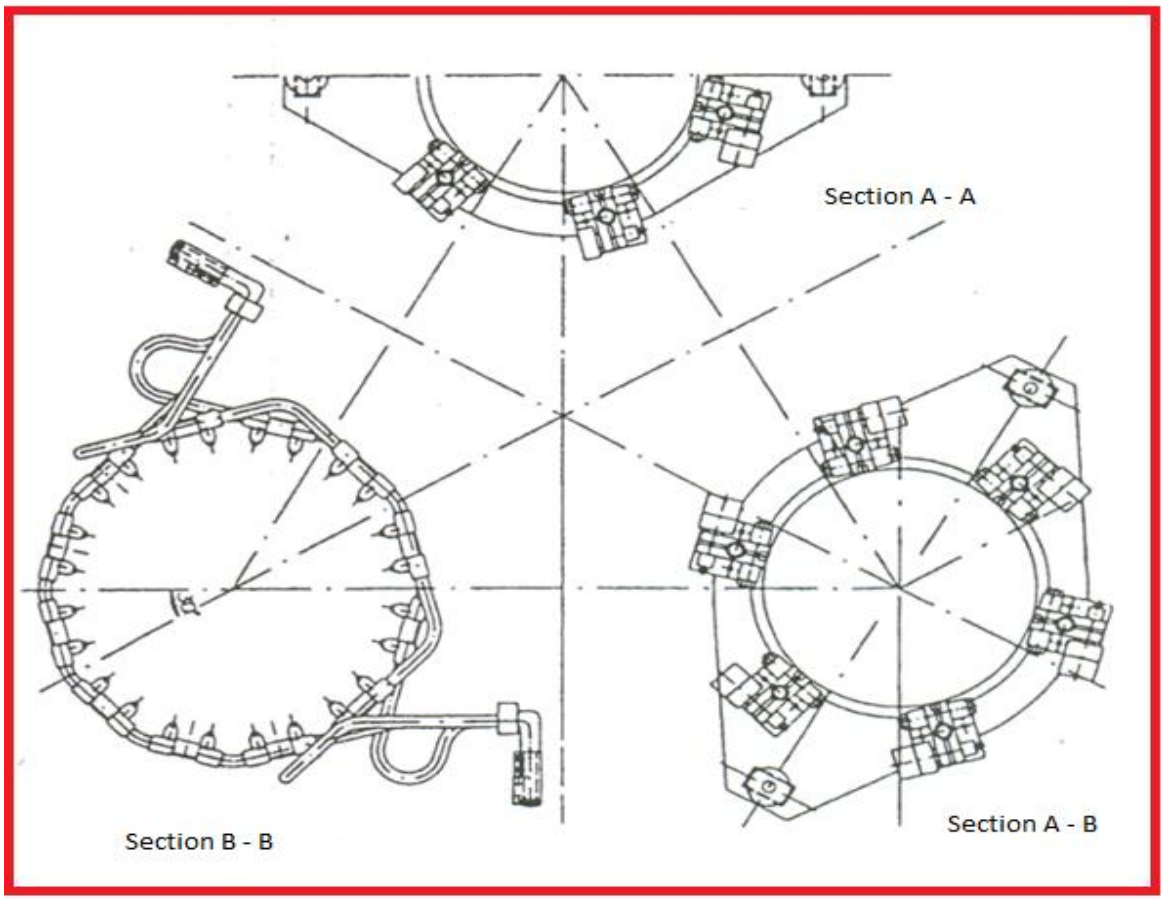

Figure 2.13: Schematic diagram for the arrangement of contact shoes around an electrode [12]

2.3.7 Shell and Lining

The shell of the furnace consists of a cylindrical vessel welded together from steel plate approximately 2cm thick and mounted on a circular platform of about 1 – 2 m from the ground [12]. The floor on the inside of the furnace shell is covered with about ½ m of refractory brick, and then with a fairly thin layer of a high temperature refractory concrete, which provides a smooth level surface. This surface is then covered up with seven layers of refractory bricks and subsequently by two layers of carbon blocks that are crossed so as to cover the gaps between the blocks.

The blocks are carefully machined and aligned so as to minimize the gaps that cause weakness in the lining. A special silicon carbide refractory and fire bricks are used around the tap holes of furnaces. The roof of the furnace is water-cooled, and is lined with high temperature refractory bricks and castable refractory.

2.4 Neutral Connection

The furnace's carbon lining is electrically connected to the molten metal and act as the neutral for the furnace's three - phase load. The electrical potential measurement of the neutral is facilitated by a copper rod imbedded in the carbon lining and connected to the side of the furnace with an insulated conductor [16]. As a result of large amounts of heat generated on large ferrochromium/ ferrosilicon furnaces, most furnaces are now operated without a neutral connection, since the copper rod does not last.

Separate neutrals are provided under each electrode, and as well as in the centre of the furnace so as to provide a means of reducing measurement errors as shown in *Figures 4.6* and *4.9*. Stainless steel is used in neutral construction and these neutrals are set into the high temperature concrete layer, flush with the surface of the concrete and then covered with a layer of carbon paste and carbon blocks.

2.5 Conclusion

This chapter described the overview of the SAF construction and their properties in the production of ferro-chrome, ferro-silicon and others. The associated equipment that constitutes the SAFs was also discussed, that included the furnace transformers, knapsack connection, bus tubes, flexible cables, furnace electrodes, electrodes columns, contact shoes, shell lining, and the neutral connections. The cooling systems of both the furnace transformers and the furnace shells were also outlined, with more emphasis on maintaining the desired temperatures for the furnace operations. The next chapter 2 will focus on the various electro-thermal variable parameters available in operations of the furnace.

CHAPTER THREE

ELETRO-THERMAL VARIABLE PARAMETERS OF SUBMERGED ARC FURNACES

3.1 Introduction

This chapter describes the various electro-thermal variable parameters present in SAF operations. The discussion of these variables will include their description, effects and variations as these impacts on the operation of the furnaces. There are many variable parameters present in furnace operations but this chapter will only focus on the variables focused on voltage, resistance, and temperature and energy consumption.

3.2 Voltage

3.2.1 Supply Voltage Variation

Load fluctuation results in the change in the *rms* value, but installed automatic regulation compensate for those changes within a few tens of seconds. Variations in magnitude of the supply voltage can be a problem when dealing with very long lines supplying SAFs. Any variation in the magnitude of the supplied voltage outside the range of +10% / -15% boundaries from nominal voltage may result in premature ageing, preheating or malfunctioning of the connected equipment [17].

3.2.2 Supply Voltage Dips

The supply voltage dips represent temporary reduction of voltage below a set threshold and its duration of phenomena is limited to 1 minute [17]. When the voltage is decreased for a period longer than a minute, it is considered as a magnitude variation. Sag is a term that is also used in some technical communities, but the latest efforts for EMC standard consistency defines dip as the preferred term.

Some standards use the term voltage depth instead of voltage dip and specify a voltage depth of 90% as equal to a retained voltage of 10% [17].

When determining the dip threshold, a sliding reference can be used for the calculation to avoid the problem with the transformer ratios when measurements are taken on both the LV and MV side of the system. The retained voltage can be expressed as a % or *p.u.* of the *rms* value before the voltage dip. The end threshold is typically 1% higher than the start threshold due to the problem that may arise if a measured value is near to the start of a dip threshold [17].

Voltage dips results due to failures in the network or the presence of excessively inrush currents. They cause malfunctioning in most equipment such as relays and contactors, which drop out if the dip is 60% for longer than I cycle as shown in *Fig. 3.1*.

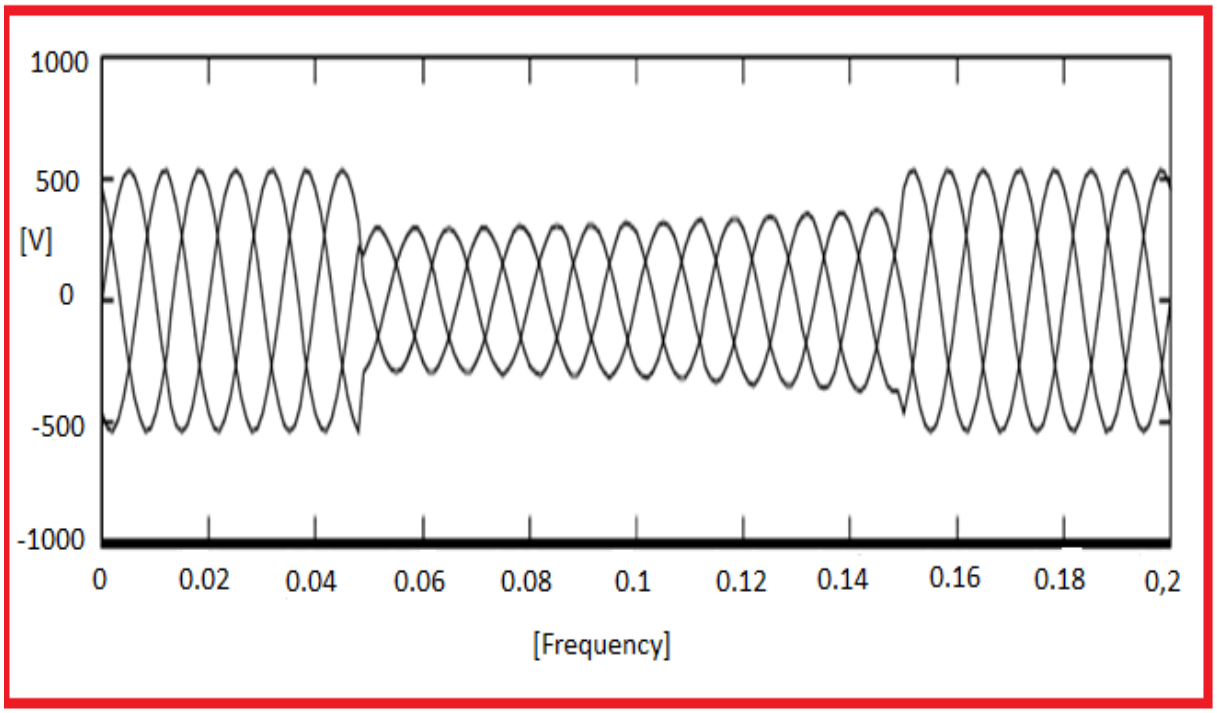

Figure 3.1: Characteristic graph of a three – phase system voltage dip [17].

3.2.2 Supply Voltage Swells

Voltage swells results from instantaneous voltage increases (opposite to dips) and same attributes are employed for the classification of swells as for dips as shown in *Fig. 3.2.* Voltage swells originate from single line ground failures (SLG), upstream failures, switching off of large load or switching on of large capacitors [18]. Since voltage swells usually last for a short period, there is no significant impact on equipment, however, light bulbs can burn out and safety problems may arise.

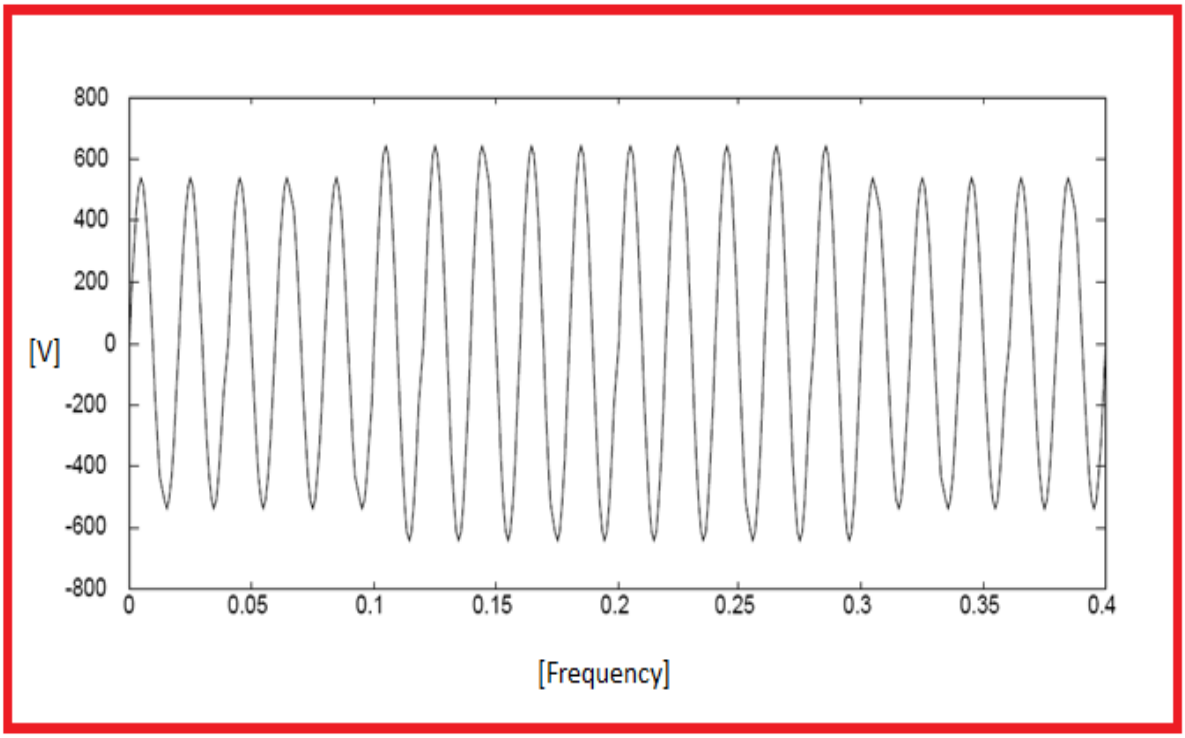

Figure 3.2: Graphical representation of voltage swells [17].

3.2.3 Rapid Voltage Changes

The rapid voltage changes are fast changes in a voltage between two steady conditions as a result of switching on or off of large loads such as SAFs. When rapid voltage changes exceed the dip or the swell voltage threshold, it results in a dip or swell. Rapid voltage changes thresholds measurements involve ascertaining the following parameters as shown in *Fig. 3.3* [17]:

- the minimum rate of change
- the minimum duration of steady state conditions
- the minimum difference between two steady states
- the steadiness of state conditions.

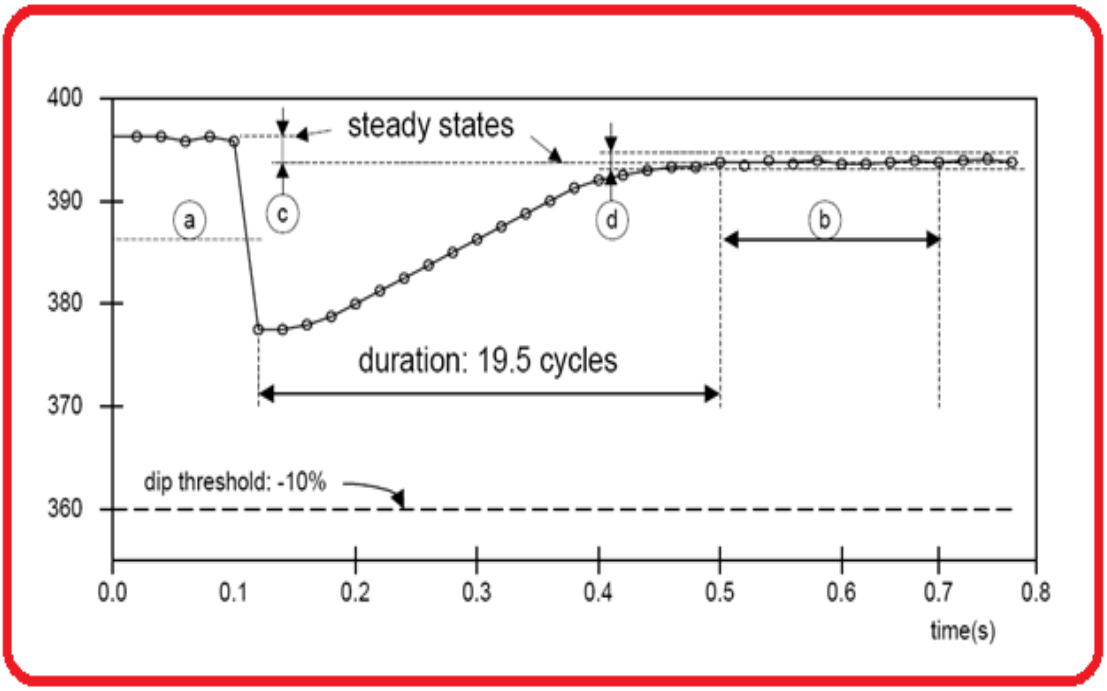

Figure 3.3: Characteristic graph of a rapid voltage change [17].

3.2.4 Supply Voltage Unbalances

Supply voltage unbalances (imbalance) arise as a result of inequality of the *rms* values of voltage or phase angles and the consecutive phases. A voltage unbalance is a ratio of the negative sequence component to the positive sequence component. The voltage unbalance occurs in SAFs when current consumption is not balanced during the 3 cycles of processing (operation) or a faulty condition before tripping [18]. They impact negatively on three - phase asynchronous motors by causing overheating and a tripping of protective devices.

3.2.5 Voltage Interruptions

An interruption is classified as a network's isolation from any source of supply. It creates a specific voltage that is above zero, a short period after the interruption commences. The interruption is detected as a voltage (U) that drops below an interruption threshold of 1%, 5% or 10% of the declared voltage [17].

The duration of an interruption is measured in the same manner as that of the voltage dip duration after setting an interruption threshold, and this technique creates a short circuit fault that can appear as a short interruption in one section of the network and a dip in another.

Voltage interruptions are classified as short term or long term. Short interruptions are introduced by a fault condition in a network, resulting in the operation of switchgears. Since there are complex schemes in SAFs operations for reclosing purposes, the limits for short interruption ranges from 1 or 3 minutes [18], depending upon the reclosing operation as shown in *Fig. 3.4.*

The long interruptions are in excess of the short interruption duration limit and arise due to a fault conditions that cannot be terminated with a control sequence and the occurrence of the final tripping of a circuit breaker, such as the SF6. In SAFs operations, interruptions can cause disruption in production, increase the risk of equipment damage or even injury.

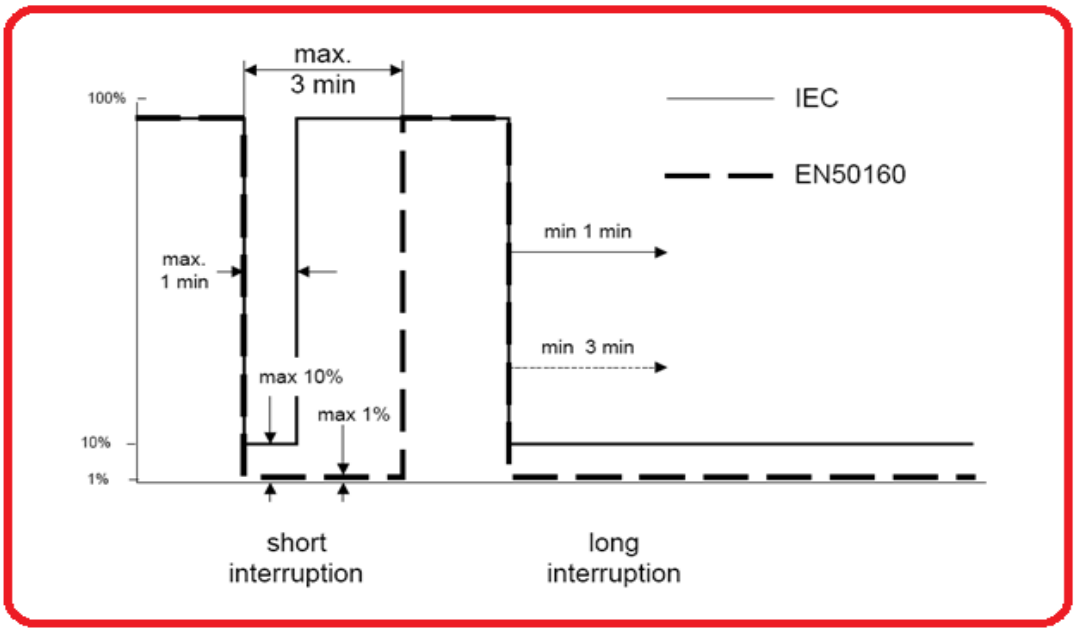

Figure 3.4: IEC and EN50160 standard Interruption threshold and duration definitions [17].

3.2.6 Transient Over-voltages

Transient over-voltages are short, highly damped momentary voltage or current disturbance that are classified as impulsive over voltage and oscillatory over voltage as shown in *Fig. 3.5.* Impulsive transient over-voltages are unidirectional disturbances that are caused by lighting and have a high magnitude but low energy, with a frequency range of above 5 KHz with durations of *30 - 200 μs* [17].

The oscillatory transient over-voltages are caused by switching, ferro-resonance or the system's response to an impulsive overvoltage. Switching over-voltages are characterised by high energy and are classified as low *(<5 KHz)*, medium *(5 kHz< f <500 KHz)* and high frequency *(> 500 KHz)* transients [17]. In SAFs operations, transient over-voltages cause the immediate failure or degradation of transformers, capacitors or semiconductors and cable isolations.

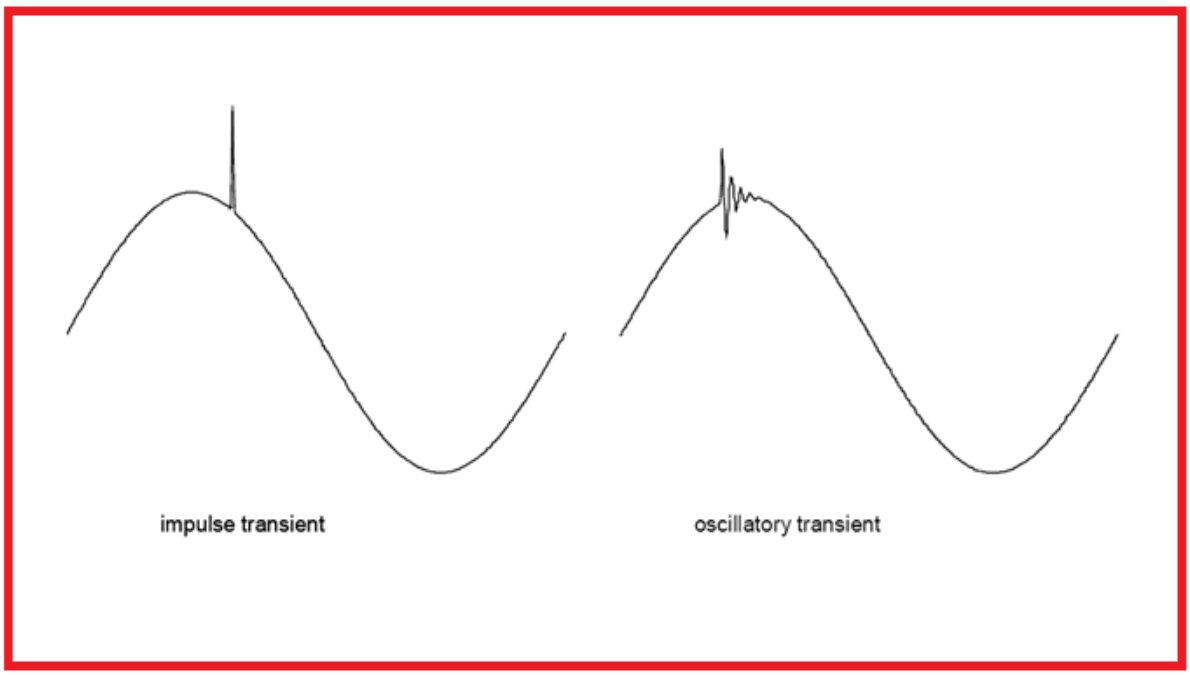

Figure 3.5: Impulse and oscillatory transients' waveforms [17].

3.3 Energy

In all electrical installations, electric conductors are selected in such a way that the heat generated, and thus the loss of energy, are minimized. The work is done through transporting the current in a conductor and the energy required for doing this provides the heat. This is known as the heating effect of an electric current and is given by the Joule's law. Joule's law states that the heat generated in an electrical conductor is directly proportional to the square of current, the resistance of the conductor and the time in seconds as shown in equation (3.2) below.

$$Heat/Energy = I^2 Rt \quad joules \qquad (3.2)$$

The amount of energy the furnace consumes to make either ferrochrome or ferromanganese is designated as specific energy consumption, and it describes the quantity of electrical energy (kilowatt-hour) used to produce a unit weight (ton) of the desired alloy product [19]. Specific energy consumption is important because it is a measure of performance of the furnace and it determines the quantity of the metal that can be made at a given rate of energy input.

3.4 Resistance

The production rate of a furnace is directly proportional to the resistance of the furnace, because the heat required for reduction and smelting is directly proportional to the resistance of the furnace. The resistance of the furnace is dependent on the following factors:

Physical Parameters

- The length of the electrode
- The distance of the tip of the electrode from the bath
- The depth of the electrode in the mix.

Physical condition of the raw materials in the furnace

- Amount of fine in raw materials
- Percentage moisture in the reductant materials
- All the factors that may influence the chemical and metallurgical changes that take place in the future.

The resistance is influenced most characteristically by reductant. Almost all parameters of the reductant have an influence on the resistance of the furnace [19]. The furnace resistance is made up of two components namely:

- resistance between the electrode tip and the molten material in the crucible bottom, R_a
- resistance due to the unmelted charge materials, R_b

The total resistance is given by the formula:

$$R_T = \frac{1}{\frac{1}{R_a} + \frac{1}{R_b}} \tag{3.2}$$

It is thus obvious that if either one of the components of the total resistance is very much greater than the other, its contribution to the total can be ignored. When $R_b \gg R_a$, then R will change in direct proportion to the and vice versa.

- **Two resistances are approximately the same order, i.e.** $R_c = R_a$

When the electrodes are raised under this condition, the area of contact between the electrode and the raw charge will be reduced, resulting in the reduction of current while the length of the arc between tip and bath is increased and the resistance thus increased [19]. The total power input will be decreased and also the input power will be increase as the electrodes are lowered. The furnace load will respond immediately to any electrode movement under this condition and will be stabilised on the new level as soon as the movement is stopped.

- **When** $R_a \gg R_c$ **, then** R_c **will be the predominant resistance**

The total heat generated will be made up of the heat generated in the unmolten charge. This situation develops if a highly acidic slag exists at the bottom of the crucible and the electrodes dip into it. The heat generated in the reaction zone will not be sufficient to raise the temperature of the slag to the desired level [19]. This situation usually causes slag boiling, disturbance of the equilibrium in the crucible, undrainable slag and a generated deterioration of the furnace conditions. The power will respond very sluggishly to the electrode movement and will not be able to stabilise at new level but will fall as the mix is melted and the layer is reduced.

- **When** $R_c \gg R_a$ **, exists,** R**, approximately equal to** R_a

Under this condition, more heat becomes generated on the electrodes than necessary, causing hot gas blows due to overheating of the reacting materials. The power will respond to the slightest movement of the electrodes and even to the slight movements of the charge and it will be virtually impossible to obtain a stabilised load.

3.5 Temperature

3.5.1 Cooling Water

In order to ensure normal operation of a SAF, closed loop water cooling system, cooling water temperature and the heat load must be controlled. It is critical to protect the lining of the furnace's important equipment so as to minimize the prevalent causes of damages in SAF operations [20], which include:

- **Excessive heat load:** This is as a result of bad operating conditions, increase in the age of the furnace and also the damaged furnace walls.

These can be minimized by:

- ✓ Additional thermal load monitoring equipment to monitor and improve the distribution of gas flows.
- ✓ Ensuring normal operation of the furnace in stable conditions in addition of micro-coolers, etc.
- ✓ Ensure furnace production safety extended life, intelligent decision on creating the conditions through the furnace cooling system, water temperature and the cooling of the walls of the furnace (shell cooling)
- ✓ Monitoring the heat exchange process and making decisive judgments.

It is essentially important to cool the walls and the walls should be in direct contact with the cooling components. The water pipes that pass through different parts of the furnace walls are installed with measurement devices to detect the corresponding temperatures in them.

3.5.2 Electrodes Temperature

Temperatures greatly influence the electrical behaviour of electrodes in arc furnaces. Hence, the temperature profiles along the electrodes can be used as a compliment to electrical measurements in monitoring the furnace operation [21]. The basic structure of an ELSA electrode is shown in *Fig. 3.6* and consists of a central column of graphite, which acts as mechanical support and a steel casing. Söderberg - type paste is introduced between the graphite / carbon and the casing.

This paste is subject to different temperature conditions along the column, which make it, evolve through different states, ranging from raw paste in the upper part of the steel casing to the baked paste in the area of the contact plates. As shown in Fig. 3.6, the temperature of slag ranges from *1650 – 1700*℃, whilst that of metal is $<$ *1600*℃.

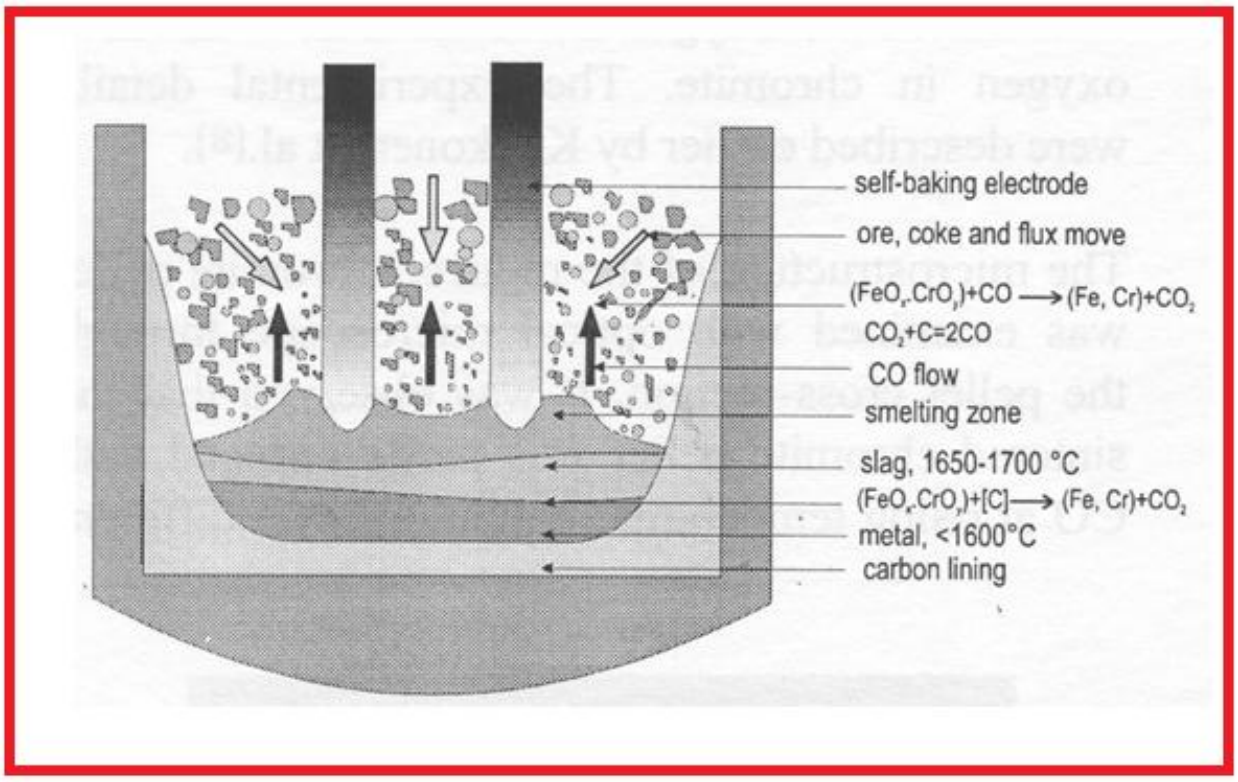

Figure 3.6: Schematic diagram of the SAF constituents [21].

3.5.3 Infrared (IR)

The Stefan-Boltzman's law states that the radiator of a blackbody or the total emissive power of a blackbody (E_b) is direct ratio to the fourth power of thermodynamics temperature (T) [22]. It is expressed by the following equation:

$$E_{(\lambda,T)} = \delta T^4 \qquad (3.1)$$

where: σ is the Stefan-Boltzmann constant

In the same temperature, the ratio of the monochromatic light of an object and the monochromatic light of black object is taken as the monochromatic blackbody degree or emissivity (ε). The monochromatic light of object (E) is less than blackbody's (E_b) or the

emissivity (ε) is not greater than one [22]. Thus, the emissivity (ε) is defined by the following expression:

$$\varepsilon = \frac{E(\lambda, T)}{E_b(\lambda, T)} \qquad (3.2)$$

The theoretic foundation of the technology of infrared temperature measuring is given by the following equation [22]:

$$E(\lambda, T) = \varepsilon E_b(\lambda, T) = \varepsilon \sigma T^4 \qquad (3.3)$$

Emissivity is the ability of an object to emit or absorb energy. Perfect emitters have an emissivity of 1, emitting 100% of incident energy. The emissivity may vary with temperature and spectral response (wavelength). Some shine metal surfaces offer difficulty taking accurate temperature measurements when infrared thermometers are used unless they are adjusted for emissivity.

The infrared thermometer gives an accurate temperature measurement and its emissivity is adjusted to fit with the emissivity of measurement of materials as shown in *Fig. 3.7*. The infrared thermometer has a capability of giving an accurate temperature measurement and its emissivity is adjusted to fit with the emissivity of measurement of any material.

Figure 3.7: Simulation of an IR Thermometer measurement reading at ε =1.00 [22].

For non-contact temperature measurement, the infrared thermo - graphic detector is used in conjunction with the infrared thermometers to obtain an accurate temperature measurement [23].

3.6 Conclusion

This chapter described the various electro-thermal variable parameters present in SAF operations. A discussion of these variables that include voltage, resistance, and temperature and energy was given that include their description, effects and variations. The preceding chapter 4 will focus on how these variable parameters are measured during the operations of SAFs.

CHAPTER FOUR

MEASUREMENT OF VARIABLE PARAMETERS IN SUBMERGED ARC FURNACES

4.1 Introduction

This chapter gives a detailed description of the various measurement techniques available in the measurement of variable parameters in submerged arc furnaces. These include the typical PQ measuring system, PQ analyser, voltage and current and the electrode-to-bath voltage. Temperature measurements that include the electrodes profiles, the IR temperature measurement of the furnace transformers will also presented. An amalgamated variable parameter measurement (AVPM) system is proposed as the best alternative to some of the shortfalls experienced in variable measurement in SAFs.

4.2 Power Quality Measurement

Power Quality meters are used to measure a number of parameters that include voltage, active and reactive power every minute. The overall measuring system's accuracy depends on the precision of the incorporated furnace current and voltage transformers and also the transducers utilized. The electro-thermal variable parameters in SAF operations are measured and controlled by a number of meters combined together systematically as shown in *Fig. 4.1.*

A typical measuring system [24] consists of the field instrument transformers (voltage and current transformers), measuring transducers (used to interface the sampling device with the field transformers), sampling device, and the real time analysis system as shown in *Fig. 4.2.* Although all precautions are taken to ensure that the measurements made by the recording instruments are accurate, the field instrument transformers usually cannot be changed or adjusted. Since instrument transformers typically have a flat magnitude response up to 10 kHz, their phase response may not be flat, or linear, at frequencies above the fundamental frequency. The sampling cards may introduce a phase shift between signals on different channels which are usually assumed to be sampled at the same time.

Figure 4.1: Control room panel meters for the measurement of electro-thermal variables (45 MVA SAFs Wonderkop Chrome Processing Plant, SA (2008)).

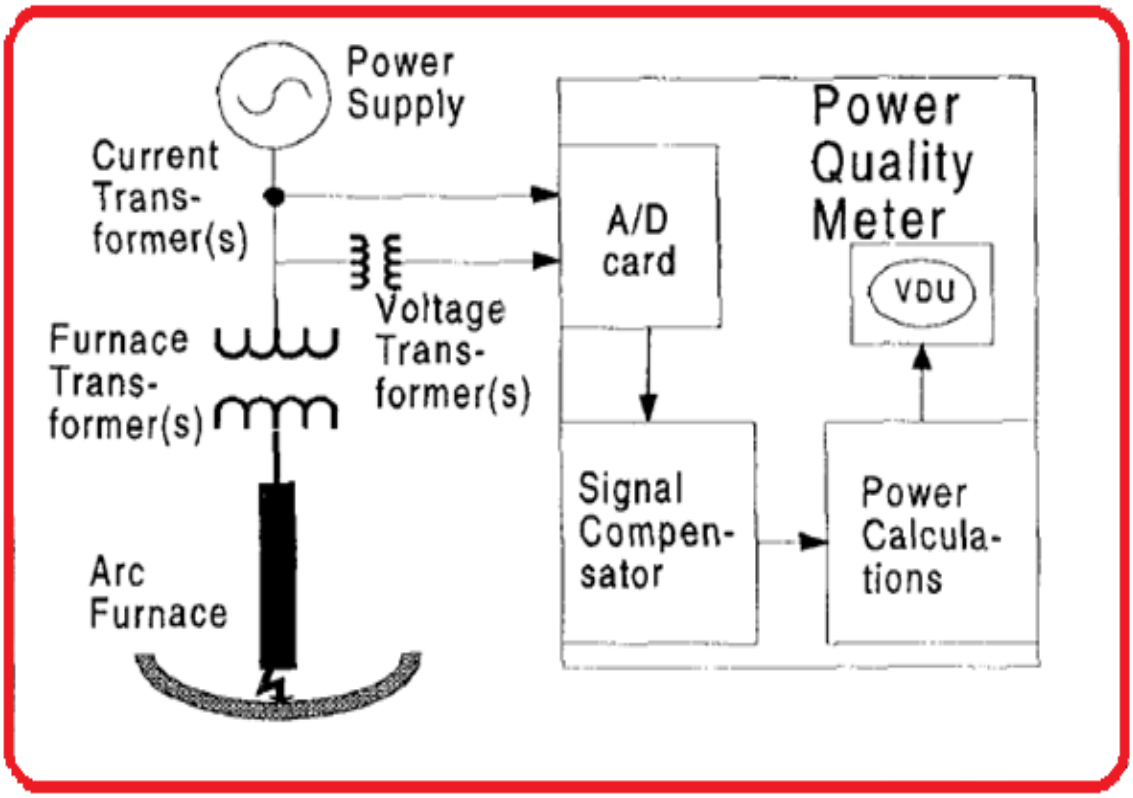

Figure 4.2: Power Quality measuring system [24].

Power measurements may be significantly affected by errors that are magnified when the power factor is much less than unity [25]. The phase shift introduced by the instrument transformers and the sampling devices can give rise to significant effects on the overall system measurement accuracy. The use of the Power Quality Analyser (PQA) has proved excellence in many applications of the measurement of power quality in SAFs loads, presenting accuracy, compensation and minimal measurements errors.

4.2.1 Power Quality Analyzer (PQA)

The Power Quality Analyzer (PQA) consists of an Intel –based processing unit connected to its own instrument current transformers and voltage transformers, via a 16 – bit analog-to-digital card [17]. The software modules have been designed to perform real-time calculations in the multi-tasking environment, which combines the power quality measurements that requires many meters. The PQA incorporates modules that allow calculations to be easily added or removed to suit individual requirements. The power quality calculations are grouped into three separate modules, namely, the basic electrical module (BEM), the advanced electrical module (AEM) and the arc furnace module (AFM). The input signal and calculation results are assessed or viewed whilst calculations are being performed and data access is achieved by the reading output data files to a local machine or by remote connection of the machine through TCP/IP network connection.

4.2.1.1 Basic Electrical Module (BEM)

The Basic Electrical Module provides the standard power calculations and with its flexible user-defined output capabilities. It is useful in evaluating a wide range of electrical problems on-line that include, fault-induced voltage dips, short-term *rms* variations, long-term *rms* variations, phase imbalance, asymmetrical operation and low power factor.

4.2.1.2 Advanced Electrical Module (AEM)

The Advanced Electrical Module provides detailed waveform calculations that include harmonics, flicker, and voltage dip classification. The harmonic calculation outputting facility is very flexible, allowing storage of discrete harmonic components and also the magnitude of the continuous frequency spectrum. Both outputs of the AEM module may be configured to limit the data storage to that outside user-defined thresholds.

4.3 Measurement of Voltage and Current

The voltage and current measurement method shown in *Fig. 4.3* is based on observing the mutual correlation between the electrode currents and the total power supplied into the furnace by utilizing the fast, natural fluctuation of currents and power supplies into the furnace and on estimation observations [24].

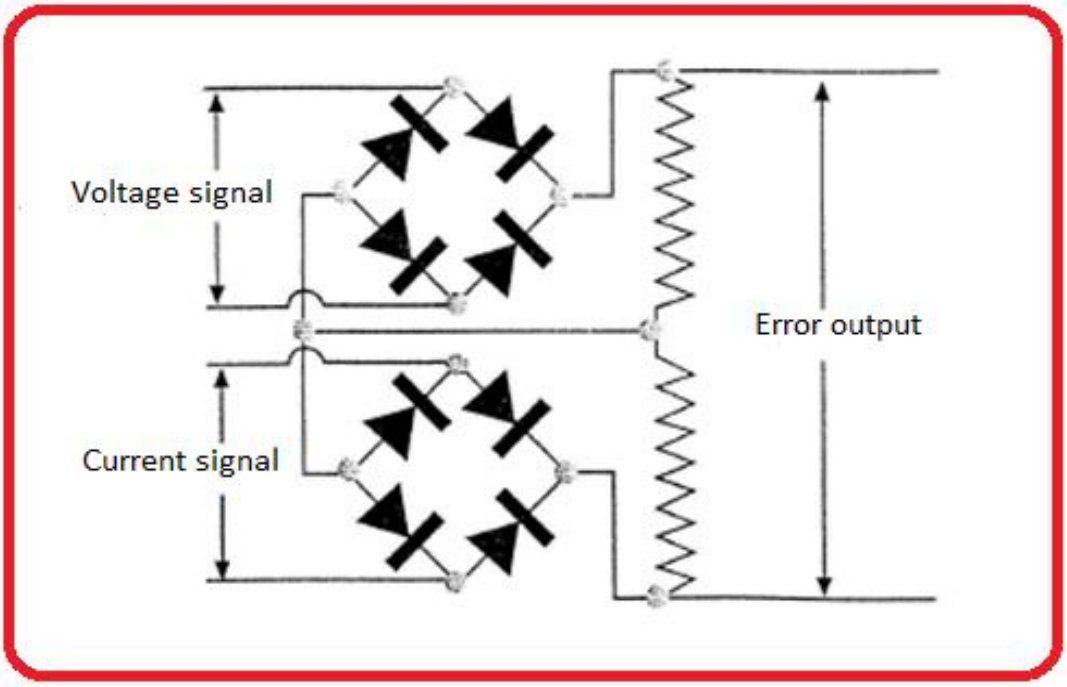

Figure 4.3: Typical configuration for voltage and current measurements in three-phase SAF [24].

The block diagram in *Fig. 4.4* shows how the information required in the estimation is collected by performing a plurality of successive current and voltage measurements of adjacent instants at various energy distributions of the furnace [26]. The measurement results are then used to calculably determine the estimates for the electrode related voltages, impedances and powers. The electrode-related powers are further split into the electric arc power and voltage or else, power and voltage loss caused by resistive conduction. The effect of the mutual impedances is automatically taken into account in estimation.

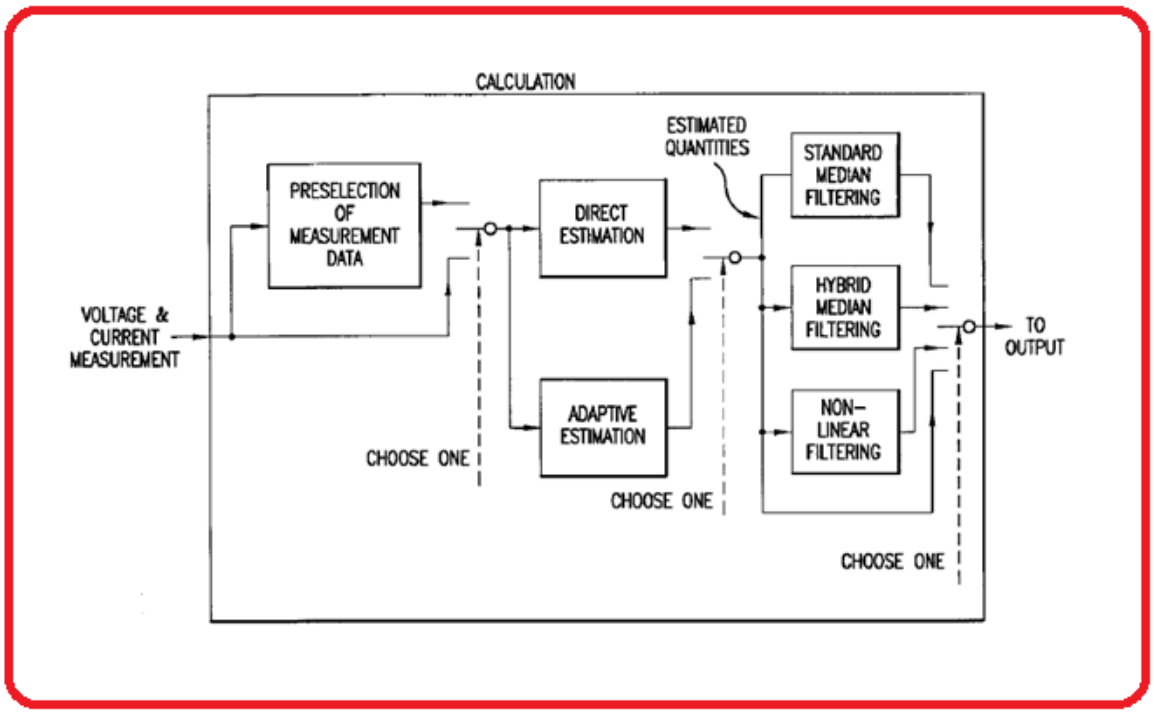

Figure 4.4: Block diagram of a voltage and current [26].

4.3.1 Voltage Dips

Using the PQ Analyser, through the AEM module, the voltage dips are characterized by profiling the fault-induced voltage variations on a Computer Business Equipment Manufacturers Association (CBEMA) curve [24]. The voltage excursions are saved by duration and the magnitude using a detailed output which gives the shape of the voltage excursion.

When assessing dips, the *rms* voltage ($U_{rms1/2}$) is calculated over a single cycle or a half cycle and is refreshed each 10 *ms* (every half of a cycle) [24]. The voltage dip is characterised by parameters such as dip threshold, dip starting time, dip duration and retained voltage (U_{ret}) as shown in *Fig. 4.5.*

The dip threshold can either be automatically set or manually set by the user to represent part of nominal U_n or declared U_c (U_{dec} in some standards) voltage and usually varies from 0.9 U_c for troubleshooting to 0.65 U_c for contractual purposes [24].

The dip starts when $U_{rms1/2}$ drops below the dip threshold and ends when $U_{rms1/2}$ rises above the dip threshold. The difference between end and start time is known as the dip duration and

is determined in seconds or cycles. The retained (residual) voltage (U_{ret}) is the lowest $U_{rms1/2}$ value recorded during a dip. The minimum set of attributes which describes a dip is a pair (U_{ret}, duration), although some instruments store more data such as the average voltage during the dip period or the shape of $U_{rms1/2}$ voltage.

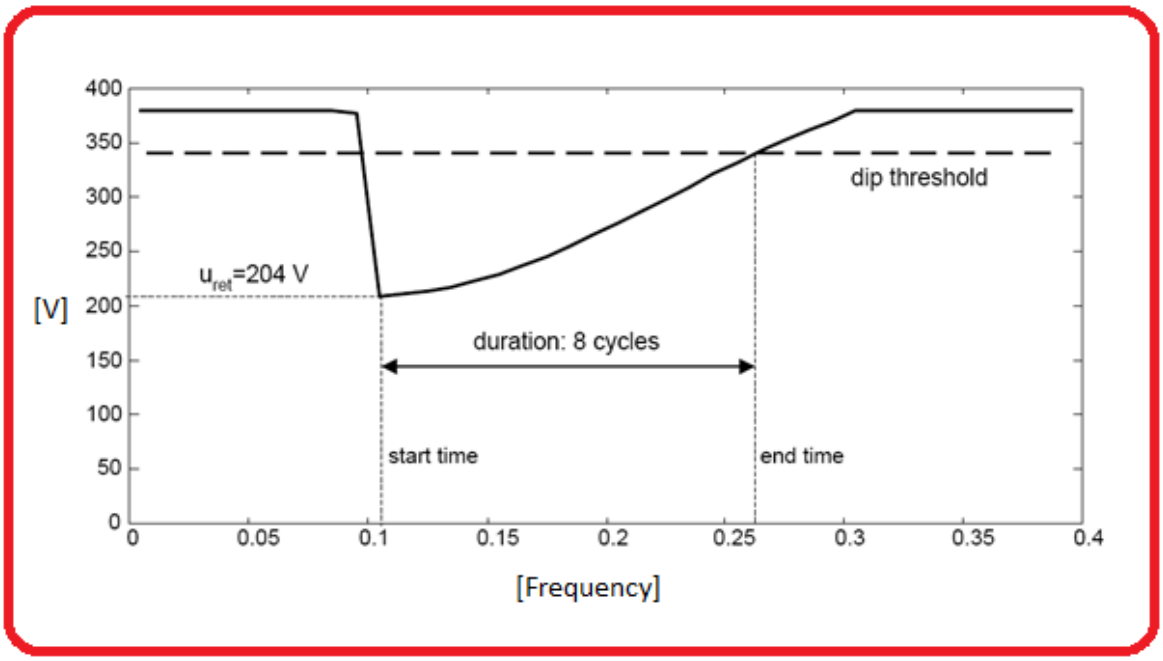

Figure 4.5: Graphical representation of dip voltage attributes [24].

4.3.2 Electrode-to-Bath Voltage

The measurement of the electrode-to-bath voltages in a SAF is affected by the induced voltage errors in the measuring leads, emanating from the high currents flowing in the secondary circuit. *Fig. 4.6* shows the researcher's proposal in the form of diagrams on how these measurements can be approximated.

The AC current (I), induces a voltage in the measuring leads, **VBCN**, as shown in *Fig. 4.7*, resulting in a passage of electromagnetic flux through area **A**. The measured voltage, E_{VN}, will be different from E_{VN}' (actual voltage) by an induced error voltage as expressed by *Bretthauer and Timm* equation [9]:

$$E_{M1} - E_{DE} = \mu \,.\, b \,.\, f \,.\, log_e\,[1 = +(1+\frac{a}{r})] \,.\, I \qquad (4.1)$$

Where; μ - *is the magnetic permeability of the medium.*

f - *alternating current frequency.*

The voltage E_{VN} is typically 180 V and error percentages of approximately 12% are possible [9].

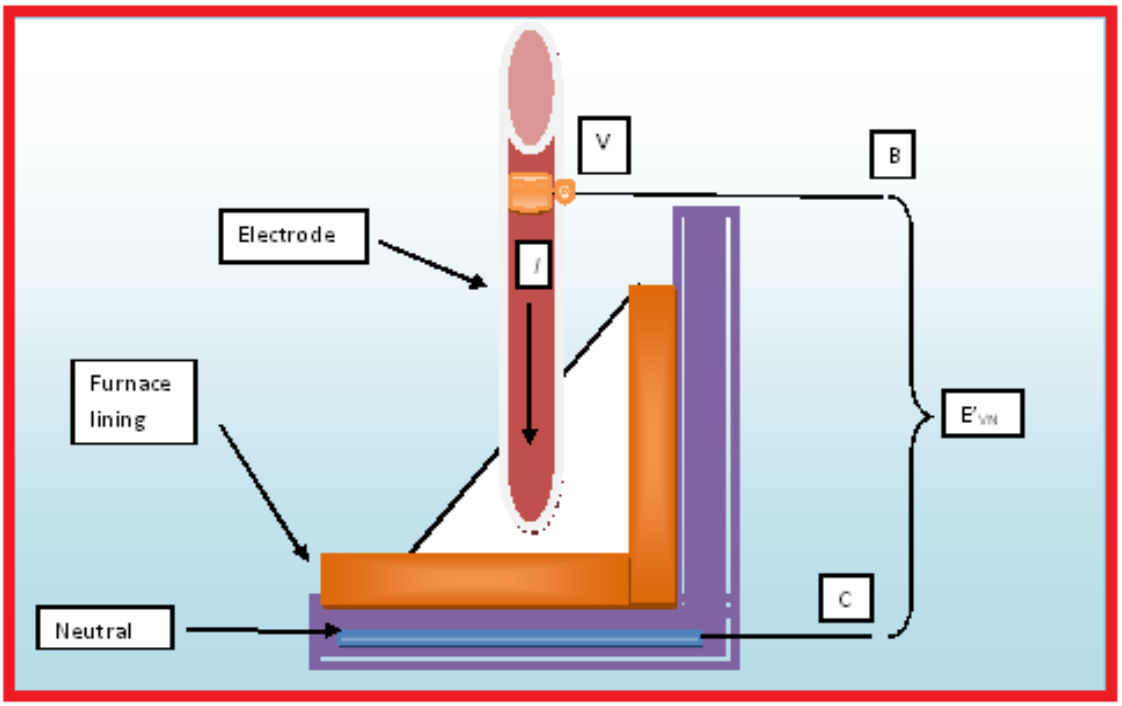

Figure 4.6: Measurement of the electrode-to-bath voltage.

- **Calculation of induced voltages of a typical 65 MVA SAF.**

Given Data:

Electrode current, I = 100 KA

a/r = 2

b = 3m

f = 50Hz

μ_o (for air) is assumed as 4 π x 10^{-7} V.s/A.m

Induced voltage is:

$$V_{induced} = 4 \times 110^{-7} \times 3 \times 50 \times log_e[1+2] \times 100 \times 10^3$$

$$= 20.71V$$

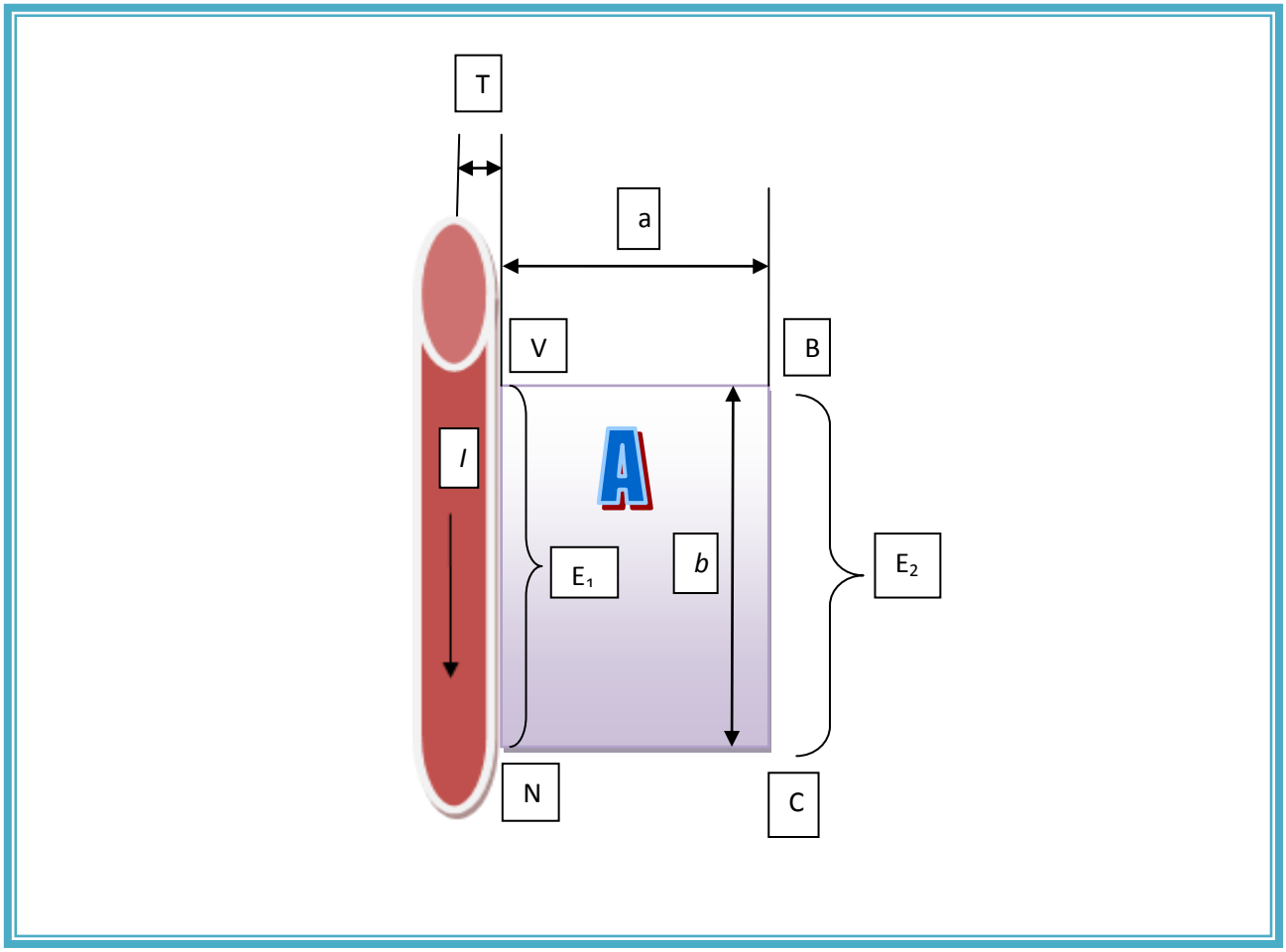

Figure 4.7: Equivalent representation of the electrode-to-bath voltage measurement.

The induced errors of the electrode-to-bath voltage measurement can be compensated by a technique based on the examination of the mutual inductance relationships in a three-conductor system as shown in the researcher's proposed diagram in *Fig. 4.8*.

The measurement of the electrode-to-bath voltage can be divided into two terms, namely the correct voltage, E_{10} and an error term, E_{OM}, which are proportional to the currents flowing in the circuit. Since the mutual inductances, $L_{3M,\,12}$ and $L_{1M,\,23}$ are based on the geometry of the furnace and the measuring system, they are considered constant for calculation purposes, but they have to be measured. If the values of the mutual inductances are known and the current and voltage parameters measured, then a suitable compensation circuit can be constructed so as to convert the erroneous measurements of electrode-to-bath voltages to accurate values.

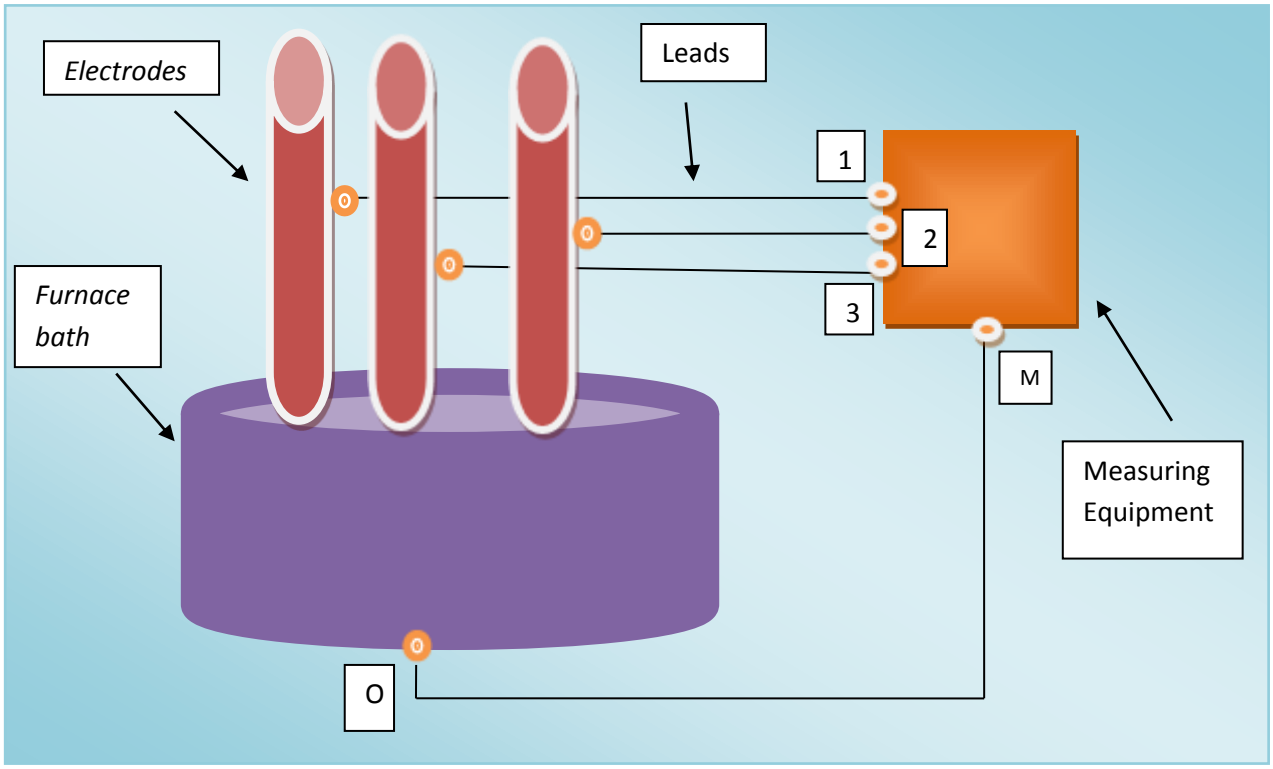

Figure 4.8: Technique to compensate induced errors in electrode-to-bath voltages measurement on the leads.

4.3.2.1 Error Minimization in Electrode-to-Bath Voltages Measurements

In arc furnaces, the geometry of the secondary circuit is almost symmetrical, such that the inductances L_1, L_2 and L_3 can be approximated equal. These inductances can be approximated equally by bringing out the leads from the furnace in a symmetrical manner. This is achieved by connecting the neutral to the carbon lining in the middle bottom part of the furnace. The researcher proposed a diagram in *Fig. 4.9,* were three separate leads are brought from the neutral connection to the sides of the furnace shell adjacent to each electrode. The leads are connected to the electrode before being taken away from the furnace as twisted-pair cables.

The arrangement in *Fig. 4.9* facilitates symmetry of the measuring loop for each electrode and also same size as other loops. The two reasons for this arrangement are:

- The central region of the SAF (commonly used in ferrochrome) is generally a “dead” region in which each phase constitutes a separate bath.

- The use of neutral connections under each electrode results in the measurement being less sensitive to changes in the position of the floating neutral connection, which affects the magnitudes of the inductances L_1, L_2 and L_3.

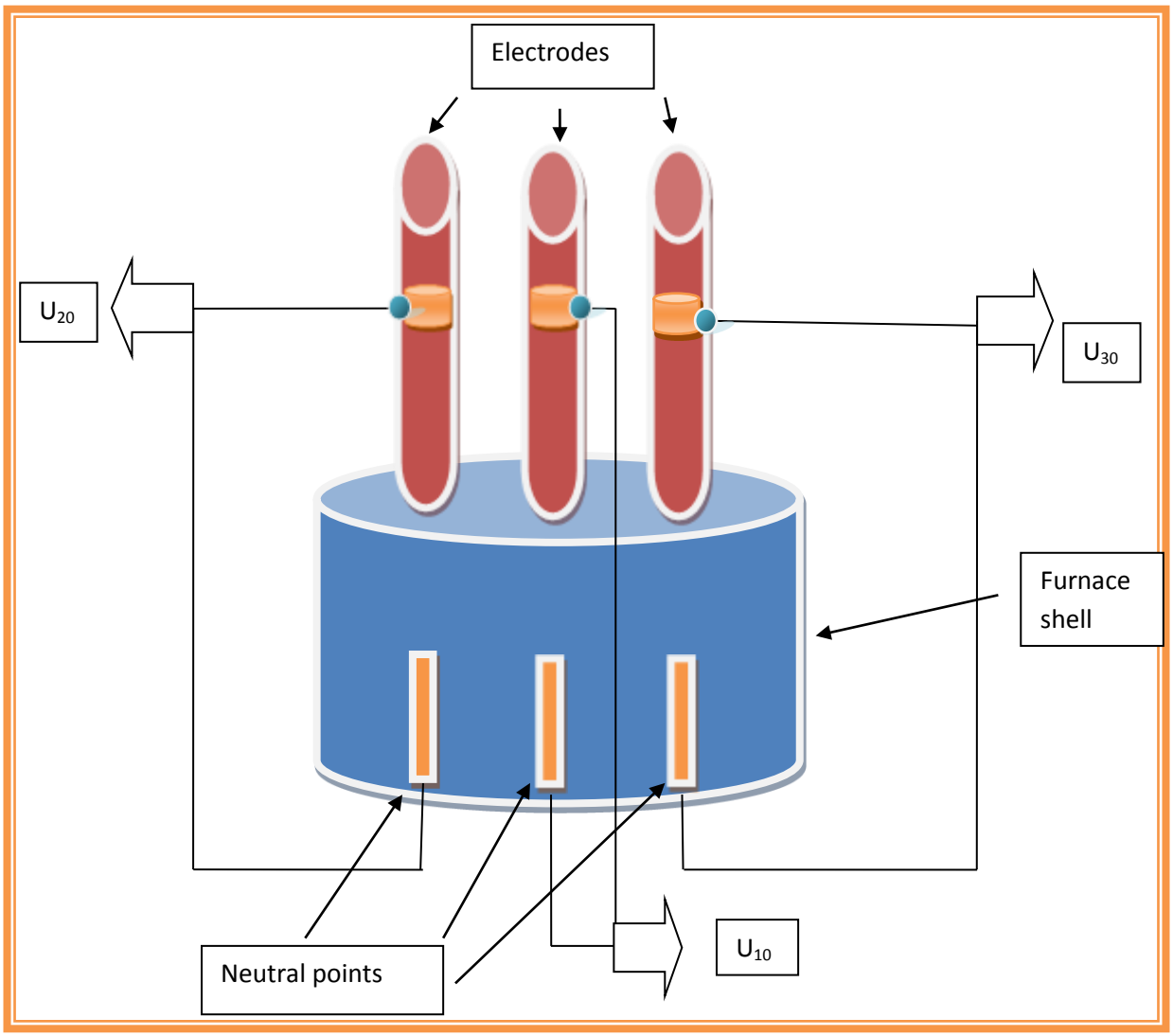

Figure 4.9: Schematic diagram showing the wiring arrangement for the electrode-to-bath measurements.

This system of arrangement *(Fig. 4.9)* has a major advantage especially when it is used on large ferrochromium furnaces, in that it provides accurate measurements of the voltages.

4.4. Temperature Measurement

In order to ensure normal operation of a SAF, two aspects need to be monitored. Firstly, electrodes' temperature should be maintained to minimise the effects of electrode breakages and this can be achieved by using pairs of thermocouples between the electrodes to record the temperature values.

Secondly, the furnace shell cooling water temperature has to be maintained low at accepted levels by controlled digital thermometers that incorporates temperature sensors.

4.4.1 Electrodes Temperature Profiles

During the operation of arc furnaces, the bottom part of the electrode is gradually consumed, resulting in the column being gradually moved to lower positions. Thus, from time to time new material has to be added to the top of the structure, either by screwing the nipples of the existing and the new graphite segments or by introducing raw paste inside the steel casing.

In instances were new segments had to be added, pairs of thermocouples are pasted to them in opposite diagonal positions so as to allow the determination of temperature both in the centre and in the outer part of the furnace [21]. Thermocouples are connected to signal converters to linearization and calibration the output signals as shown in *Fig. 4.10*.

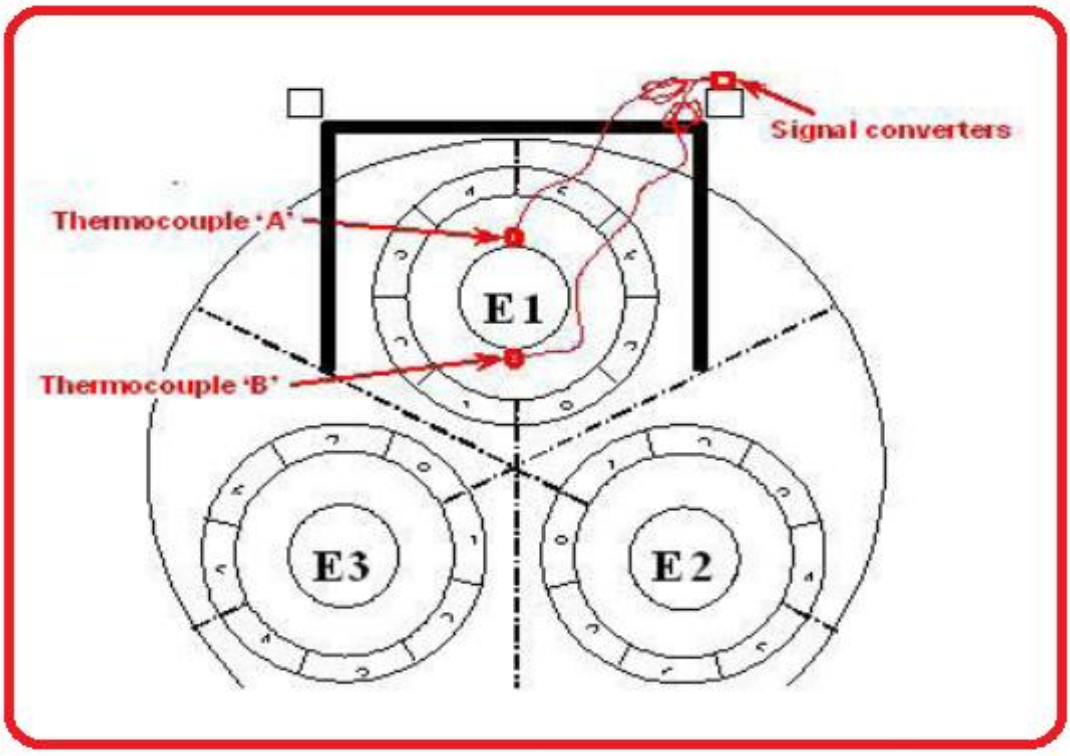

Figure 4.10: Location of thermocouple pairs in electrode, E1 [21].

The converters provide isolation between the measurement system, data logging and the processing system by means of optocouplers. The temperature profiles along the column can be obtained by distributing several pairs of thermocouples at different heights.

As the electrode consumption continues, the thermocouples move down, hence the electrical contact with the measurement system must be guaranteed. The measured temperature curves of the electrodes as a function of the height reveal the variation of the height in time as shown in *Fig. 4.11* shows.

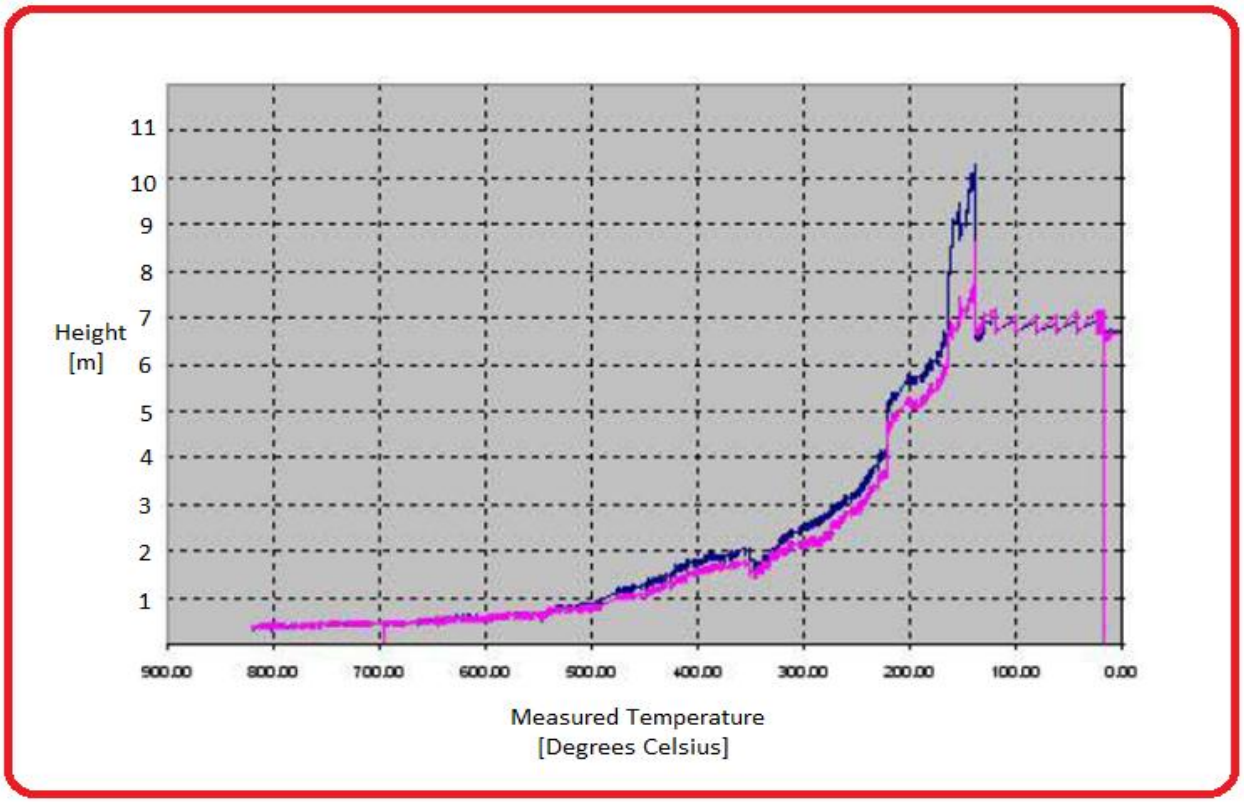

Figure 4.11: Simulation of the measured temperature vs column height of an electrode [21].

The measured temperature characteristic curves show that the height (distance to the combustion area) has a strong influence in the temperature, with variations due to the working conditions. The temperature limit of the thermocouples can be easily identified and it determines the minimum height at which measurements can be performed. The thermocouples used must be able to work at least until the contact plates area is reached. The major disadvantage of this type of measurement is that as thermocouples move down due to electrode consumption, they may lose the electrical contact with the measurement system.

4.4.2 Infrared (IR) Temperature Measurement

The furnace transformer consists of the primary terminal (high voltage side) and the secondary terminal (arc furnaces side) and it steps down the voltage with high current as

shown in *Fig. 4.12*. The primary and secondary sides of the transformers are connected in the delta / delta configuration.

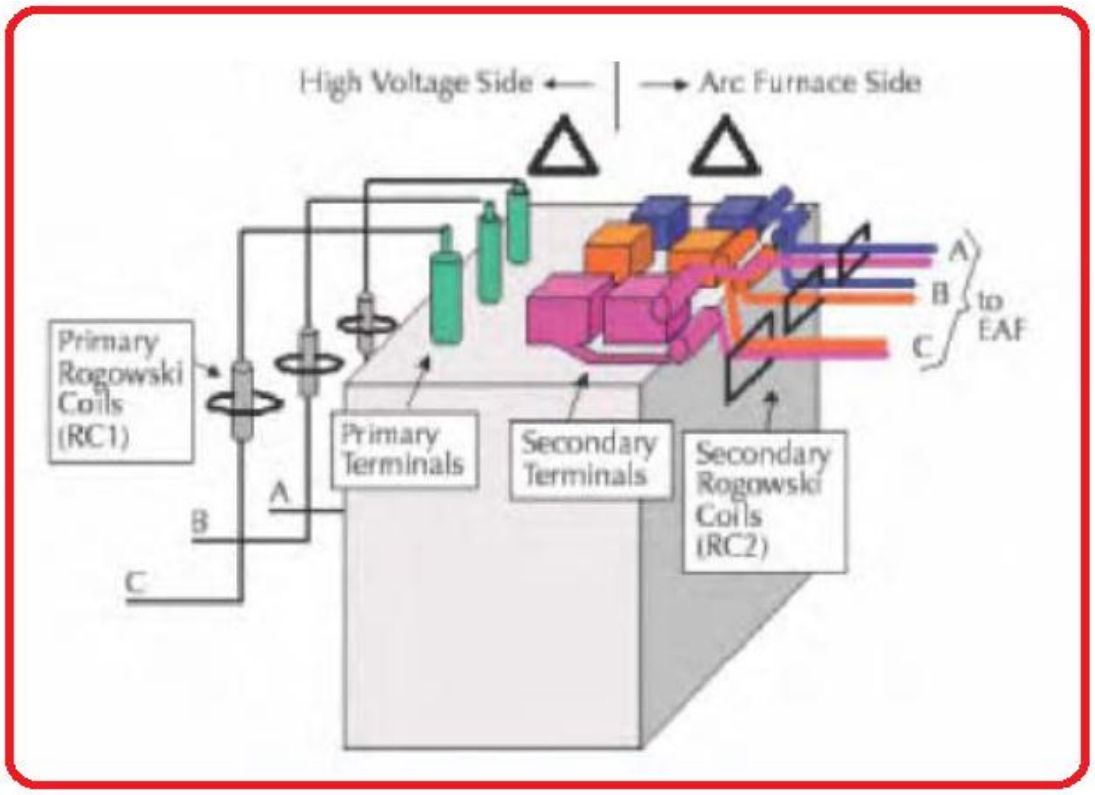

Figure 4.12: Diagram showing the various parts of the SAF transformer [22].

Its temperature is an important parameter that needs to be measured and controlled to prevent breaking down due to over storage heat in the cooling system. Infrared (IR) temperature measurement technique with no destruction measured temperature field, quick response and high stability is employed in many applications [21]. The temperatures of the bus bars in the primary and secondary side of the furnace transformer can be measured by the IR thermometer and have its image captured by the VarioCAM head, as shown in *Fig. 4.13*.

4.5 Major Shortfalls of the Existing Measurement Techniques

Though the previously discussed measurement techniques can be relied on for electro-thermal variable measurements, they present a number of constraints that include the follows:

- In temperature measurements, the thermocouples move down due to electrode consumption, they may lose electrical contact with the measurement system, resulting in no measurements.

- The on-line measurement of the electrode resistance is difficult to achieve with the desired accuracy.
- The phase shift introduced by the instrument transformers and the sampling devices can give rise to significant effect on overall system measurement accuracy.

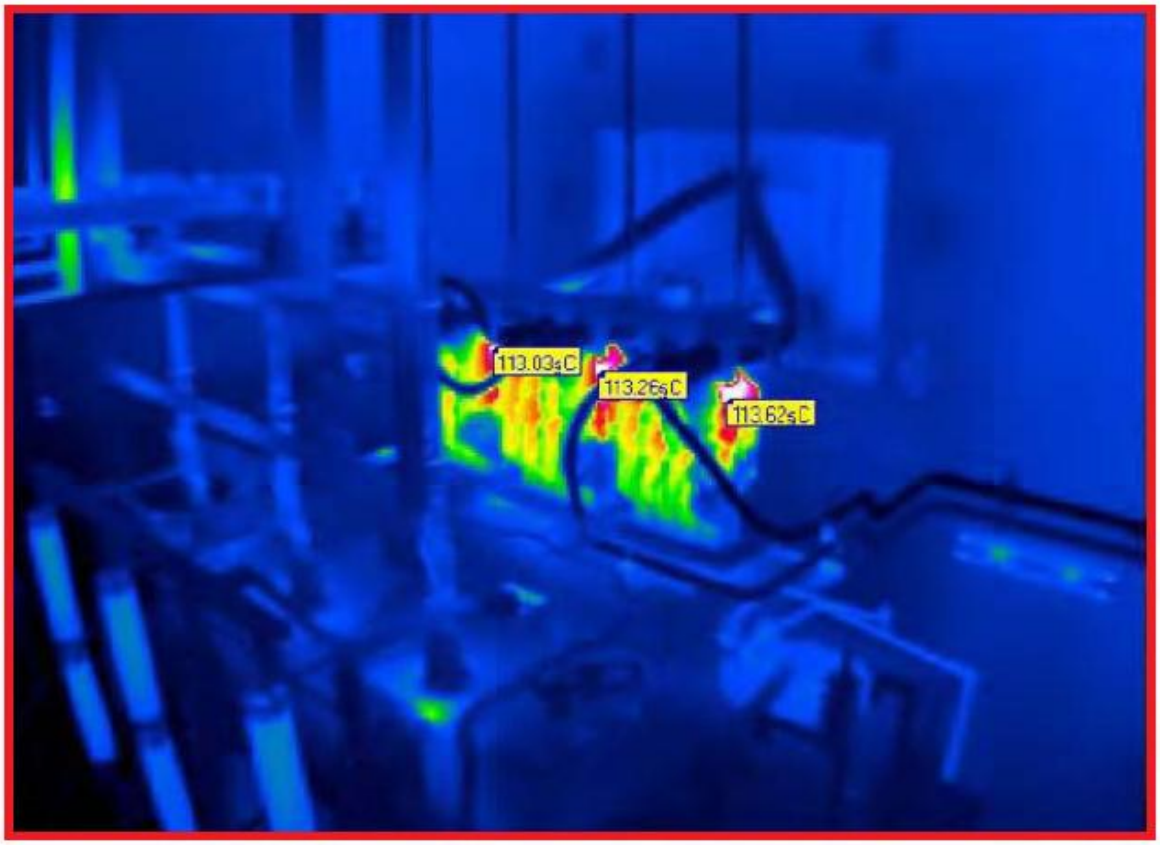

Figure 4.13: Simulation of the IR temperature image (ε=0.8) of bus bars at a given load captured by VarioCAM head at Wonderkop Chrome Processing Plant.

4.6 Amalgamated Variable Parameters Measurement (AVPM) System

The shortfalls presented by the existing measurement techniques electro-thermal variables in arc furnaces can be mitigated by a proposed Amalgamated Variable Parameter Measurement (AVPM) system as shown in Appendix C. The proposed AVPM system is a technique that combines different measurement philosophies into multifunctional measuring equipment for both the primary and secondary sides of the furnace. It incorporates measurement and control of a number of electro-thermal variable parameters that include harmonic, temperature, voltage, current, electrode resistance and others.

It is made up of a number of modular blocks that include:

- Current and Voltage Calculation Module (CVCM)
- Power Calculation Module (PCM)
- IR Temperature Calculation Module (ITCM)
- Electrode – to – bath voltage Calculation Module (ECM)
- Electrode Resistance, Impedance Calculation Module (ERICM)
- Waveform Calculation Module (WCM)

4.7 Conclusion

This chapter presented a detailed description of the various measurement techniques available in the measurement of variable parameters in submerged arc furnaces. These include the typical PQ measuring system, PQ analyser, voltage and current, electrode-to-bath voltage for the primary side. Temperature measurements that include the electrodes profiles, the IR temperature measurement of the furnace transformers were also presented. The amalgamated variable parameter measurement (AVPM) system was proposed as the best alternative to some of the shortfalls experienced in electro-thermal variable measurements in SAFs. The next chapter 5 will focus on the modeling and simulation of the electro-thermal variables based on the neural networks (NN).

CHAPTER FIVE

MODELLING OF SUBMERGED ARC FURNACE ELECTRO-THERMAL VARIABLES BASED ON THE NEURAL NETWORKS

5.1 Introduction

This chapter presents the modelling and simulation for SAFs using the back-propagation neural networks. An overview of the neural network model, architecture, and transfer functions will also be outlined and discussed. The design SAF NN model architecture and its defining neural network algorithm will be described. The design model will be simulated by the Neural Network Fitting Tool GUI, using the real furnace plant samples. The design SAF NN model's output power will then be compared with the real furnace plant power output to verify its performance.

5.2 Neural Networks (NN)

An Artificial Neural Network (ANN) is an information processing paradigm that is inspired by the way biological nervous systems, such as the brain, process information. The first artificial neuron model was proposed in 1943 by the neurophysiologist Warren McCulloch and the logician Walter Pits [27].

The key element of the ANN's paradigm is the novel structure of the information processing system. It is composed of a large number of highly interconnected processing elements (neurons) working in unison to solve specific problems. An ANN is configured for a specific application, such as pattern recognition or data classification, through a learning process. Learning in biological systems involves adjustments to the synaptic connections that exist between the neurons [28]. Neural networks, with their remarkable ability to derive meaning from complicated or imprecise data, can be used to extract patterns and detect trends that are too complex to be noticed by either humans or other computer techniques.

5.2.1 Back-propagation

One of the most commonly used supervised neural network model is the back-propagation network that uses the back-propagation learning algorithm [7]. It was first described by Paul Werbos in 1974, but it was not until 1986, through the work of David E. Rumelhart, Geoffrey

E. Hinton and Ronald J. Williams [29], that it gained recognition, which led to a "renaissance" in the field of artificial neural network research.

The back-propagation is described as the generalization of the Widrow-Hoff learning rule of multiple-layer networks and nonlinear differentiable transfer functions. Back-propagation can also be defined as the manner in which the gradient is computed for nonlinear multilayer networks [29]. There are a number of variations on the basic algorithm that are based on other standard optimization techniques, such as the Conjugate gradient and Newton methods.

The input vectors and the corresponding target vectors are used to train a network until it can approximate a function, associate input vectors with specific output vectors, or classify input vectors in an appropriate way as defined by users [29]. In back-propagation, networks with biases, a sigmoid layer, and a linear output layer are capable of approximating any function with a finite number of discontinuities. When the back-propagation network is properly trained it tends to give reasonable answers of the inputs that they have never seen.

In general, the back-propagation algorithm looks for the minimum of the error function in weight space using the method of gradient descent. Since this method requires computation of the gradient of the error function at each iteration step, the continuity and differentiability of the error functions must be guaranteed. Obviously, the kind of activation function other than the step function should be used. The back propagation neural network is essentially a network of simple processing elements working together to produce a complex output. The combination of weights which minimizes the error function is considered to be a solution of the learning problem.

5.2.2 Feed-forward Artificial Neural Network

Feed-forward artificial neural networks do not have feedback (loops), they allow signals to travel one way only that is from input to output as shown in *Fig. 5.1*. The output of any layer does not affect that same layer, thus they tend to be straight forward networks that associate inputs with outputs. They find their applications in pattern recognition [30].

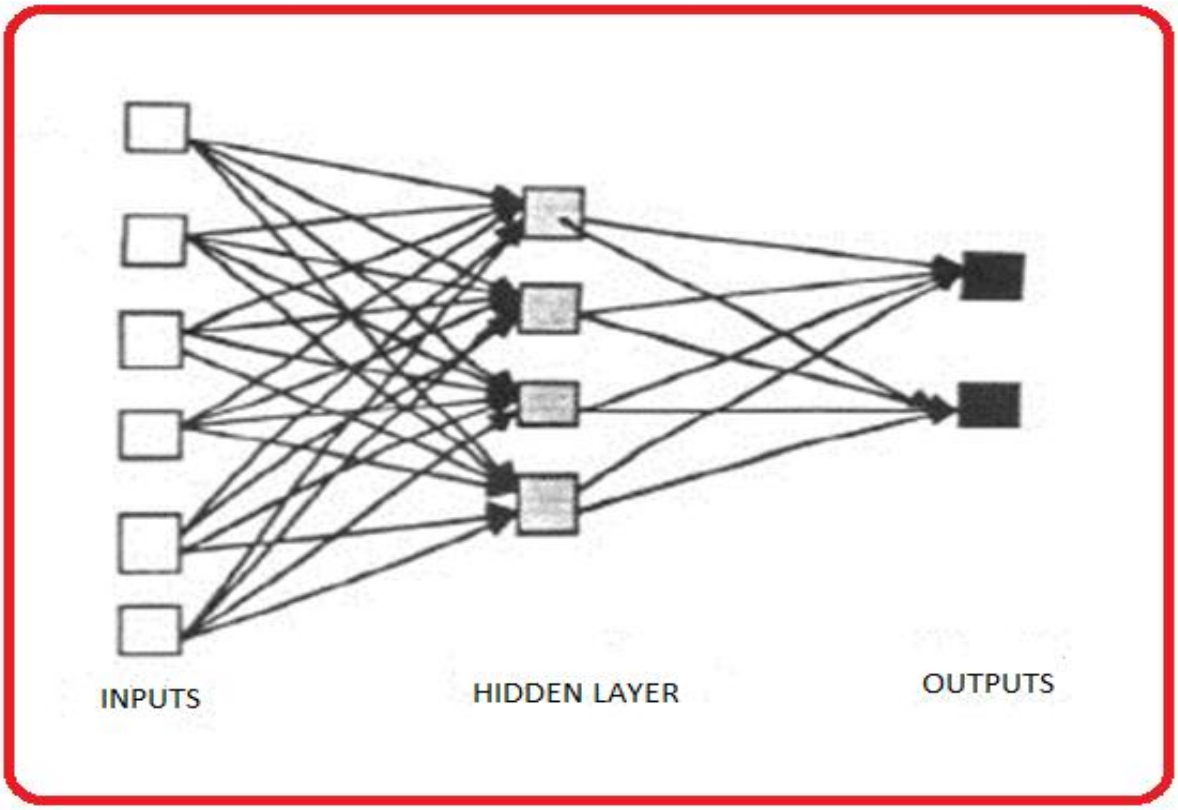

Figure 5.1: Simple feed-forward network diagram [30].

5.3 Neural Model

An elementary neuron model [30] consists of the inputs and the general neutron, with P_R inputs, weighted with an appropriate, ω is shown in *Fig. 5.2*. It output is defined by equation:

$$a = f(W.p + b) \qquad (5.1)$$

The neuron consists of a bias, *b*, which is summed with the weighted inputs to form the net input, *n*. This sum, *n*, is the argument of the transfer function, *f*, which can be defined by the user as follows:

$$n = w.p + b \qquad (5.2)$$

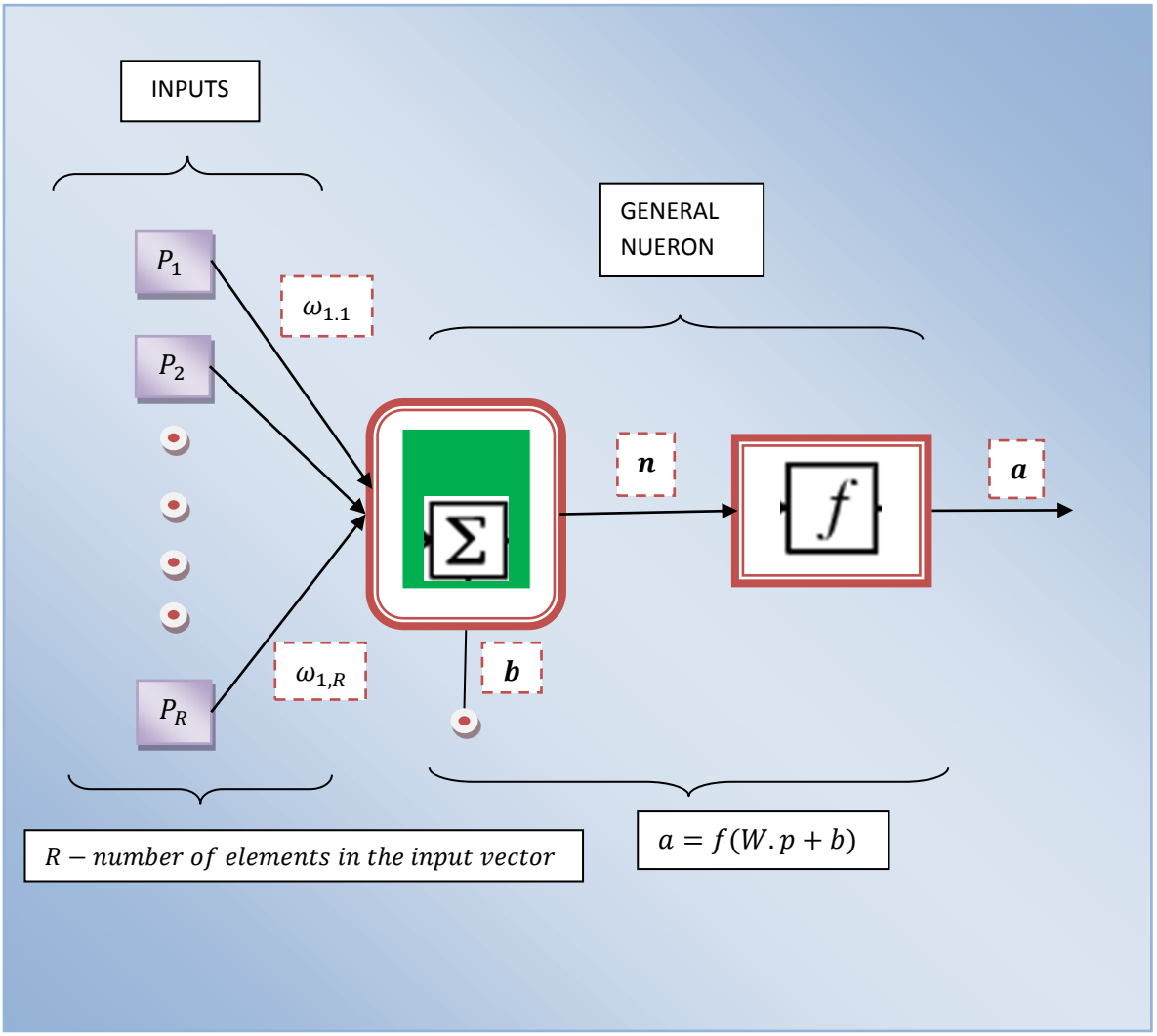

Figure 5.2: Basic elementary neural model diagram [30].

5.4 Transfer Functions

Majority of neural networks pass the output of their layers through activation or transfer functions, which scale the output of the neural network into proper ranges [31]. There are three types of transfer functions that are implemented in back-propagation multilayer neural networks namely, the log-sigmoid transfer function (*logsig*.), tan-sigmoid transfer function (*tansig*.) and the linear transfer function (*purelin*.). Different activation functions can be implemented for each layer of the neural network, but usually the sigmoid activation function is favoured for the last section as it is the default choice of the feed-forward layer class.

5.4.1 Log-sigmoid transfer function *(logsig.)*

The function, *logsig*, takes the input which can have any value between plus and minus infinity, and squashes the output into the range 0 to 1, as shown in *Fig. 5.3*.

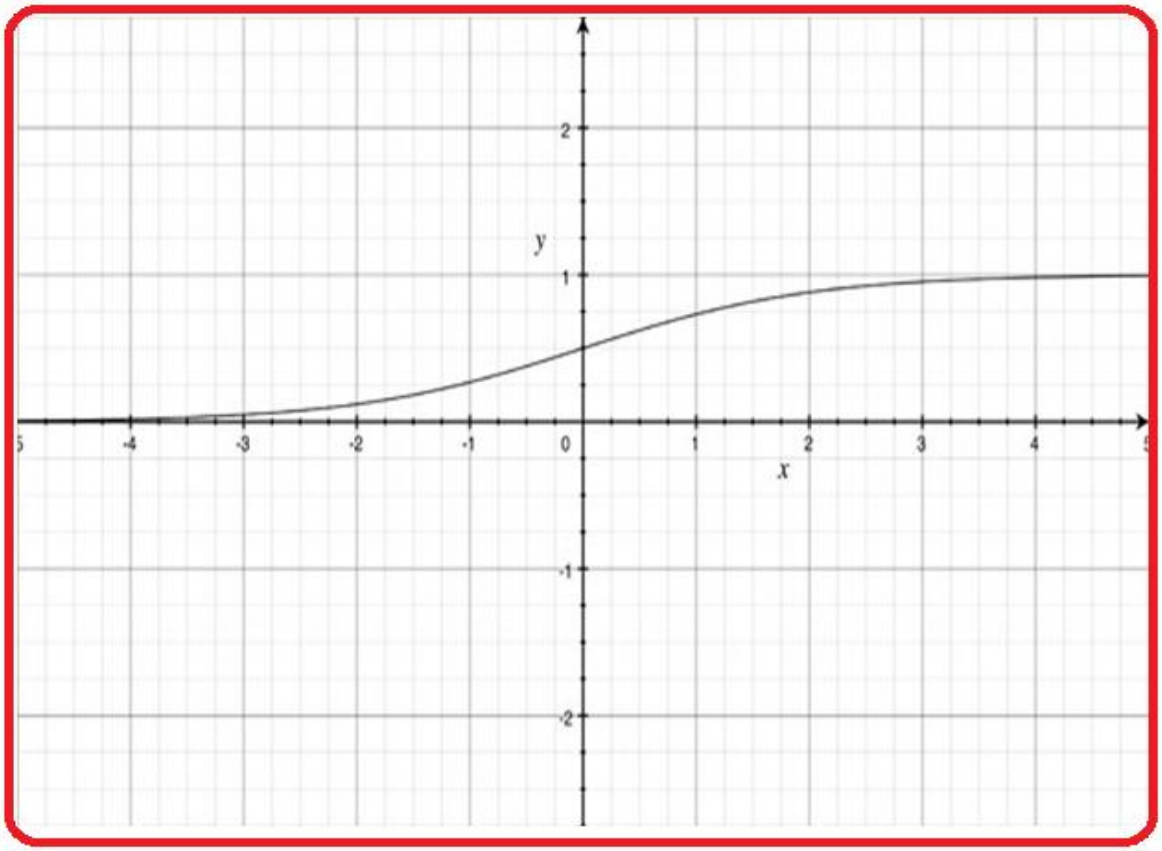

Figure 5.3: Log-sigmoid transfer function.

The sigmoid function is defined by the mathematical expression:

$$f(x) = \frac{1}{1 + e^{-x}} \tag{5.3}$$

and the log-sigmoid transfer function:

$$a = logsig(n) \tag{5.4}$$

The log-sigmoid transfer function is commonly finds its application in back-propagation networks, as it is differentiable.

5.4.2 Tan-sigmoid transfer function *(tansig.)*

Alternatively, multilayer networks can use the tan-sigmoid transfer function (*tansig.)* as shown in *Fig. 5.4.*

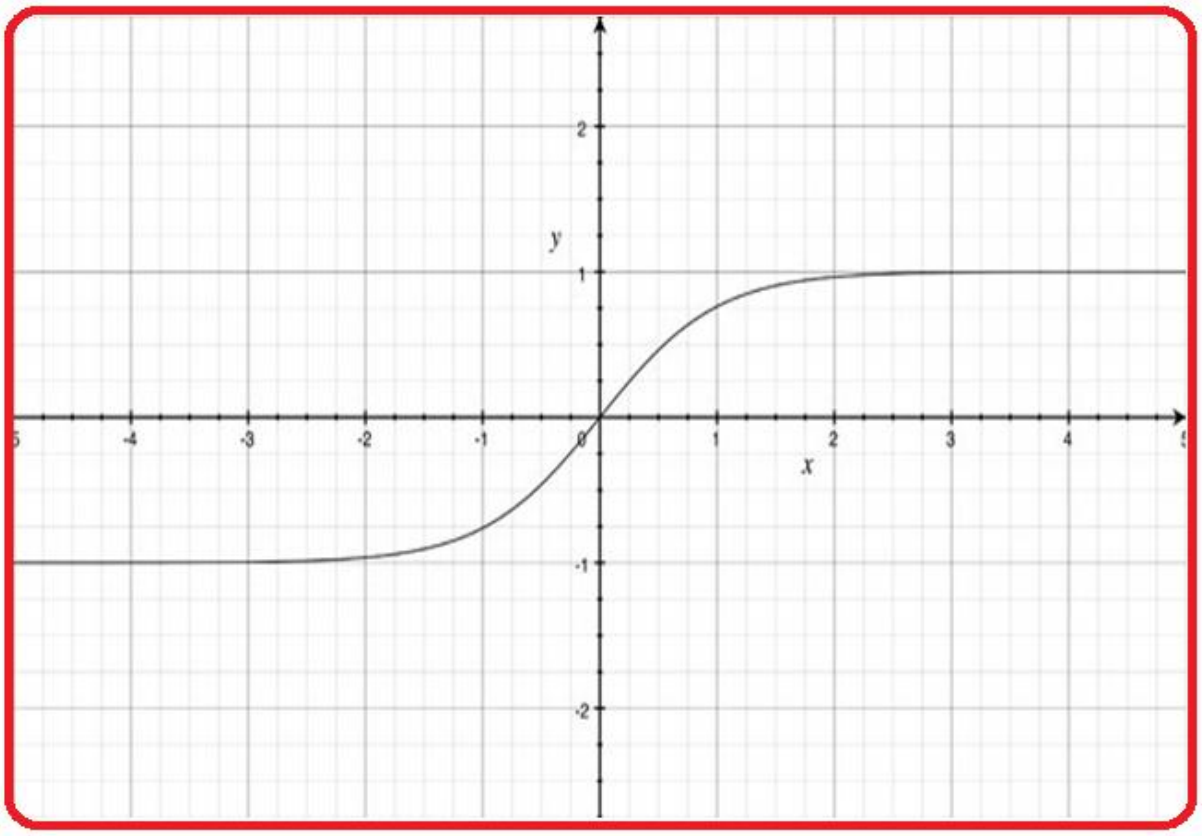

Figure 5.4: Tan-sigmoid transfer function.

The TANH function is defined by the mathematical expression:

$$f(x) = \frac{e^{2x} - 1}{e^{2x} + 1} \qquad (5.5)$$

and the tan-sigmoid transfer function:

$$a = tansig(n) \qquad (5.6)$$

5.4.3 Linear transfer function *(purelin.)*

The linear transfer function (*purelin.)* is used in back-propagation networks and is shown in *Fig. 5.5*.

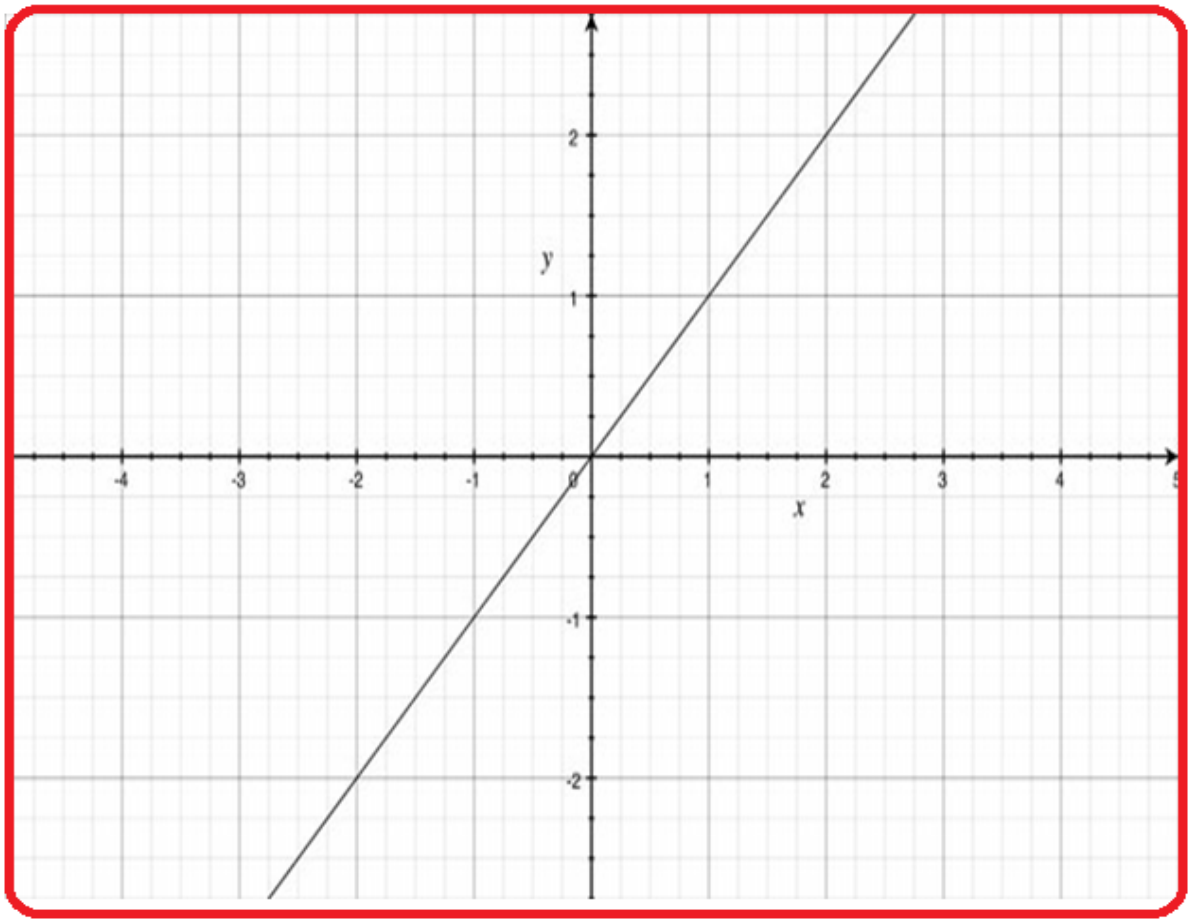

Figure 5.5: Purelin transfer function.

The linear function is defined by the mathematical expression [31]:

$$f(x) = x \tag{5.7}$$

and the linear transfer function:

$$a = purelin(n) \tag{5.8}$$

5.5 Design Submerged Arc Furnace Neural Network Model (SAF NN)

The design SAF NN model consists of two-layer feed-forward network with the default tan-sigmoid transfer function in the hidden layer with 20 neurons and the linear transfer function in the output layer. The units in each layer receive their inputs units of a layer directly below and send their output to units in a layer directly above the unit. There are no connections within a layer and the inputs (N_i) are fed into the layer of the hidden units (N_h). The input units are merely "fan out", meaning that no processing taking place in them.

The activation of the hidden layer within design model is a function, F_i, of the weighted inputs plus a bias as defined by the following equation:

$$y_k\,(t+1) = \mathcal{F}_k\big(s_k(t)\big) = \mathcal{F}_k\left(\sum_j w_{jk}\,(t) y_j(t) + \theta_k(t)\right) \qquad (5.9)$$

As reiterated earlier on in Chapter 4, three important electro-thermal variables, that include the voltage, resistance and temperature, are chosen as the inputs to the SAF NN model. The outputs of the hidden units are distributed to the next layers (N_h), until the last layer of the hidden units, which are again fed into a layer of outputs units (N_o) as shown in *Fig. 5.6.* The output variable is power which is optimized by the PSO algorithm as discussed in chapter 6.

5.6 Implementation and Simulation

5.6.1 Assembling the Training Data

A set of electro-thermal variables (resistance, voltage and temperature and power) define the input vector and the target vector of the 45 MW SAF Wonderkop Chrome Processing Plant (WCP) are assembled as shown in Appendix A. The input vector **(*inputvalue*)** is defined by *3 x 120* matrix *representing 120 of 3* which comprise of voltage, resistance and temperature. The target vector **(*power*)** is defined by a *1 x 120* matrix *representing 120 of 1* which comprise of output power variables. Both the input and the target vectors comprise of 120 samples each. It should be noted that only the first *84* samples are used to train neural network and the last *36* samples are used to validate and test the trained neural network.

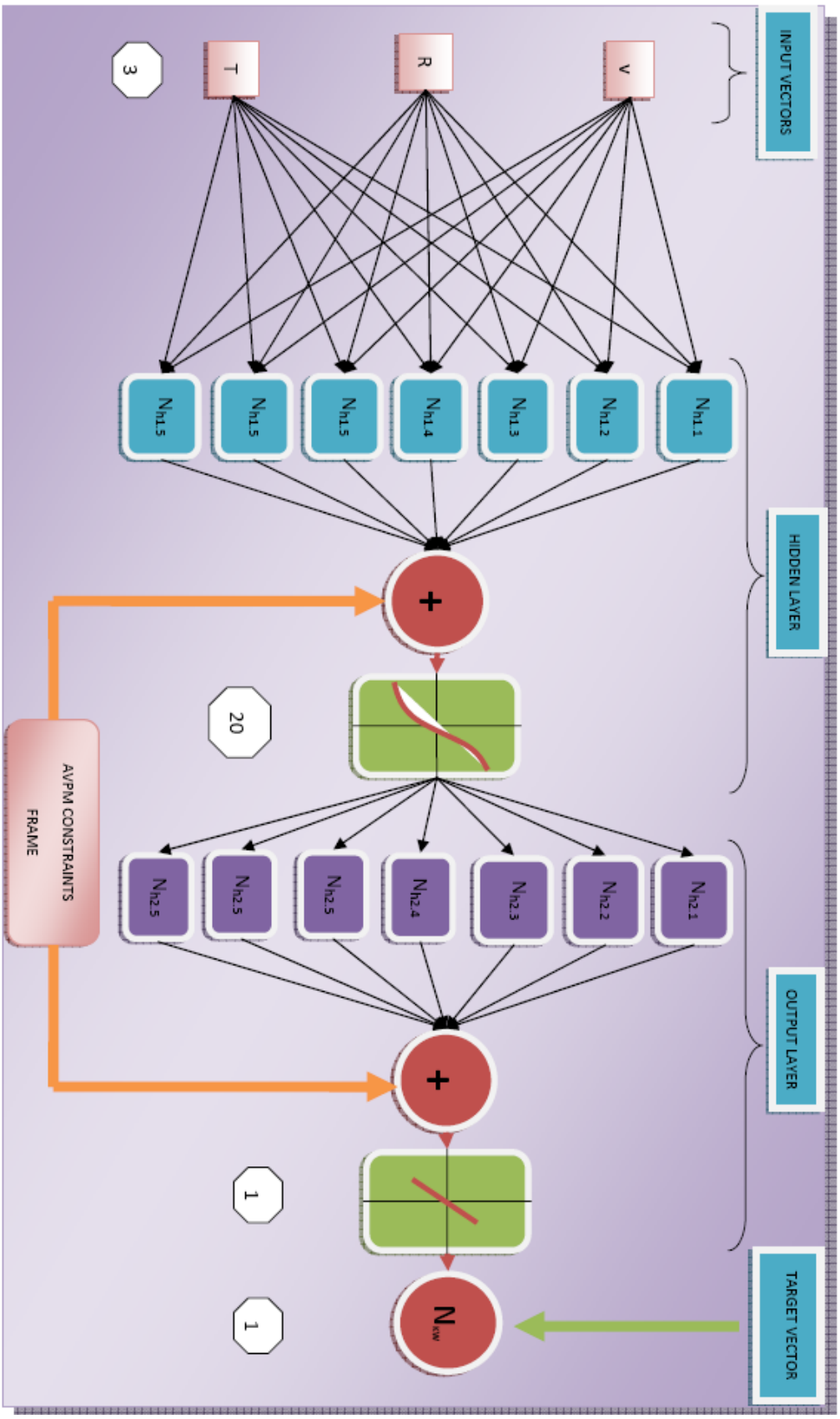

Figure 5.6: Design SAF Neural Network (NN) Model Structural Layout.

5.6.2 Simulation

The design SAF NN model structure is composed of *20* neurons in one hidden layer and one output neuron since there is only one target value associated with three input vectors. The Neural Network Fitting Tool GUI is utilized for simulating the SAF NN model and is activated by the command, "*nftool"*, which displays the Neural Network Fitting Tool window as shown in *Fig. 5.7.*

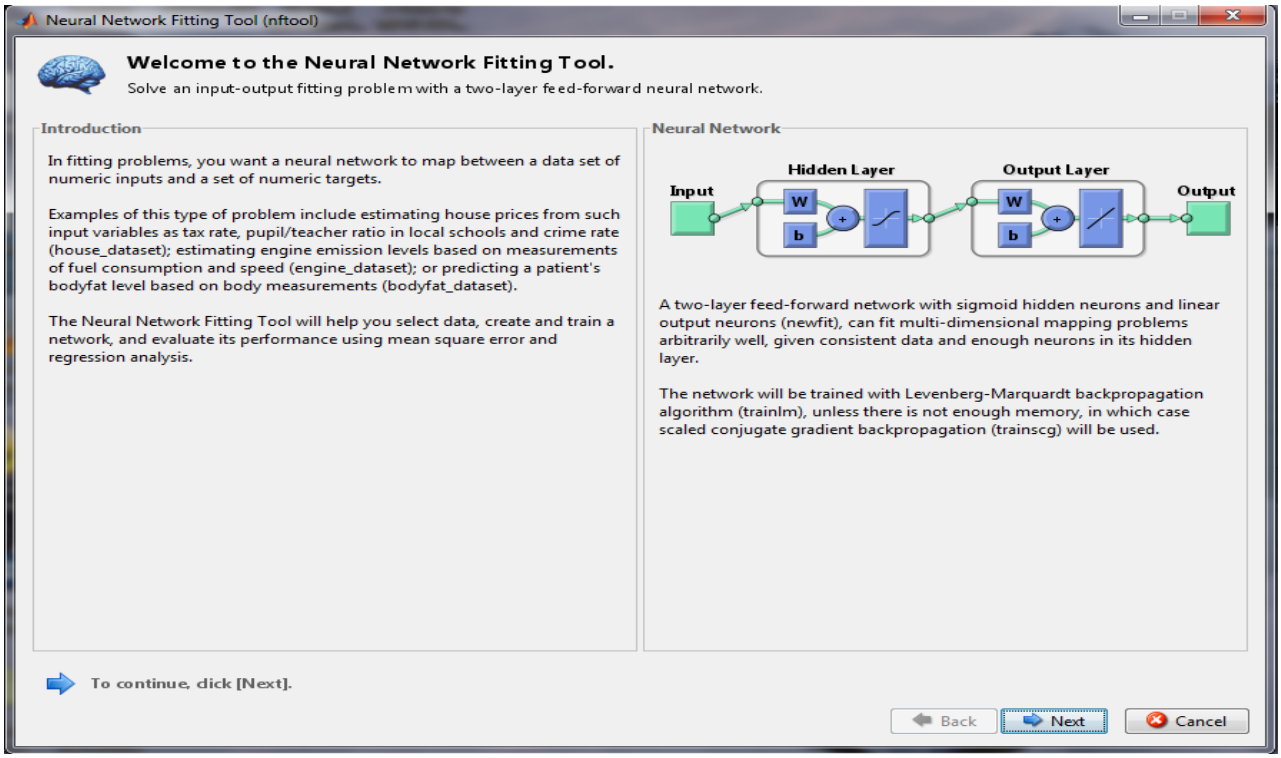

Figure 5.7: Neural Network Fitting Tool window.

Activating the "*next tab*" opens the *Select Data* window where the data is selected and set as the *"inputvalue"* and *"power"* and loaded as shown in *Fig. 5.8.* The validation and test data window is displayed when the "next" tab is activated with each test data set at *15%* of the original data as shown in *Fig. 5.9.*

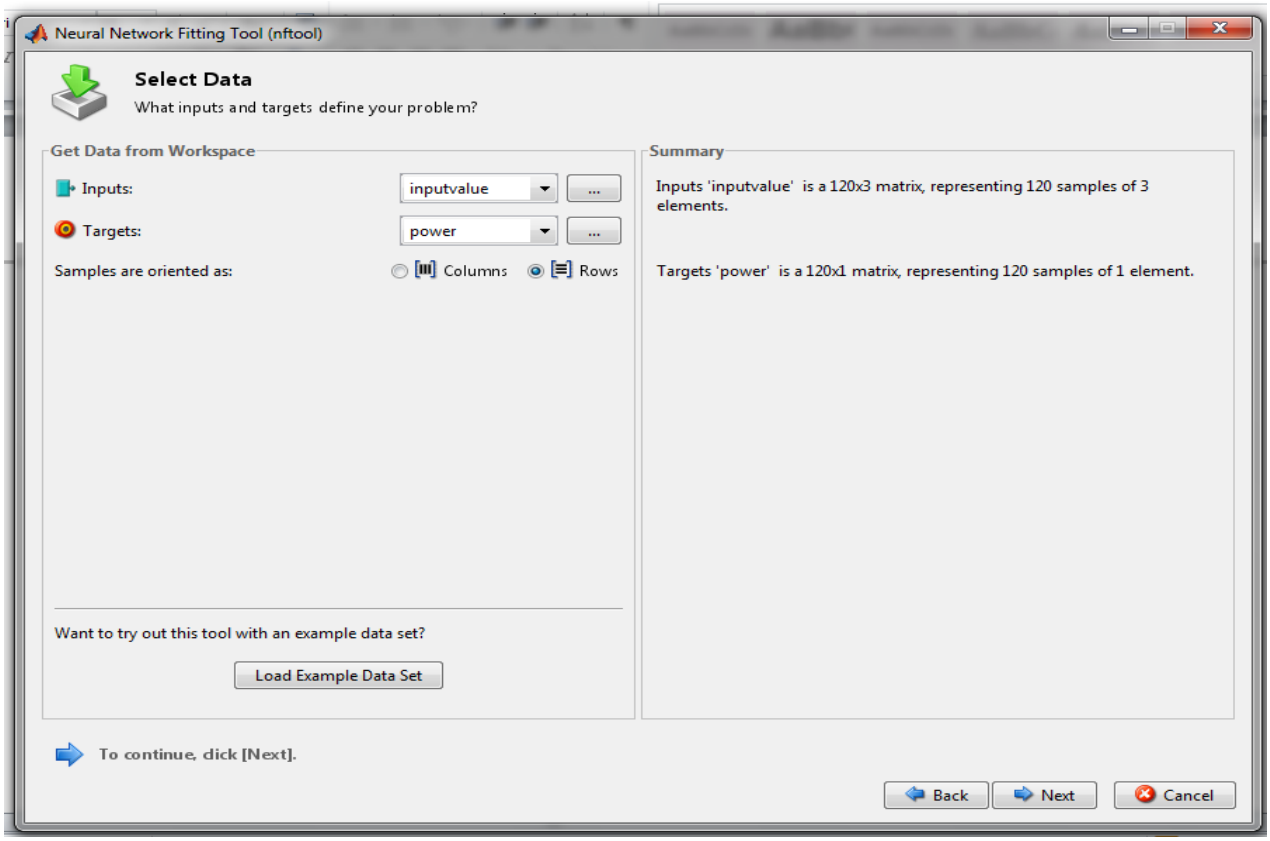

Figure 5.8: Select Data window.

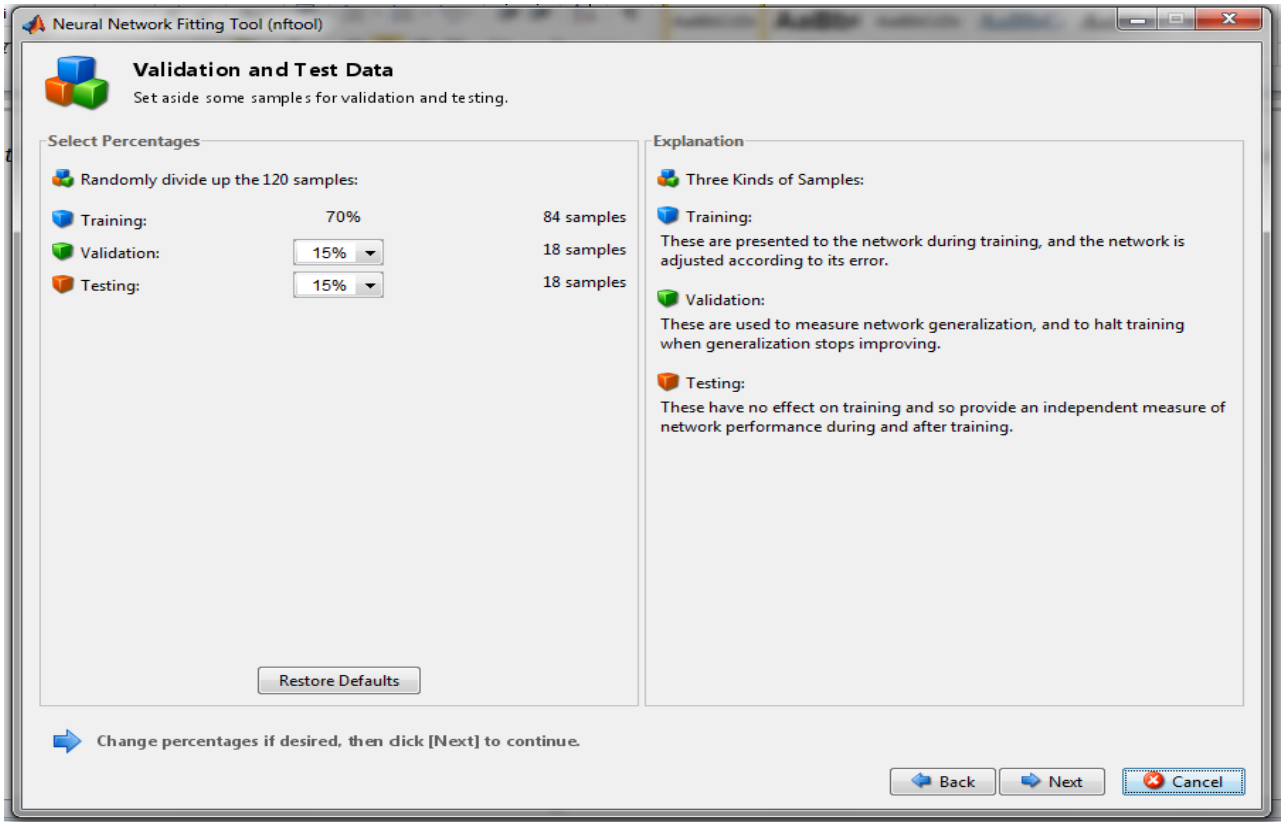

Figure 5.9: Validation and Test Data window.

The activation of the *"next"* tab in *Fig. 5.9* facilitates the adjustment of the number of neuron to *20* on the network size as shown in *Fig 5.10*.

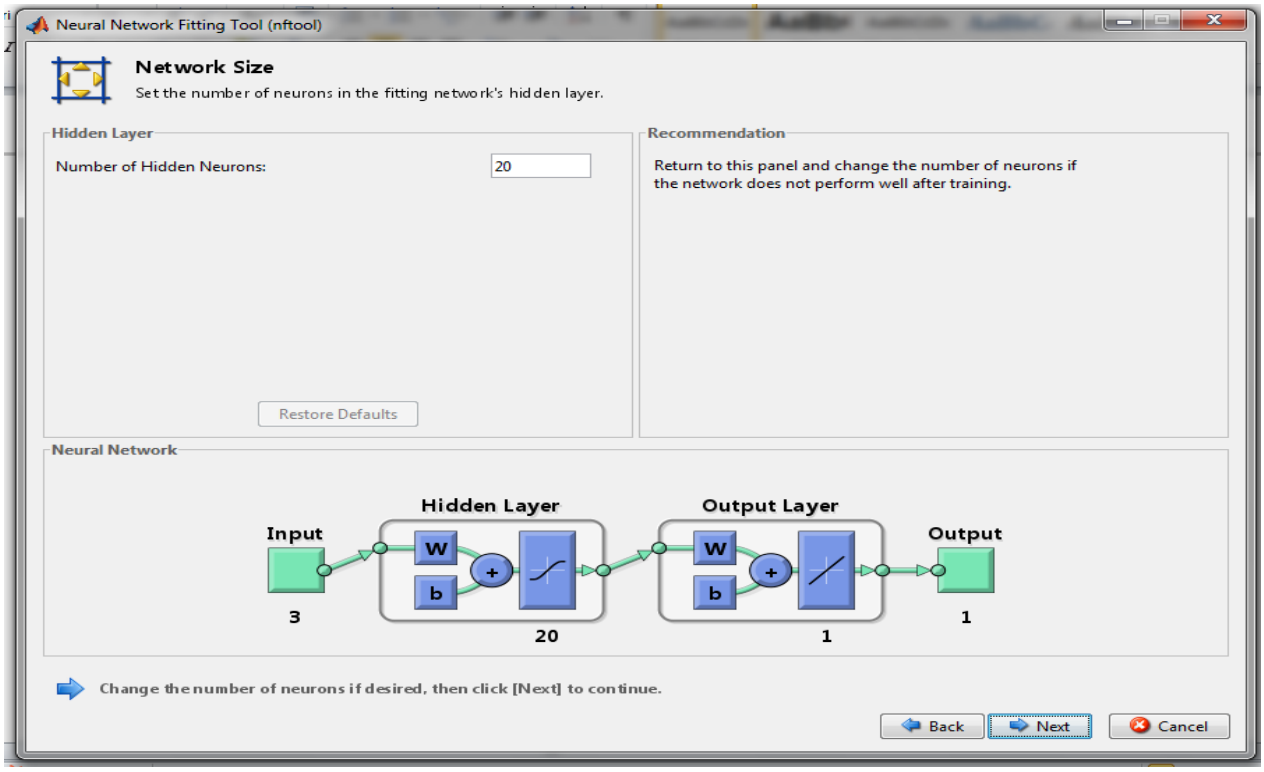

Figure 5.10: Network Size Data window.

The design SAF NN model is trained using the Levenberg-Marquardt back-propagation with *84* samples being used for training, *18* for validation and the other 18 for testing as shown in *Fig. 5.11* after the activation of the "*next*" tab on the Network Size window in *Fig.5.10*. The training of both the input and the target vectors is done over a number of times and it automatically stops when generalization stops improving. The stopping of training is reflected by an increase in the mean square error of the validation samples, thus, indicating achievement of the best results.

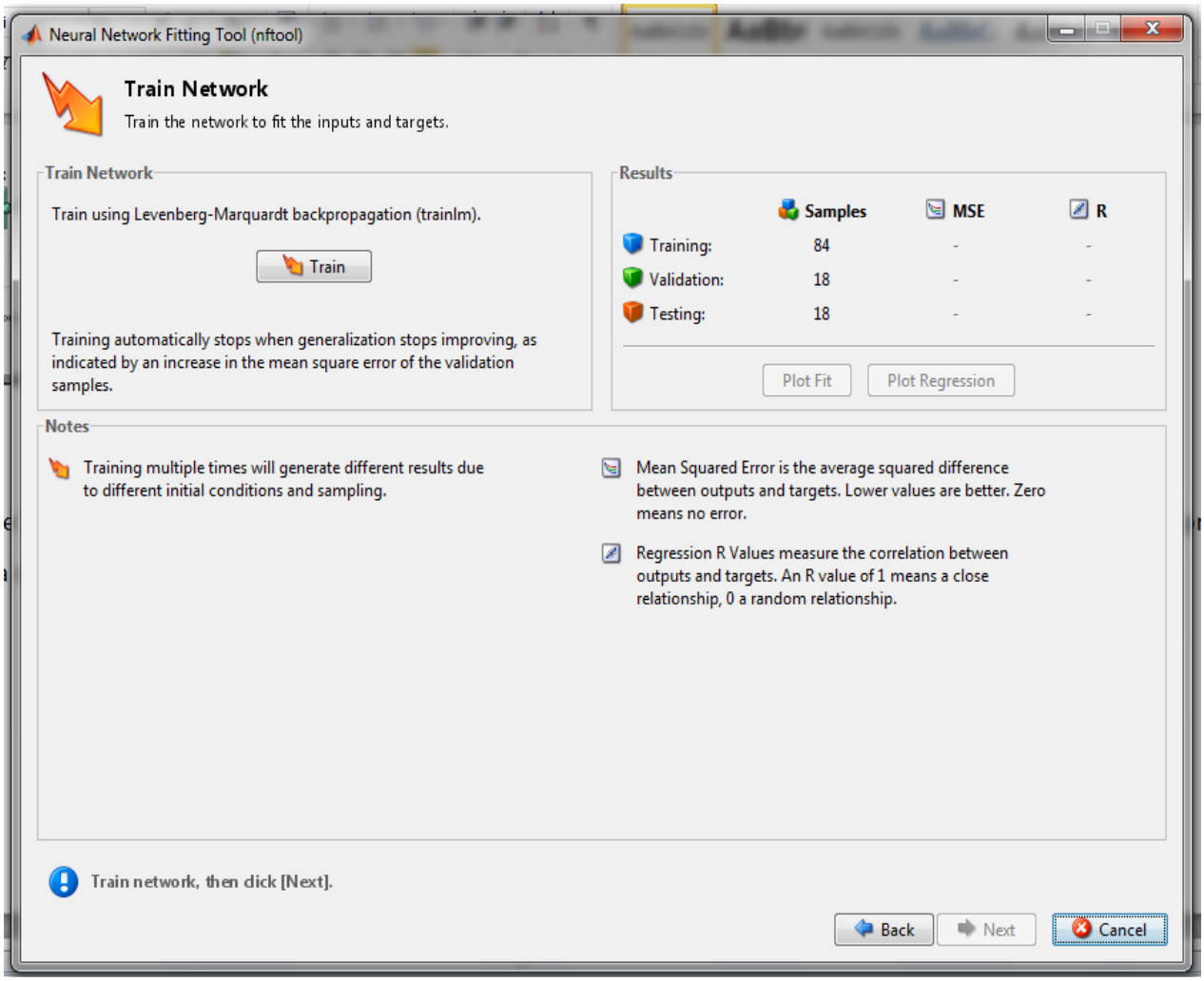

Figure 5.11: Train Network Data window.

The training stopped when the validation error increased for *6* iterations, which occurred at *10* iterations as shown in *Fig.5.12*. The performance *(plotperform)* characteristics depicted in *Fig. 5.13* shows that the result of the plot of the training errors, validation errors and test errors is reasonable because of the following considerations:

- The final mean-square is small.
- The test set error and the validation set error has similar characteristics.
- There is no significant over fitting that has occurred by iteration *4*, where the best validation performance occurs).

The training state characteristics generated during the SAF NN model training is shown in *Fig. 5.14*.

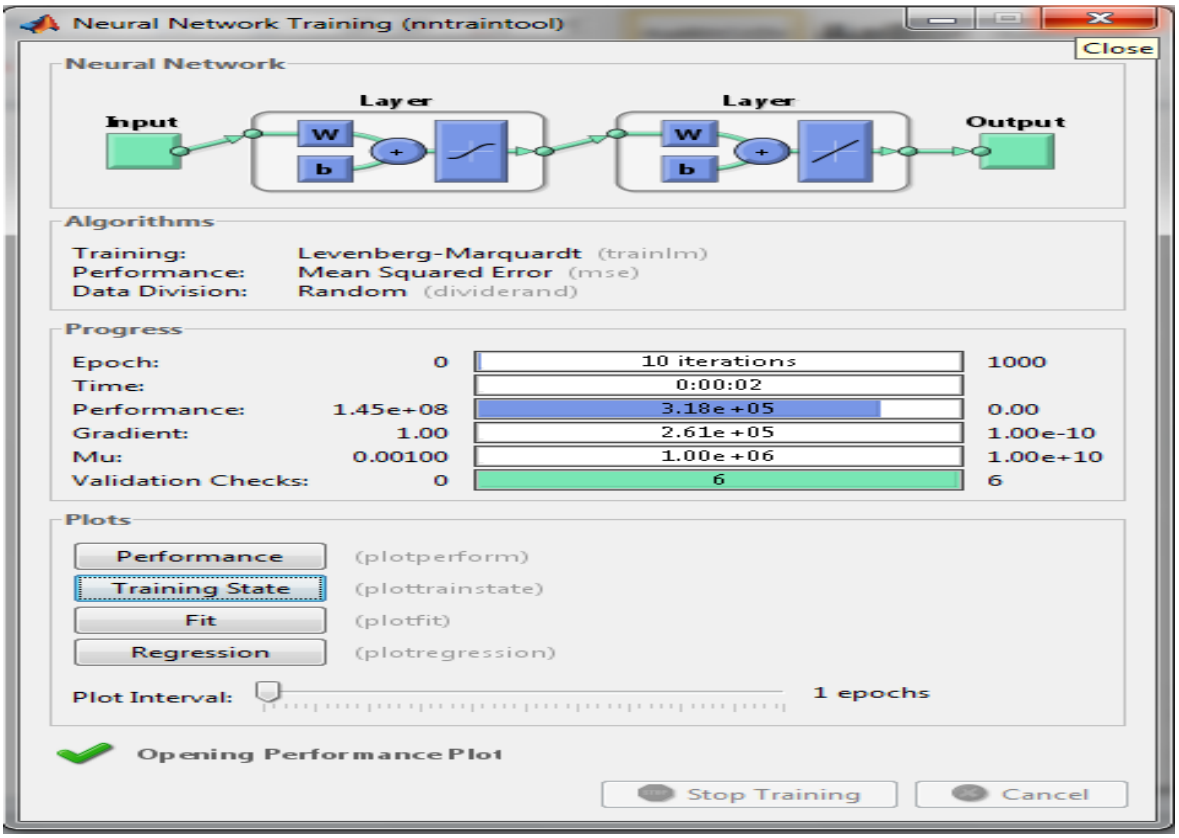

Figure 5.12: Neural Network Training window.

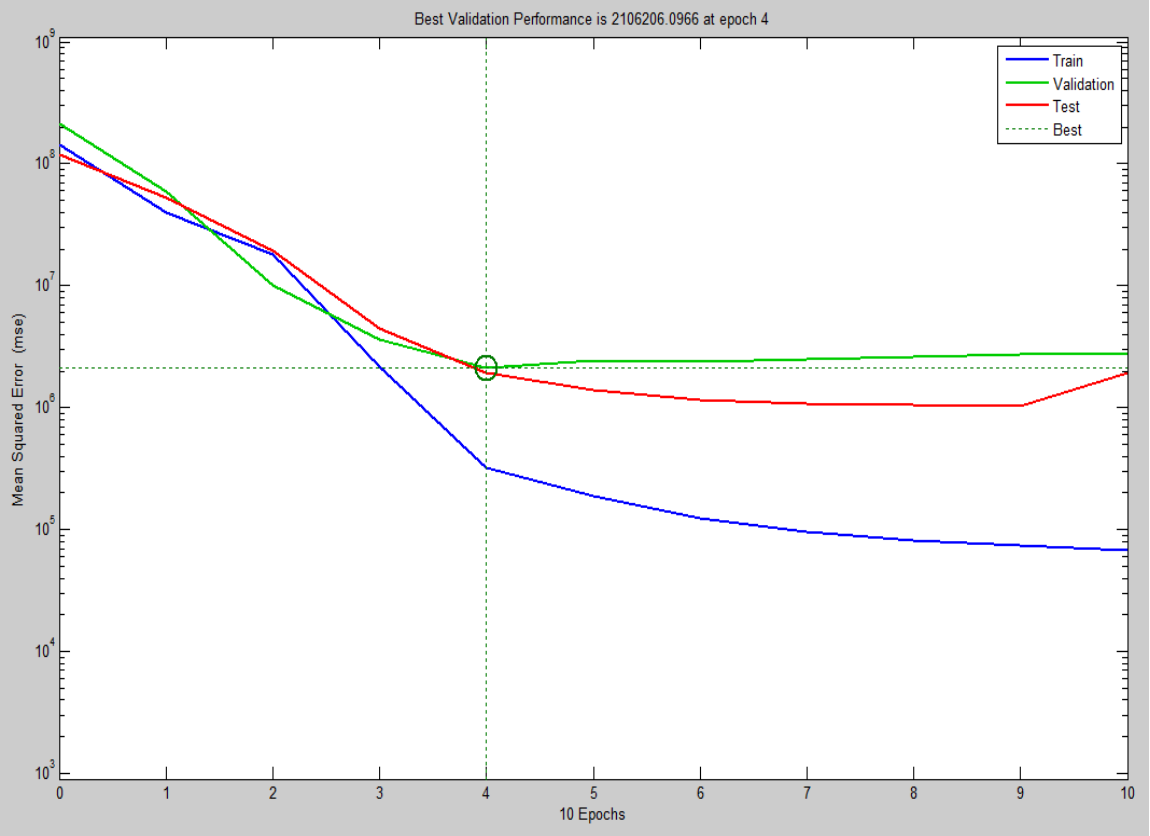

Figure 5.13: Simulated Best Validation Performance characteristics.

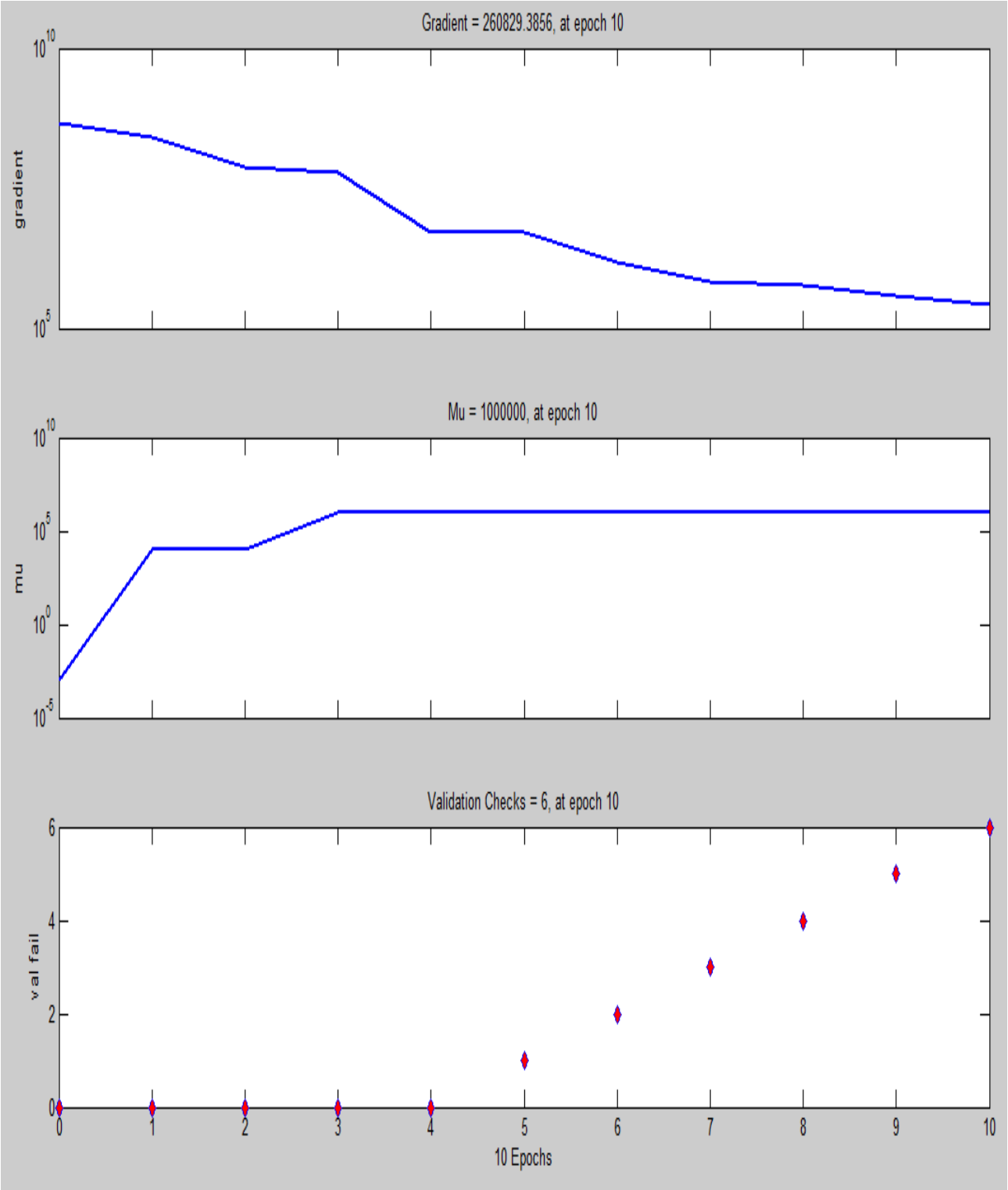

Figure 5.14: Simulated Training State Characteristics.

The linear regression performance between the SAF NN model outputs and the corresponding target (power) shows that the model's output tracks the targets very well for training and validation, with the R-value being over *0.98* for the total response as shown in *Fig. 5.15.*

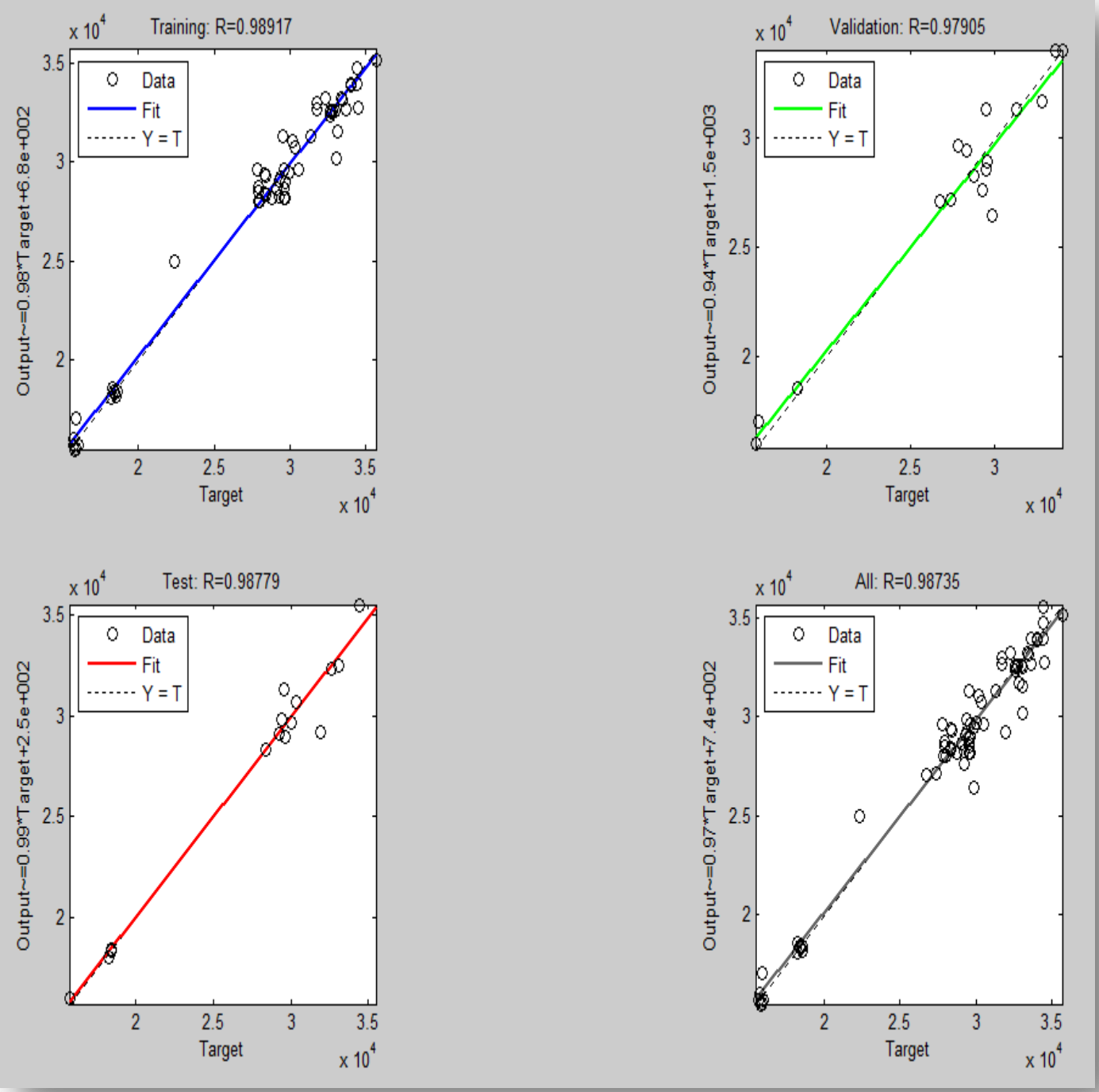

Figure 5.15: Simulated Regression Characteristics.

5.6.3 Comparison of the SAF NN model output vs Real Furnace Data Samples

The output of the SAF NN model and the real data reveals some similarities that can be used to judge the model's performance as compared to the real plant. The real furnace power

samples and the trained SAF NN model output are shown in the plot characteristics in *Fig. 5.16.* From *Fig. 5.16*, it can be seen that The trained SAF NN model output characteristics shows some similarities with the real furnace output, although the last *36* samples were not used for training the design model.

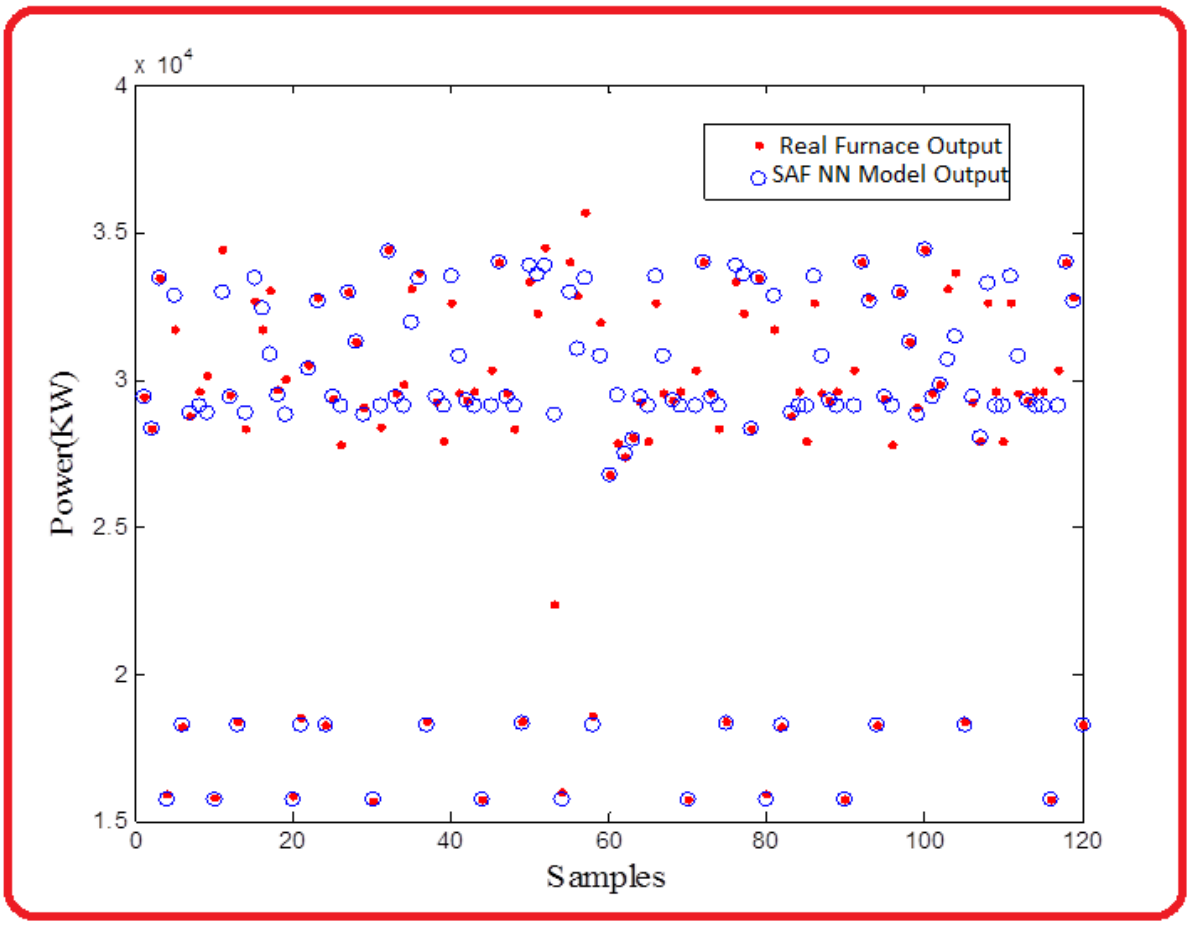

Figure 5.16: Comparison of the SAF NN model output versus real furnace output data (power).

5.6 Conclusion

This chapter presented the modelling and simulation for SAFs using the back-propagation neural networks. An overview of the neural network model, architecture, and transfer functions was outlined and discussed. The design SAF NN model architecture and its defining neural network algorithm were described. The design model was simulated by the Neural Network Fitting Tool GUI, using the real furnace plant samples. The design SAF NN model's output power was then be compared with the real furnace plant power output to verify its performance.

CHAPTER SIX

ENERGY OPTIMIZATION OF THREE - PHASE SUBMERGED ARC FURNACES

6.1 Introduction

To reduce the production costs, it is necessary to optimise the power or energy cost. In this chapter, we only focus on power as energy cost can be determined directly by power. The particle swarm optimization is used to optimize the power cost. Firstly, this chapter presents a brief introduction of the general concept of the particle swarm optimization and their paradigms. Secondly, the PSO based SAF NN optimization method is proposed and this method comprises the SAF NN model and the particle swarm optimizer. Neural network model of the SAF plant is used as the objective function as it is impossible to use the real SAF Plant. Finally, the optimization results will be tested using the real samples as the objective function is not the real plant.

6.2 Overview of Particle Swarm Optimization (PSO)

The particle swarm optimization (PSO) is originally attributed to Kennedy, Eberhart and Shi [32] [33] and was first intended for simulating social behavior [34] as a stylized representation of the movement of organisms in a bird flock or fish school as shown in *Fig. 6.1*.

PSO is regarded as a metaheuristic that makes few or no assumptions about the problem being optimized and can search very large spaces of candidate solutions. However, PSO is easy to use due to its simple mechanism and also does not use the gradient of the problem being optimized, meaning that they do not require the differentiation of the optimization problem as is required by classic optimization methods such as gradient descent and quasi-newton methods.

The problem of PSO optimization is of having a population of candidate solutions, dubbed particles, and moving these particles around in the search-space according to simple mathematical formulae over the particle's position and velocity. Each and every particle's movement will be influenced by its local best known position and also guided toward the best known positions in the search-space, which are then updated as better positions are found by

other particles. Thus, this is expected to move the swarm toward the best solutions. The social topology that is commonly used is the ring, in which each particle has just two neighbors, but there are far more [31]. The social topology is not necessarily fixed as it can be adaptive (SPSO, stochastic star, [35] TRIBES, [36] Cyber Swarm [37]).

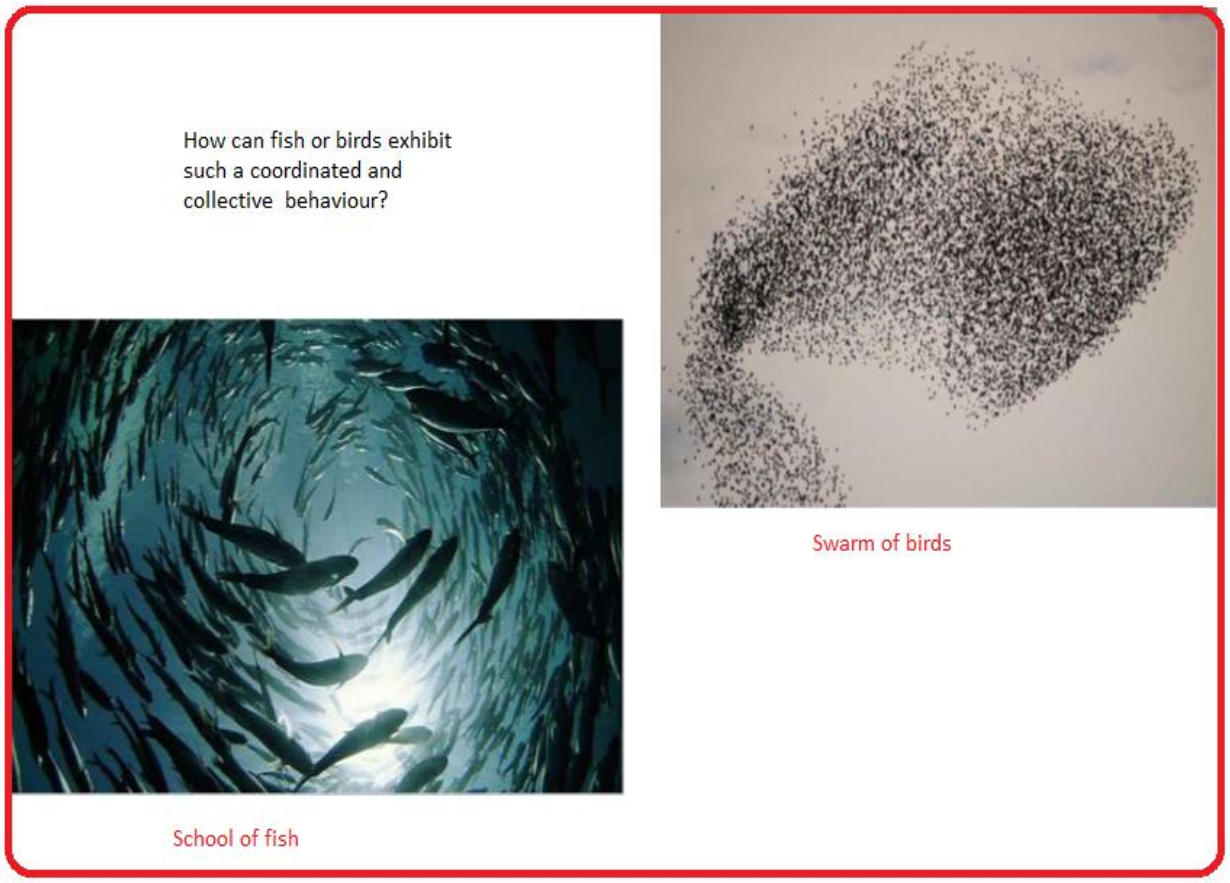

Figure 6.1: Pictures showing the movement of organisms in fish school and bird flock.

6.3 General Concept of the PSO

Particle swarm optimization (PSO) consists of a swarm of particles and each particle resides at a position in the search space. The fitness of each particle represents the quality of its position. The particles fly over the search space with a certain velocity. The velocity (direction and speed) of each particle is influenced by its own best position found so far and the best solution that was found so far by its neighbors. At last the swarm eventually converges to optimum positions.

It has found many applications in the field of engineering and computer science were the optimization problems are partially irregular, noisy, change over time, and others. With regard to computer science, the particle swarm optimization (PSO) is a computational method that

optimizes a problem by iteratively trying to improve a candidate solution with regard to a given measure of quality.

6.4 PSO Description

Many systems require solving one or more nonlinear optimization problems. While analytical methods might suffer from slow convergence, and the curse of dimensionality, heuristics-based swarm intelligence can be an efficient alternative. Particle swarm optimization algorithm was considered as one of the most effective optimization algorithms. The particle swarm optimization (PSO) algorithm is a population - based technique proposed firstly to solve many real optimization problems by use of the following functional optimization equations [38]:

$$f(X_i) = \min(g(X_i), X_i = [x_i^1, x_i^2, \ldots . x_i^n, \qquad (6.1)$$

subject to $p_j(X_i) \leq 0, j = 1,2, \ldots, k$

Here, $g(.)$ is the objective function without constraint; $X_i(t)$ denotes the position vector of particle i consisting of n variables. Every candidate solution of $f(X_i)$ is called a "particle". $p_j(X_i)$ is the j^{th} constraint.

A PSO system consists of a multiple candidate solutions that coexists and collaborate simultaneously, where each solution is called a "particle", flies in the problem search space looking for optimal position to land [38]. As time passes through its quest, the particle adjusts its position according to its self "experience", with respect to the neighboring particle experience. The particle experience is built by the tracking and memorization of the best position encountered, thus the PSO possesses a memory, where every particle remembers the best position it has reached during the past.

The PSO system also combines local search method, (achieved through self-experience) with the global search methods (achieved through neighboring experience), in an attempt to balance exploration and exploitation.

6.5 PSO Paradigms

There are two factors that characterized a particle status on the search space, namely, its position and velocity.

The particle searches the domain of the problem, according to:

$$V_i(t+1) = \omega V_i(t) + c_1 R_1 (P_i - X_i(t)) + c_2 R_2 (P_g - X_i(t)), \quad (6.2)$$

$$X_i(t+1) = X_i(t) + V_i(t+1), \quad (6.3)$$

where; $V_i = \left[v_i^1, v_i^2, \cdots v_i^n \right]$ is the velocity of particle i; $X_i = \left[x_i^1, x_i^2, \cdots x_i^n \right]$ represents the position of particle i; P_i represents the best previous position of particle i (indicating the best discoveries or previous experience of particle i); P_g represents the best previous position among all particles (indicating the best discovery or previous experience of the social swarm); ω is the inertia weight that controls the impact of the previous velocity of the particle on its current velocity; R_1 and R_2 are two random weights whose components r_1^j and r_2^j $(j = 1, 2 \cdots, n,)$ are chosen uniformly within the interval $[0,1]$ which might not guarantee the convergence of the particle trajectory; c_1 and c_2 are the positive constant parameters. Generally the value of each component in V_i should be clamped to the range $[-v_{\max}, v_{\max}]$ to control excessive roaming of particles outside the search space.

Equation *6.2* is utilized to determine the new velocity according to its previous velocity and to the distance of its current position from both its historical and neighbor's positions. The simple PSO algorithm is as follows:

Step 1 (*Initialisation*): *For each particle i in the population*:

Step 1.1: initialize X_i *randomly.*
Step 1.2: initialize V_i *randomly.*
Step 1.3: initialize f_i .
Step 1.4: initialize P_g *with the index of the particle with the best function value among the population.*
Step 1.5: initialize P_i *with a copy of* X_i , $\forall i \leq N$.

Step 2 : *Repeat until a stopping criterion is satisfied*:

Step 2.1: Find P_g *such that* $f[P_g] \leq f_i$, $\forall i \leq N$.
Step 2.2: for each particle , X_i *if* $f_i < f_{best}[i]$, $\forall i, \leq N$.
Step 2.3: for each particle i , *update* X_i *according to equation 2 and 3.*
Step 2.4: evaluate f_i *for all particles.*

Here, *N* denotes the size of population, f_i represents the function value of the i^{th} particle, and $f_{best}[i]$ represents the local-best function value for the best position visited by the i^{th} particle.

6.6 PSO based SAF Neural Network (NN) Model Power Optimization

The particle swarm optimization (PSO) and NN model are combined together to form the PSO based SAF NN model. The particle swarm optimization was used to optimize the power variables based on the SAF neural network model. The inertia weight that controls the impact of previous velocity of electro-thermal variable parameters on their current ones, for this optimizer is, $w = 0.729$. Also there are positive constant parameters called acceleration coefficients (c_1, c_2) which control the maximum step size and is defined as, $c_1 = c_2 = 1.49445$. The optimization evolution characteristic and the Matlab 2010a code for the model are shown in *Fig. 6.4* and Appendix B respectively.

6.6.1 Training of the SAF NN Model

A set of electro-thermal variables data samples that include resistance, voltage and temperature are chosen as the input vector and the target vector (power) of the 45 MW SAF Wonderkop Chrome Processing Plant (WCP) are shown in *Fig. 6.2*, *6.3* and *6.4* respectively.

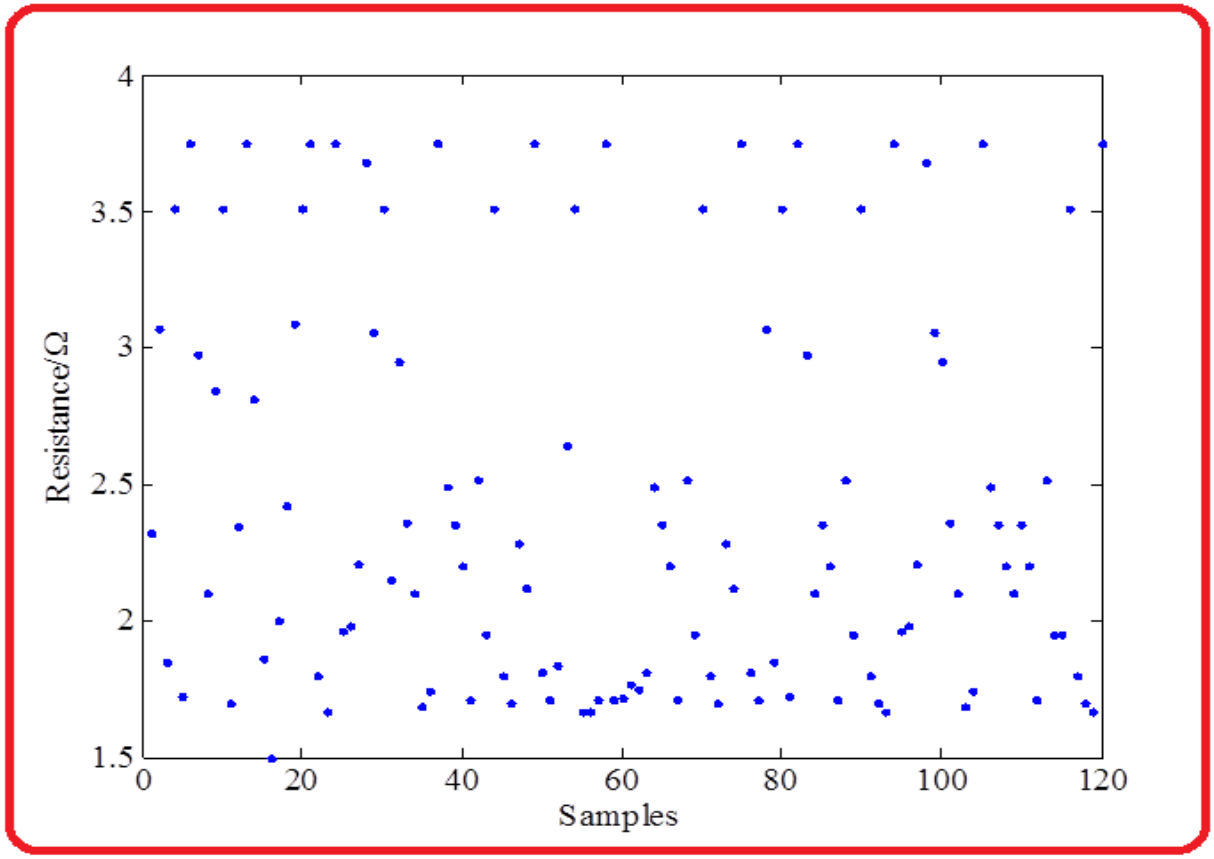

Figure 6.2: SAF Resistance samples.

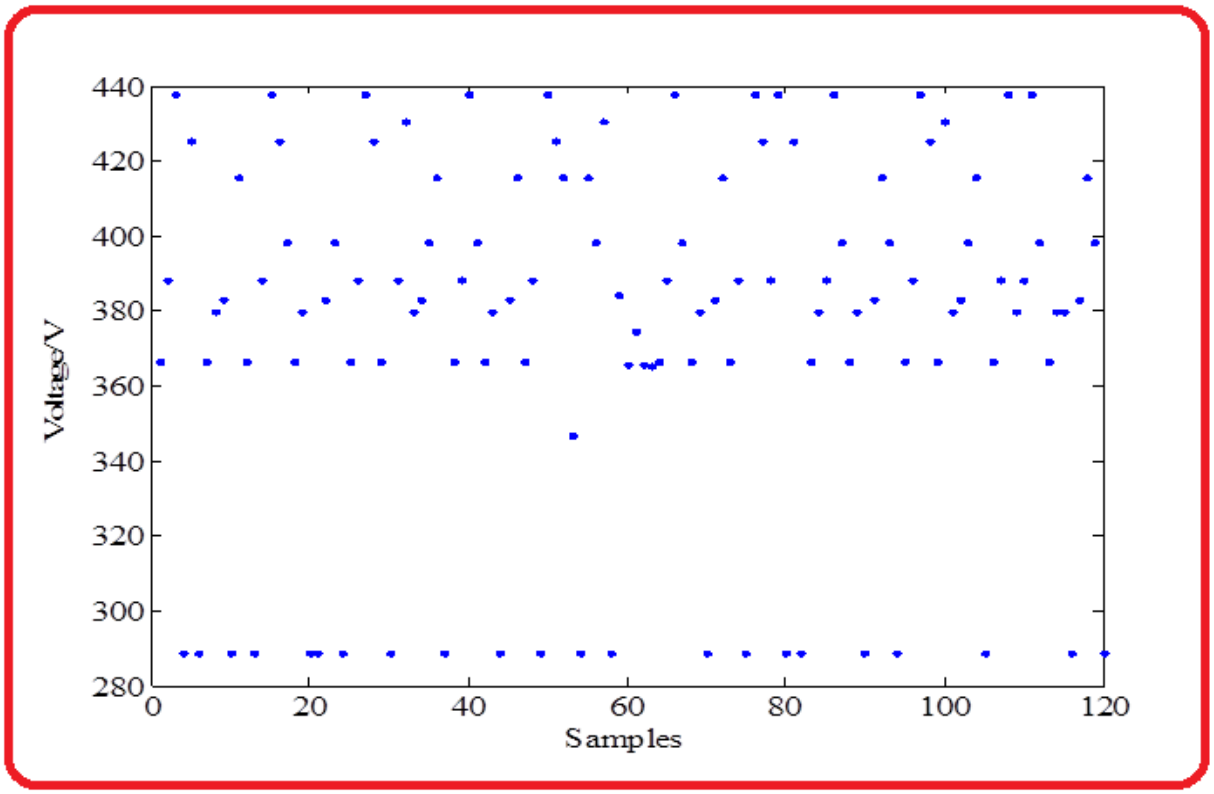

Figure 6.3: SAF Voltage samples.

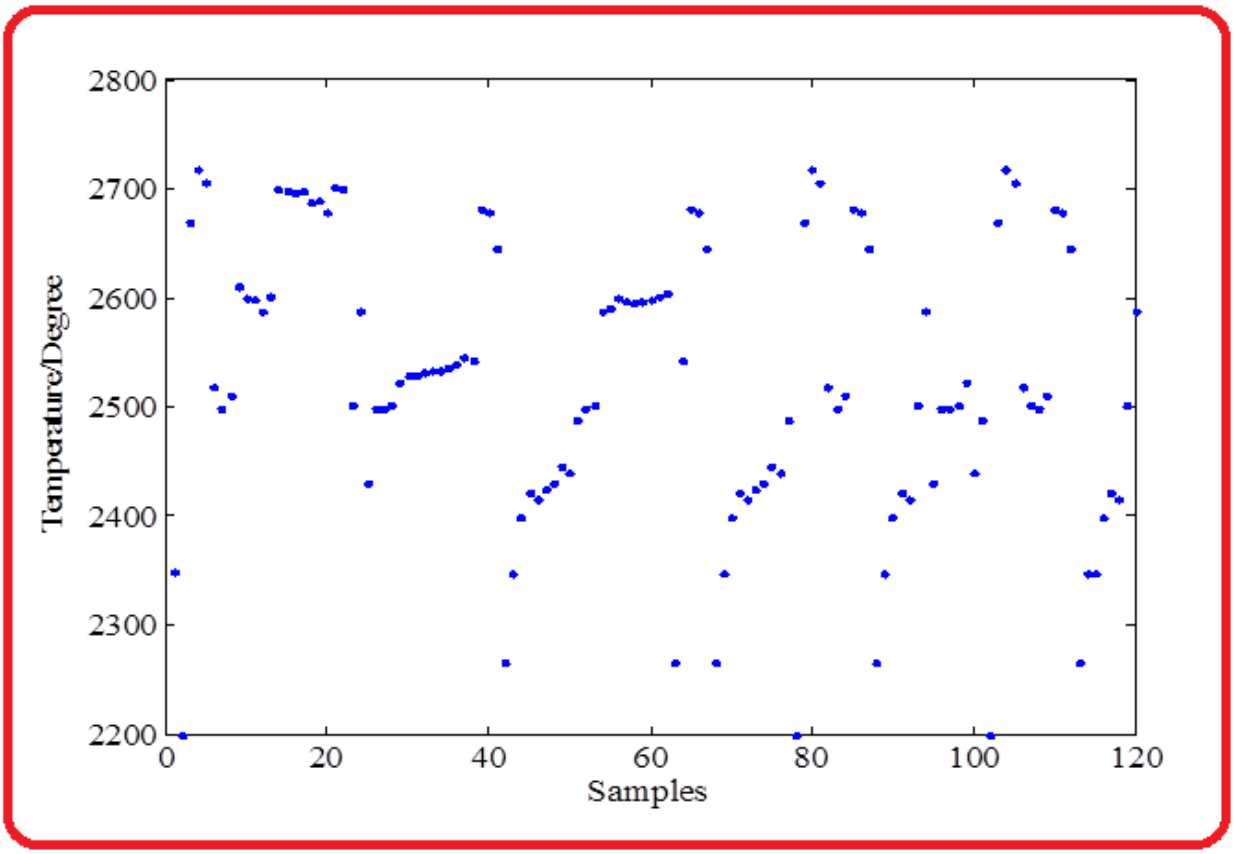

Figure 6.4: SAF Temperature samples.

The training of the PSO based SAF NN model was done considering a sample of *84* parameters *(0-84)*. The other *36* samples were reserved for the validation and testing of the model. The power evolution characteristic of the PSO based SAF NN model for *100* iterations is shown in *Fig. 6.5*, which is based on the trained neural network model.

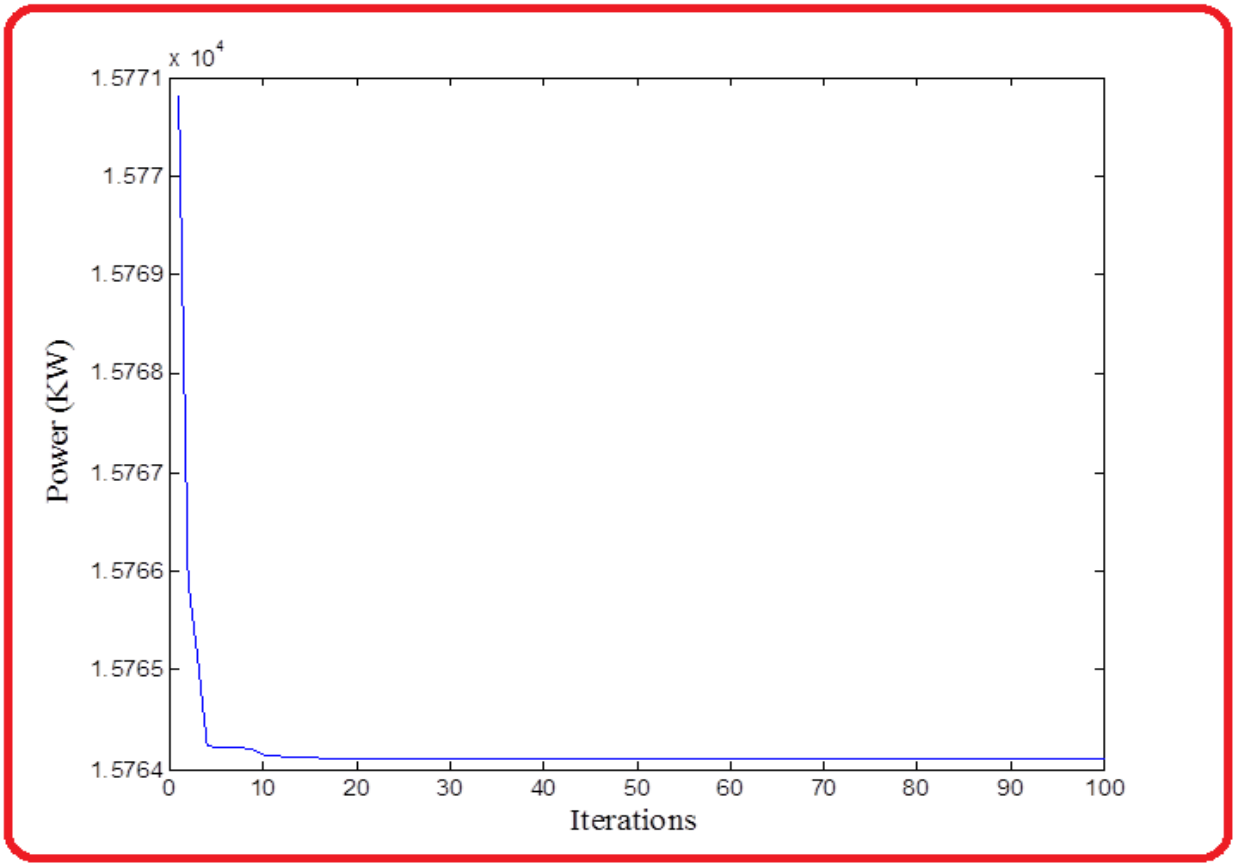

Figure 6.5: Power evolution characteristic of the PSO based SAF NN Model.

The minimum power and the corresponding variables of the PSO based SAF NN model is shown in *Table 1*.

TABLE 1: OPTIMUM /SUB OPTIMUM RESULTS OF PSO BASED SAF NN MODEL.

VARIABLES			**TARGET**
TEMPERATURE [℃]	**VOLTAGE** $[V]$	**RESISTANCE** $[\Omega]$	**POWER** (KW)
27I7,0	288.5	3.5	15764

6.6.2 Optimum / Sub-Optimum Results Testing

As the optimal result is obtained, it is necessary to test the results as the optimal result that is based on the neural network model other than the real SAF plant. Firstly, we should find the lower and near values of the samples comparing with optimal power of the neural network based method.

Here we give a redundancy of *0.5%*, that is, the value of power less than $157764 + (\max\_P - \min\_P) \times 0.5\%$ should be found, where $\max\_P$ is the maximum power sample and $\min\_P$ is the minimum power sample. The comparison of the optimal value of the PSO based SAF NN model output and furnace plant (real) output data are shown in *Table 2*. In *Table 2*, the calculated deviation percentage (%) of the PSO based SAF NN model output and the real SAF Plant output for the considered electro-thermal variables.

TABLE 2: DEVIATION % OF THE REAL SAF PLANT OUTPUT DATA Vs PSO BASED SAF NN MODEL

SAMPLE REF. NUMBER	TEMPERATURE [°C]				VOLTAGE [V]				RESISTANCE [Ω]				POWER [KW]	POWER [KW]
	PLANT	MODEL	DIFF.	% Div.	PLANT	MODEL	DIFF.	% Div.	PLANT	MODEL	DIFF.	% Div.	PLANT	MODEL
10	2599	2717	118	0.04	288.5	288.5	-	0	3.5133	3.5	0.0133	0.38	15814.28	15764
30	2529	2717	188	0.07	288.5	288.5	-	0	3.5133	3.5	0.0133	0.38	15706.37	15764
44	2399	2717	318	0.12	288.5	288.5	-	0	3.5133	3.5	0.0133	0.38	15733.71	15764
70	2399	2717	318	0.12	288.5	288.5	-	0	3.5133	3.5	0.0133	0.38	15733.71	15764
90	2399	2717	318	0.12	288.5	288.5	-	0	3.5133	3.5	0.0133	0.38	15733.71	15764
116	2399	2717	318	0.12	288.5	288.5	-	0	3.5133	3.5	0.0133	0.38	15733.71	15764

From *Table 2*, it can be seen that the *%* error deviation derived from the sample of electro-thermal variable parameters namely, temperature, voltage and resistance are $> 0.2\%$, $0\% \; and \; > 0.4\%$ respectively. The percentage difference of the model and real plant outputs are negligible and in some cases nil, implying that the model is a true replica of the real plant and can be implemented in a real plant furnace scenario.

6.7 Optimization Performance Improvements Techniques

The performance of the proposed PSO based SAF NN model can be further improved by employing a number of techniques to attain the desired optimum performance of the model. These techniques include:

- Combining the SAF NN model with other optimizers
- Alleviating the premature convergence (optimization stagnation) by reversing and perturbing the movement of the PSO particles.
- Using multiple swarms (multi-swarm optimization) to avert premature convergence.
- Adapting the behavioral parameters of the PSO during optimization.

6.8 Conclusion

The particle swarm optimization algorithm used to optimize the power (energy) in the SAF NN model was presented. The description of the particle swarm optimisation, PSO paradigms, proposed PSO based SAF NN model was given. The proposed model was used as an objective function to replace the real SAF Plant. The PSO based SAF NN model results were tested with the real SAF plant samples to verify its performance. The proposed design model results were similar to the results of the real plant furnace, making it acceptable. The preceding chapter will draw up the conclusions of the theses and the future works that can be done in the field of neural networks and particle swarm optimisation with regard to SAFs operations.

CHAPTER SEVEN

CONCLUSIONS AND FUTURE WORKS

This chapter briefly summarizes the findings and contributions of this thesis and gives the future research directions.

7.1 Summary

The work presented in this thesis has addressed one of the most crucial issues in three-phase submerged arc furnaces (SAF) that include measurement, modeling and optimization of the SAFs. This thesis focused on the modeling and optimization of electro-thermal variables in three-phase submerged arc furnaces. The imbalances in the measurement and control of electro-thermal variable parameters results in correspondingly large imbalances in the distribution of the output power during submerged arc furnaces' operations. This scenario is detrimental to the furnace metallurgical operations, thus the focus of this research thesis is to strike the balance in achieving the accurate modelling and optimise the power (energy).

The modelling and optimization of electro-thermal variables was motivated by the need for constant electrical output power. The identification of common electro-thermal variable parameters and how they are measured was carried out in chapters 3 and 4 respectively. A combined solution for the effective and accurate measurement of the electro-thermal variables, in the form of an amalgamated variable parameter measurement (AVPM) system was proposed in chapter 5. The submerged arc furnace plant was modeled using the Neural Network Fitting GUI of Matlab 2010a software.

In chapter 6, the SAF plant was modelled using the neural networks and then optimized by the PSO algorithm to form a PSO based SAF NN model. The optimal results were also validated using the real furnace plant results and produced results were acceptable. This gave green light for a possible implemented in real life environment to improve the status quo and hence efficiency of SAFs.

7.2 Future Research

Throughout this thesis deliberation several new directions for future research presented themselves that include the following:

- Combining the SAF NN model with other optimizers to optimize energy.
- Alleviating the premature convergence (optimization stagnation) by reversing and perturbing the movement of the PSO particles.
- Using multiple swarms (multi-swarm optimization) to avert premature convergence.
- Adapting the behavioral parameters of the PSO during optimization.
- Verifying the proposed amalgamated variable parameter measurement system (AVPM)

List of Publications and Presentations

1. Amos Amadi, Zhengui Wang, Energy optimization of submerged arc furnace, 2012 International Conference on Systems and Informatics (ICSAI 2012), Yantai, China 19-20 May 2012: 800-804 (EI indexed).
2. Amos Amadi, "Optimization of energy in three-phase submerged arc furnaces", 23 July 2012, PG Student Seminar, Florida Campus, UNISA, South Africa.

APPENDIX: A: INPUTS AND TARGET VECTORS SAMPLES FOR THE 45 MVA SAF (WONDERKOP CHROME PROCESSING PLANT)

ELECTRO-THERMAL VARIABLES														TARGET VECTORS	
TIME	RESISTANCE				Current (KA)				VOLTAGE (V)				Temp.	POWER	ENERGY
INTERV.	E1	E2	E3		E1	E2	E3		E1	E2	E3			(KW)	(KWh)
(30 MIN)	R1	R2	R3	R	i1	i2	i3	I_L	V1	V2	V3	V_L			
T_1	2.1	2.1	2.77	2.32	84.3	84.3	84.3	84.3	289	158	188	366.4	2349	29417.31	14708.65252
T_2	2.73	2.27	4.21	3.07	84.7	77.4	68.5	76.87	286	187	200	388.3	2200	28363.93	14181.9631
T_3	2.14	2.12	1.29	1.85	86.5	81.3	70.8	79.53	299	197	263	437.9	2670	33450.08	16725.04224
T_4	4.27	4.18	2.09	3.51	49.6	55	67.5	57.37	300	100	100	288.5	2717	15914.31	7957.152798
T_5	2.14	1.75	1.28	1.72	85.7	86.2	63.6	78.5	284	290	163	425.2	2706	31734.41	15867.20442
T_6	2.56	4.37	4.32	3.75	64	69	67.5	66.83	300	100	100	288.5	2518	18239.82	9119.907628
T_7	2.89	3.931	2.11	2.98	84.3	84.3	84.3	84.3	289	158	188	366.4	2499	28759.5	14379.75125
T_8	2.14	2.18	1.99	2.1	72.1	83.2	90.8	82.03	291	189	178	379.7	2511	29635.34	14817.67248
T_9	3.77	2.89	1.88	2.85	74.8	82.5	90.6	82.63	286	179	199	383.1	2610	30153.5	15076.74909
T_{10}	4.27	4.18	2.09	3.51	49.6	55	67.5	57.37	300	100	100	288.5	2599	15814.28	7907.137842
T_{11}	2.11	1.72	1.27	1.7	75.8	91.5	90.9	86.07	290	250	180	415.4	2598	34414.17	17207.08353
T_{12}	2.12	2.73	2.19	2.35	84.3	84.3	84.3	84.3	289	158	188	366.4	2588	29514.69	14757.34603
T_{13}	2.56	4.37	4.32	3.75	64	69	67.5	66.83	300	100	100	288.5	2601	18397.13	9198.566168
T_{14}	4.11	3.11	1.21	2.81	84.7	77.4	68.5	76.87	286	187	200	388.3	2699	28319.57	14159.78534
T_{15}	2.13	2.19	1.26	1.86	86.5	81.3	70.8	79.53	299	197	263	437.9	2698	32692.06	16346.02798
T_{16}	2.12	1.17	1.21	1.5	85.7	86.2	63.6	78.5	284	290	163	425.2	2697	31737.11	15868.55639
T_{17}	2.14	1.87	1.99	2	75.8	91.5	90.9	86.07	293	215	182	398.1	2698	33043.4	16521.69758
T_{18}	2.39	2.77	2.11	2.42	84.3	84.3	84.3	84.3	289	158	188	366.4	2688	29648.77	14824.38647
T_{19}	3.11	3.89	2.27	3.09	72.1	83.2	90.8	82.03	291	189	178	379.7	2689	30002.02	15001.0091
T_{20}	4.27	4.18	2.09	3.51	49.6	55	67.5	57.37	300	100	100	288.5	2679	15898.95	7949.473466
T_{21}	2.56	4.37	4.32	3.75	64	69	67.5	66.83	300	100	100	288.5	2701	18523.77	9261.88634
T_{22}	2.1	2.1	1.2	1.8	74.8	82.5	90.6	82.63	286	179	199	383.1	2699	30524.16	15262.08172
T_{23}	2.1	1.7	1.2	1.67	75.8	91.5	90.9	86.07	293	215	182	398.1	2501	32793.67	16396.83329
T_{24}	2.56	4.37	4.32	3.75	64	69	67.5	66.83	300	100	100	288.5	2588	18261.51	9130.753425
T_{25}	2.11	2.11	1.67	1.96	84.3	84.3	84.3	84.3	289	158	188	366.4	2430	29374.71	14687.35586
T_{26}	2.32	2.35	1.27	1.98	84.7	77.4	68.5	76.87	286	187	200	388.3	2499	27812.38	13906.18874
T_{27}	3.17	2.17	1.29	2.21	86.5	81.3	70.8	79.53	299	197	263	437.9	2498	32968.41	16484.20283
T_{28}	4.11	4.71	2.22	3.68	85.7	86.2	63.6	78.5	284	290	163	425.2	2501	31322.77	15661.38741
T_{29}	3.11	3.18	2.88	3.06	84.3	84.3	84.3	84.3	289	158	188	366.4	2523	29094.75	14547.37553

T_{30}	4.27	4.18	2.09	3.51	49.6	55	67.5	57.37	300	100	100	288.5	2529	15706.37	7853.183918
T_{31}	2.67	2.45	1.34	2.15	84.7	77.4	68.5	76.87	286	187	200	388.3	2528	28422.34	14211.17029
T_{32}	3.55	3.16	2.15	2.95	84.3	84.3	84.3	84.3	289	289	168	430.4	2531	34420.86	17210.42826
T_{33}	3.48	2.33	1.27	2.36	72.1	83.2	90.8	82.03	291	189	178	379.7	2533	29574.11	14787.05668
T_{34}	2.91	2.11	1.28	2.1	74.8	82.5	90.6	82.63	286	179	199	383.1	2534	29873	14936.49908
T_{35}	2.11	1.71	1.23	1.68	75.8	91.5	90.9	86.07	293	215	182	398.1	2537	33094.35	16547.17415
T_{36}	2.15	1.78	1.29	1.74	75.8	91.5	90.9	86.07	290	250	180	415.4	2540	33642.6	16821.29918
T_{37}	2.56	4.37	4.32	3.75	64	69	67.5	66.83	300	100	100	288.5	2546	18428.75	9214.376929
T_{38}	3.15	2.18	2.14	2.49	84.3	84.3	84.3	84.3	289	158	188	366.4	2543	29244.74	14622.36941
T_{39}	2.89	2.88	1.29	2.35	84.7	77.4	68.5	76.87	286	187	200	388.3	2681	27925.3	13962.64801
T_{40}	2.45	2.39	1.77	2.2	86.5	81.3	70.8	79.53	299	197	263	437.9	2678	32628.18	16314.0879
T_{41}	2.09	1.78	1.26	1.71	85.7	86.2	63.6	78.5	293	215	182	398.1	2645	29518.56	14759.27918
T_{42}	2.68	2.43	2.44	2.52	84.3	84.3	84.3	84.3	289	158	188	366.4	2266	29279.09	14639.54263
T_{43}	2.24	2.34	1.28	1.95	72.1	83.2	90.8	82.03	291	189	178	379.7	2347	29608.03	14804.01528
T_{44}	4.27	4.18	2.09	3.51	49.6	55	67.5	57.37	300	100	100	288.5	2399	15733.71	7866.854452
T_{45}	2.1	2.1	1.2	1.8	74.8	82.5	90.6	82.63	286	179	199	383.1	2421	30345.07	15172.53383
T_{46}	2.11	1.73	1.25	1.7	75.8	91.5	90.9	86.07	290	250	180	415.4	2415	34032.33	17016.16685
T_{47}	2.61	2.11	2.13	2.28	84.3	84.3	84.3	84.3	289	158	188	366.4	2425	29570.91	14785.45329
T_{48}	2.43	2.5	1.43	2.12	84.7	77.4	68.5	76.87	286	187	200	388.3	2430	28330.05	14165.02383
T_{49}	2.56	4.37	4.32	3.75	64	69	67.5	66.83	300	100	100	288.5	2445	18390.19	9195.095513
T_{50}	2.05	2.11	1.28	1.81	86.5	81.3	70.8	79.53	299	197	263	437.9	2439	33363.01	16681.5034
T_{51}	2.18	1.71	1.25	1.71	85.7	86.2	63.6	78.5	284	290	163	425.2	2488	32279.97	16139.98581
T_{52}	2.43	1.68	1.41	1.84	75.8	91.5	90.9	86.07	290	250	180	415.4	2499	34481.28	17240.6401
T_{53}	2.85	2.43	2.65	2.64	64	69	67.4	66.8	288	126	187	346.8	2501	22365.73	11182.8649
T_{54}	4.27	4.18	2.09	3.51	49.6	55	67.5	57.37	300	100	100	288.5	2588	16012.37	8006.183012
T_{55}	2.1	1.7	1.2	1.67	75.8	91.5	90.9	86.07	290	250	180	415.4	2591	34001.91	17000.95287
T_{56}	2.1	1.7	1.2	1.67	75.8	91.5	90.9	86.07	293	215	182	398.1	2599	32850.62	16425.30811
T_{57}	2.19	1.72	1.23	1.71	75.8	91.5	90.9	86.07	289	289	168	430.4	2597	35682.17	17841.08337
T_{58}	2.56	4.37	4.32	3.75	64	69	67.5	66.83	300	100	100	288.5	2595	18566.11	9283.057336
T_{59}	2.14	1.7	1.29	1.71	75.8	91.5	90.9	86.07	288	199	179	384.3	2596	31945.42	15972.7117
T_{60}	2.22	1.62	1.32	1.72	65.8	84.5	79.9	76.73	276	169	189	365.8	2598	26753.26	13376.62873
T_{61}	2.38	1.71	1.22	1.77	69.8	82.8	80.9	77.83	281	179	189	374.5	2601	27871.56	13935.77821
T_{62}	2.34	1.69	1.21	1.75	71.8	81.5	81.9	78.4	286	169	179	365.8	2605	27361.48	13680.73806
T_{63}	2.45	1.72	1.27	1.81	74.8	82.5	82.9	80.07	281	171	181	365.2	2266	28015.78	14007.88857
T_{64}	3.15	2.18	2.14	2.49	84.3	84.3	84.3	84.3	289	158	188	366.4	2543	29244.74	14622.36941
T_{65}	2.89	2.88	1.29	2.35	84.7	77.4	68.5	76.87	286	187	200	388.3	2681	27925.3	13962.64801
T_{66}	2.45	2.39	1.77	2.2	86.5	81.3	70.8	79.53	299	197	263	437.9	2678	32628.18	16314.0879
T_{67}	2.09	1.78	1.26	1.71	85.7	86.2	63.6	78.5	293	215	182	398.1	2645	29518.56	14759.27918
T_{68}	2.68	2.43	2.44	2.52	84.3	84.3	84.3	84.3	289	158	188	366.4	2266	29279.09	14639.54263
T_{69}	2.24	2.34	1.28	1.95	72.1	83.2	90.8	82.03	291	189	178	379.7	2347	29608.03	14804.01528
T_{70}	4.27	4.18	2.09	3.51	49.6	55	67.5	57.37	300	100	100	288.5	2399	15733.71	7866.854452

T_{71}	2.1	2.1	1.2	1.8	74.8	82.5	90.6	82.63	286	179	199	383.1	2421	30345.07	15172.53383
T_{72}	2.11	1.73	1.25	1.7	75.8	91.5	90.9	86.07	290	250	180	415.4	2415	34032.33	17016.16685
T_{73}	2.61	2.11	2.13	2.28	84.3	84.3	84.3	84.3	289	158	188	366.4	2425	29570.91	14785.45329
T_{74}	2.43	2.5	1.43	2.12	84.7	77.4	68.5	76.87	286	187	200	388.3	2430	28330.05	14165.02383
T_{75}	2.56	4.37	4.32	3.75	64	69	67.5	66.83	300	100	100	288.5	2445	18390.19	9195.095513
T_{76}	2.05	2.11	1.28	1.81	86.5	81.3	70.8	79.53	299	197	263	437.9	2439	33363.01	16681.5034
T_{77}	2.18	1.71	1.25	1.71	85.7	86.2	63.6	78.5	284	290	163	425.2	2488	32279.97	16139.98581
T_{78}	2.73	2.27	4.21	3.07	84.7	77.4	68.5	76.87	286	187	200	388.3	2200	28363.93	14181.9631
T_{79}	2.14	2.12	1.29	1.85	86.5	81.3	70.8	79.53	299	197	263	437.9	2670	33450.08	16725.04224
T_{80}	4.27	4.18	2.09	3.51	49.6	55	67.5	57.37	300	100	100	288.5	2717	15914.31	7957.152798
T_{81}	2.14	1.75	1.28	1.72	85.7	86.2	63.6	78.5	284	290	163	425.2	2706	31734.41	15867.20442
T_{82}	2.56	4.37	4.32	3.75	64	69	67.5	66.83	300	100	100	288.5	2518	18239.82	9119.907628
T_{83}	2.89	3.931	2.11	2.98	84.3	84.3	84.3	84.3	289	158	188	366.4	2499	28759.5	14379.75125
T_{84}	2.14	2.18	1.99	2.1	72.1	83.2	90.8	82.03	291	189	178	379.7	2511	29635.34	14817.67248
T_{85}	2.89	2.88	1.29	2.35	84.7	77.4	68.5	76.87	286	187	200	388.3	2681	27925.3	13962.64801
T_{86}	2.45	2.39	1.77	2.2	86.5	81.3	70.8	79.53	299	197	263	437.9	2678	32628.18	16314.0879
T_{87}	2.09	1.78	1.26	1.71	85.7	86.2	63.6	78.5	293	215	182	398.1	2645	29518.56	14759.27918
T_{88}	2.68	2.43	2.44	2.52	84.3	84.3	84.3	84.3	289	158	188	366.4	2266	29279.09	14639.54263
T_{89}	2.24	2.34	1.28	1.95	72.1	83.2	90.8	82.03	291	189	178	379.7	2347	29608.03	14804.01528
T_{90}	4.27	4.18	2.09	3.51	49.6	55	67.5	57.37	300	100	100	288.5	2399	15733.71	7866.854452
T_{91}	2.1	2.1	1.2	1.8	74.8	82.5	90.6	82.63	286	179	199	383.1	2421	30345.07	15172.53383
T_{92}	2.11	1.73	1.25	1.7	75.8	91.5	90.9	86.07	290	250	180	415.4	2415	34032.33	17016.16685
T_{93}	2.1	1.7	1.2	1.67	75.8	91.5	90.9	86.07	293	215	182	398.1	2501	32793.67	16396.83329
T_{94}	2.56	4.37	4.32	3.75	64	69	67.5	66.83	300	100	100	288.5	2588	18261.51	9130.753425
T_{95}	2.11	2.11	1.67	1.96	84.3	84.3	84.3	84.3	289	158	188	366.4	2430	29374.71	14687.35586
T_{96}	2.32	2.35	1.27	1.98	84.7	77.4	68.5	76.87	286	187	200	388.3	2499	27812.38	13906.18874
T_{97}	3.17	2.17	1.29	2.21	86.5	81.3	70.8	79.53	299	197	263	437.9	2498	32968.41	16484.20283
T_{98}	4.11	4.71	2.22	3.68	85.7	86.2	63.6	78.5	284	290	163	425.2	2501	31322.77	15661.38741
T_{99}	3.11	3.18	2.88	3.06	84.3	84.3	84.3	84.3	289	158	188	366.4	2523	29094.75	14547.37553
T_{100}	3.55	3.16	2.15	2.95	84.3	84.3	84.3	84.3	289	289	168	430.4	2439	34420.86	17210.42826
T_{101}	3.48	2.33	1.27	2.36	72.1	83.2	90.8	82.03	291	189	178	379.7	2488	29574.11	14787.05668
T_{102}	2.91	2.11	1.28	2.1	74.8	82.5	90.6	82.63	286	179	199	383.1	2200	29873	14936.49908
T_{103}	2.11	1.71	1.23	1.68	75.8	91.5	90.9	86.07	293	215	182	398.1	2670	33094.35	16547.17415
T_{104}	2.15	1.78	1.29	1.74	75.8	91.5	90.9	86.07	290	250	180	415.4	2717	33642.6	16821.29918
T_{105}	2.56	4.37	4.32	3.75	64	69	67.5	66.83	300	100	100	288.5	2706	18428.75	9214.376929
T_{106}	3.15	2.18	2.14	2.49	84.3	84.3	84.3	84.3	289	158	188	366.4	2518	29244.74	14622.36941
T_{107}	2.89	2.88	1.29	2.35	84.7	77.4	68.5	76.87	286	187	200	388.3	2501	27925.3	13962.64801
T_{108}	2.45	2.39	1.77	2.2	86.5	81.3	70.8	79.53	299	197	263	437.9	2499	32628.18	16314.0879
T_{109}	2.14	2.18	1.99	2.1	72.1	83.2	90.8	82.03	291	189	178	379.7	2511	29635.34	14817.67248
T_{110}	2.89	2.88	1.29	2.35	84.7	77.4	68.5	76.87	286	187	200	388.3	2681	27925.3	13962.64801
T_{111}	2.45	2.39	1.77	2.2	86.5	81.3	70.8	79.53	299	197	263	437.9	2678	32628.18	16314.0879

T_{112}	2.09	1.78	1.26	1.71	85.7	86.2	63.6	78.5	293	215	182	398.1	2645	29518.56	14759.27918
T_{113}	2.68	2.43	2.44	2.52	84.3	84.3	84.3	84.3	289	158	188	366.4	2266	29279.09	14639.54263
T_{114}	2.24	2.34	1.28	1.95	72.1	83.2	90.8	82.03	291	189	178	379.7	2347	29608.03	14804.01528
T_{115}	2.24	2.34	1.28	1.95	72.1	83.2	90.8	82.03	291	189	178	379.7	2347	29608.03	14804.01528
T_{116}	4.27	4.18	2.09	3.51	49.6	55	67.5	57.37	300	100	100	288.5	2399	15733.71	7866.854452
T_{117}	2.1	2.1	1.2	1.8	74.8	82.5	90.6	82.63	286	179	199	383.1	2421	30345.07	15172.53383
T_{118}	2.11	1.73	1.25	1.7	75.8	91.5	90.9	86.07	290	250	180	415.4	2415	34032.33	17016.16685
T_{119}	2.1	1.7	1.2	1.67	75.8	91.5	90.9	86.07	293	215	182	398.1	2501	32793.67	16396.83329
T_{120}	2.56	4.37	4.32	3.75	64	69	67.5	66.83	300	100	100	288.5	2588	18261.51	9130.753425

APPENDIX B: DESIGN PSO - BASED SAF NN MODEL - Matlab 2010a Code.

```
load NN_SAF    %The neural network was loaded and its name is net.

Xrmin_max = 1.0e+003 *[2.7170    0.4379    0.0037
    2.2000    0.2885    0.0015];                          %This is the range
of the system variables.

Vmax = 1;
%Xmax = 1.0;
% Xmax = Xmaxmin(1);
Xmin = -1.0;
Xmax = 1;
W     = 0.729;
c1    = 1.49445;
c2    = c1;
dim = 3;
Num_P = 20;                  %The number of particles

particle_x = -1 + 2*rand(dim,Num_P);       % in the interval [-1,1]

best_particle_x = particle_x;
Vx = Vmax*(rand(dim, Num_P) - 0.5)*2;
for i = 1:Num_P
    for j = 1:dim
        real_X(j,1) = Xrmin_max(2,j) + (Xrmin_max(1,j) -
Xrmin_max(2,j))/2*(particle_x(j,i) + 1);
    end
    fit_fun(i) = sim(net,real_X);
end
Pbest = fit_fun;
temp = min(Pbest);
Pg = min(find(Pbest == temp));


for interv = 1:100
    interv
        for i = 1:Num_P
           for j = 1:dim
            real_X(j,1) = Xrmin_max(2,j) + (Xrmin_max(1,j) -
Xrmin_max(2,j))/2*(particle_x(j,i) + 1)           end
           fit_fun(i) = sim(net,real_X);
         if Pbest(i) > fit_fun(i)
             Pbest(i) = fit_fun(i);
             best_particle_x(:,i) = particle_x(:,i);
         end
    end
   temp = min(Pbest);
   Pg = min(find(Pbest == temp));

     local_temp = [];
     for i = 1:dim
          local_temp = [local_temp; best_particle_x(i,Pg) -
particle_x(i,:)];
      end
```

```
     Vx = W.*Vx + c1.*rand(dim,Num_P).*(best_particle_x - particle_x) +...
c2.*rand(dim,Num_P).* local_temp; % [best_particle_x(1,Pg) -
particle_x(1,:);best_particle_x(2,Pg) - particle_x(2,:)];

     particle_x = particle_x + Vx;
     for i = 1:Num_P
         for j = 1:dim
                 if particle_x(j,i) > Xmax
                     particle_x(j,i) = Xmax;
                     Vx(j,i) = 0;
                 end
                 if particle_x(j,i) < Xmin
                     particle_x(j,i) = Xmin;
                      Vx(j,i) = 0;
                 end
         end
      end

       fitness(interv) = Pbest(Pg);
  end


fitness_out = Pbest(Pg);
for j = 1:dim
    real_X(1,j) = Xrmin_max(2,j) + (Xrmin_max(1,j) -
Xrmin_max(2,j))/2*(best_particle_x(j,Pg) + 1);
end
plot(fitness)
```

APPENDIX C: PROPOSED AMALGAMATED VARIABLE PARAMETERS MEASUREMENT (AVPM) SYSTEM

The proposed AVPM system is a technique that combines different measurement philosophies into multifunctional measuring equipment for both the primary and secondary sides of the furnace. It incorporates measurement and control of a number of electro-thermal variable parameters that include harmonic, temperature, voltage, current, electrode resistance and others. It is made up of a number of modular blocks that include:

- Current and Voltage Calculation Module (CVCM)
- Power Calculation Module (PCM)
- IR Temperature Calculation Module (ITCM)
- Electrode – to – bath voltage Calculation Module (ECM)
- Electrode Resistance, Impedance Calculation Module (ERICM)
- Waveform Calculation Module (WCM)

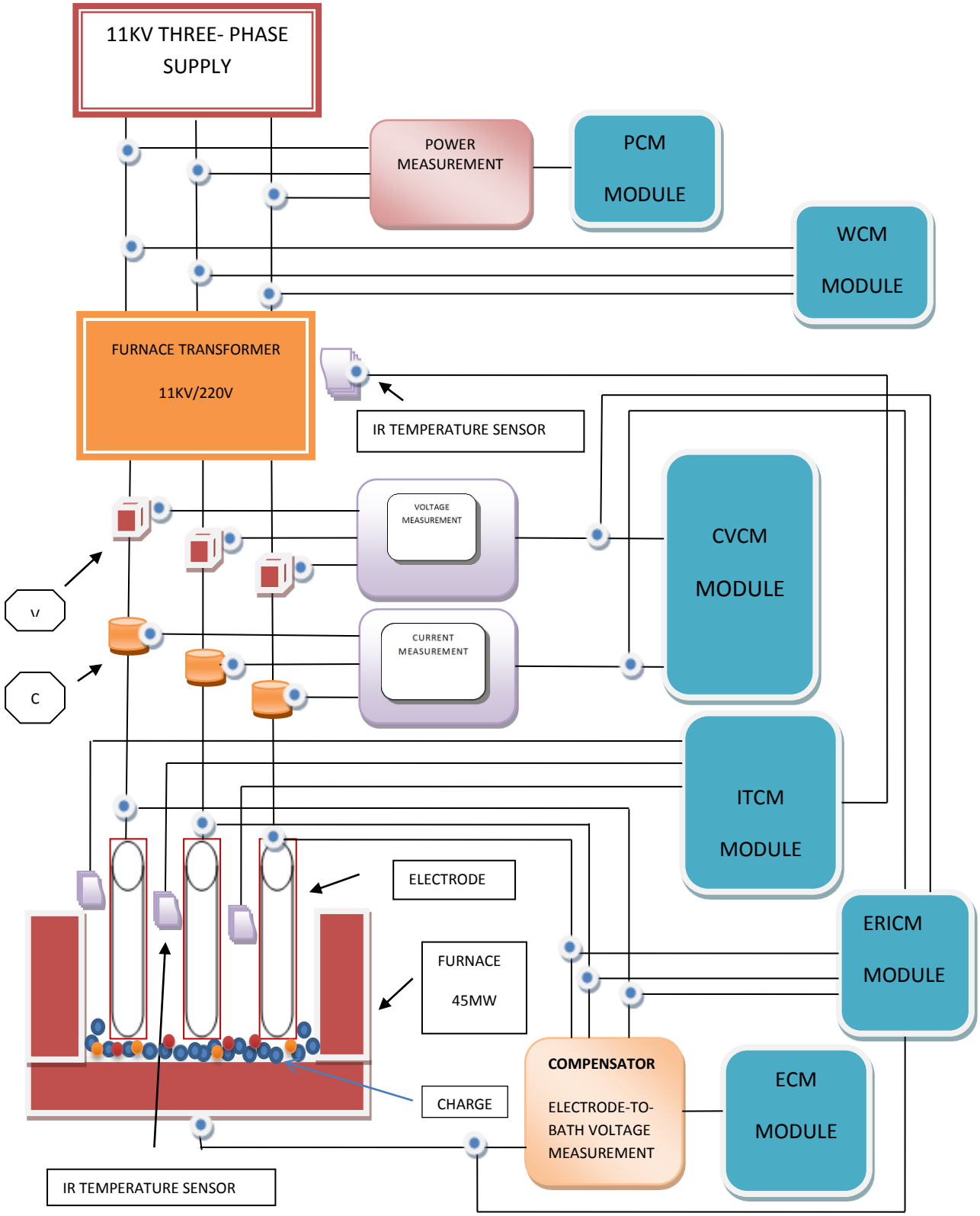

Figure C.1: Proposed Amalgamated Variable Parameters Measurement (AVPM) system diagram.

C.1 Current and Voltage Calculation Module (CVCM)

The measurement of current and voltage by the CVCM is based on observing the mutual correlation between the secondary currents and voltages measured by means of current and voltage transformers respectively. The secondary current and voltage signals are sampled separately as proposed by the researcher in *Fig. C.2.* The current and voltage parameters are measured as line voltages using resistance dividers and the divider output signals are sampled, filtered in the median filter for standard, hybrid and non-linear with resolution requirement. Their outputs are then supplied to the ammeter and voltmeter respectively of the CVCM module.

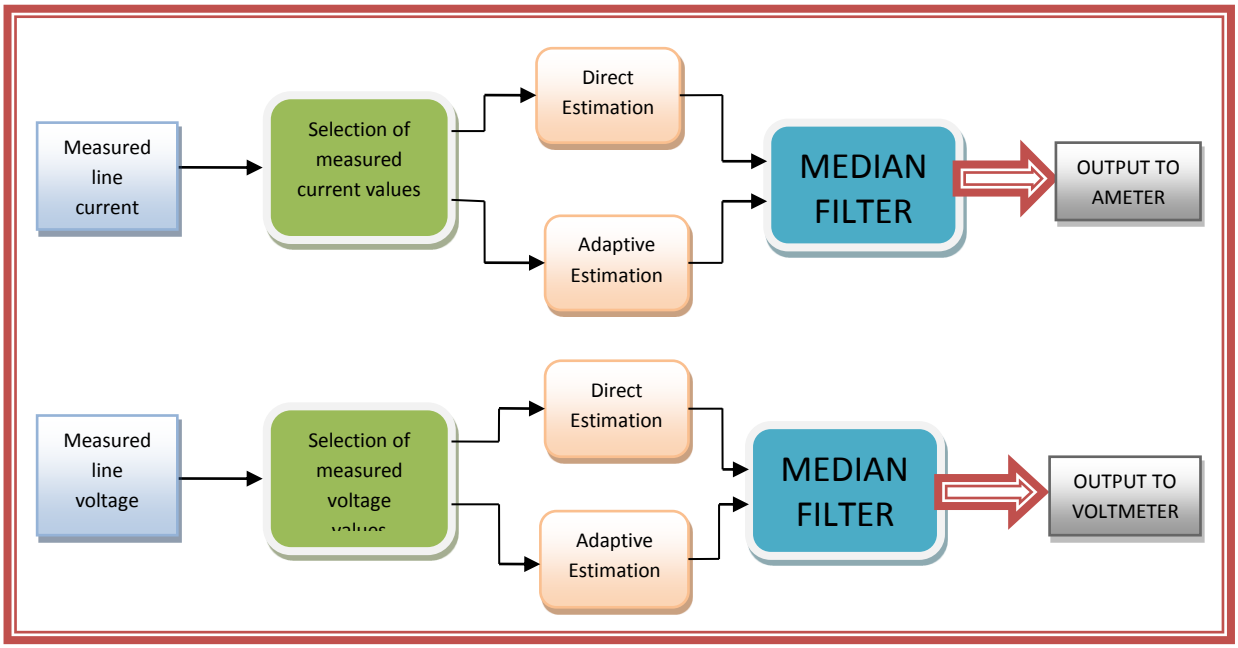

Figure C.2: Proposed Block diagram of CVCM module.

The CVCM is used to measure instantaneous three-phase voltages and currents in the SAF circuit. When connected in series with three-phase elements, it retains the three phase-to-ground or phase-to-phase peak voltages and currents. The module can output the voltages and currents in per unit *(pu)* values or in volts and amperes.

When selected to measure phase-to-ground voltages in per unit, the module converts the measured voltages based on peak value of nominal phase-to-ground voltage based on equation (C.1):

$$V_{abc}\ (p.u)\ = \frac{Vphase\ -to-ground\ (V)}{Vbase\ (V)} \qquad (C.1)$$

where:

$$V_{abc}\ (p.u)\ = \frac{Vphase\ -to-ground\ (V)}{Vbase\ (V)}$$

Also when selected to measure phase-to-phase voltages in per unit, the module converts the measured voltages based on peak value of nominal phase-to-phase voltage defined by the equation:

$$V_{abc}\ (p.u)\ = \frac{Vphase\ -to-ground\ (V)}{Vbase\ (V)} \qquad (C.2)$$

where: $V_{base} = V_{norm}\ (vrms)\ .\ \sqrt{2}$

When selected to measure currents in per unit, the module converts the measured currents based on the peak value of the nominal current defined by equation:

$$I_{abc}(p.u) = \frac{I_{abc}\ (A)}{I_{base}\ (A)} \qquad (C.3)$$

where $I_{base} = \dfrac{P_{base}\ (VA)}{\dfrac{V_{norm}\ .\ \sqrt{2}}{\sqrt{3}}}$

The steady-state voltage and current phasors measured by the CVCM module can be simulated by the Powergui block, when selecting steady-state voltages and currents in the Matlab 2010a Software.

C.2 Power Calculation Module (PCM)

The PCM module utilizes the current and voltage output signals derived from the primary side of the 11KV / 220V furnace transformer to determine the input power to the SAF. These signals are used for calculating either the powers and *rms* values or the spectra of powers and signals, for estimation purposes. The PCM module utilizes strong and abrupt variations which continuously occur in the power of the SAF as a result of the fluctuations of the furnace impedances and arc voltages. The PCM can also calculate the power for the furnace with or without neutral power connection, with measurements being taken from primary or secondary

of the furnace transformer. When the PCM is used on a furnace that is not provided with the neutral power connection, variation of a single electrode, related voltage or power has an inevitable effect on the electric parameters of other electrodes as well.

The mathematical models for the determination of the power values by the PCM module are defined by the following equations:

Apparent Power supplied into the furnace,

$$S_T = (I_1 Z_{E1} + I_2 Z_{E2} + I_3 Z_{E3})^2 \qquad (C.4)$$

True Power of the furnace,

$$P_T = (I_1 R_{E1} + I_2 R_{E2} + I_3 R_{E3})^2 \qquad (C.5)$$

Reactive Power of the furnace,

$$Q_T = (I_1 X_{E1} + I_2 X_{E2} + I_3 X_{E3})^2 \qquad (C.6)$$

where; Z_{E1} ---- Z_{E2} - *are equivalent impedances representing electrodes 1.2.and 3.*

R_{E1} ---- R_{E2} - *are real components of these impedances*

X_{E1} ---- X_{E2} - *is imaginary components of impedances*

I_1 ---- I_2 - *are absolute values of currents of electrodes.*

C.3 Infrared Temperature Calculation Module (ITCM)

In order to ensure the normal prevailing temperatures during furnace operation, the transformers, bus bars, electrodes and furnace shell temperature should be maintained to minimise heat build-up in windings, electrode breakages and furnace shell cracking respectively, by making use of the ITCM module. In bus bar temperature measurement, the IR thermometer is placed in the measurement area to provide reliable measurements results.

The proposed ITCM module by the researcher is used in conjunction with lens to collect the energy emitted by the target and detector to convert the energy to an electrical signal. The emissivity is adjusted to match the IRT calibration so as to the emit characteristics of the object being measured as shown in *Fig. C.3.*

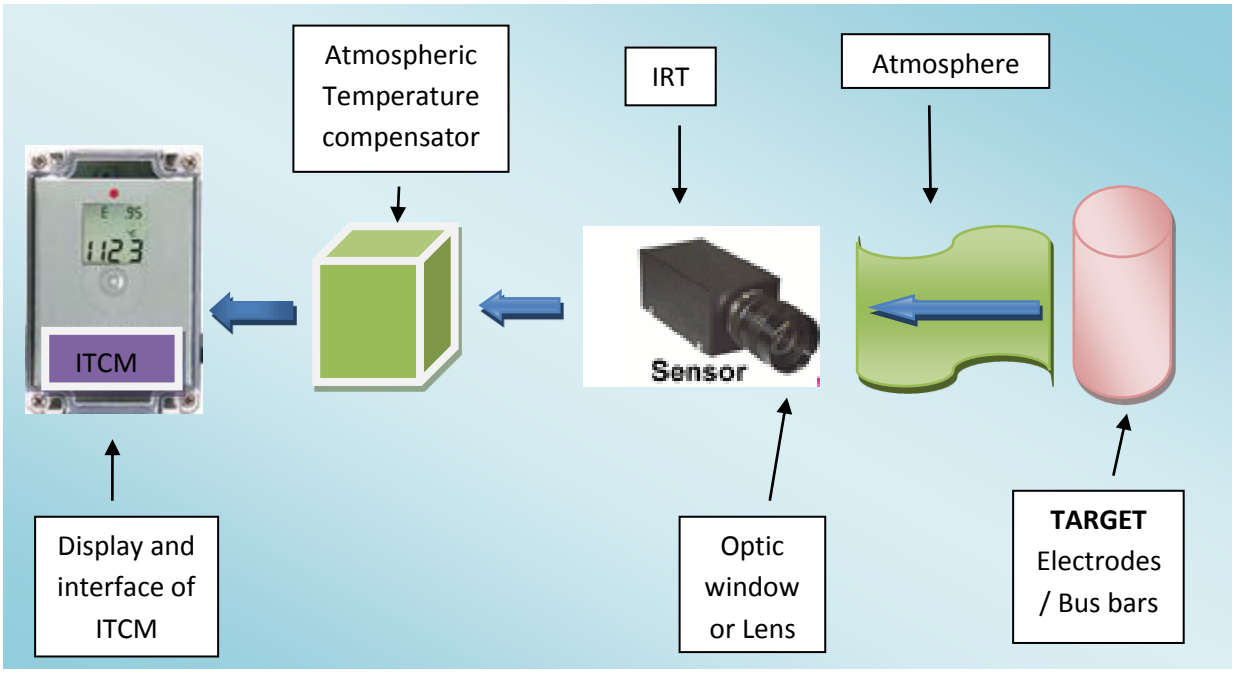

Figure C.3: Block diagram showing the proposed SAF Infrared (IR) measuring system of electrode temperature.

The infrared thermometer (IRT) measures temperature by detecting the infrared energy emitted by the electrode which is at temperatures above absolute zero (0°Kelvin). An ambient or atmospheric temperature compensation circuit is connected before the ICTM module to ensure that temperature varies within the IRT. The ambient temperature changes are not transferred to the final output (ITCM). The ICTM module is modeled to produce emission characterized by a mathematical equation that combines the absorption (**A**), reflection (**R**) and transmission (**T**) as being equal to one [20]:

$$A + R + T = 1 \qquad (C.7)$$

where:

A - *absorption*

R - *reflection*

T - *transmission*

NB: *an ideal blackbody has no reflectance (**R = 0**), so E = **1***

When used in electrode temperature measurements, the IRT lens focus the infrared (IR) energy on to a detector mounted on each electrode to convert the energy into an electrical

signal that can be displayed in the units of temperature after being compensated for ambient temperature variation by the ITCM module.

This configuration facilitates temperature measurement from a distance without contact with the object being measured. A VarioCAM head thermo-graphic system in conjunction with the IR thermometers are utilised to capture the image of the measurement area in the three electrodes and then convey the measured signals to the ITCM module for processing.

The IR temperature measurement offers a number of advantages as compared to the other temperature measurement techniques discussed previously. It can be utilized successfully to:

- Measure temperature of a moving object.
- Measure an object's temperature that is surrounded by an electromagnetic (EM) field.
- Measure the temperature of the furnace transformer's high voltage side without making any contact with it (non-contact technique).
- With the availability of high speed digital IR data acquisition it can be used for monitoring tasks requiring capability for continuous and automatic operation.

C.4 Electrode – to – bath voltage Calculation Module (ECM)

The proposed ECM module is responsible for the approximate measurement of the electrode-to-bath voltages and is capable for minimizing the induced voltage errors in the measuring leads, emanating from the high currents flowing in the secondary circuit. The researcher proposes an ECM module that incorporates an in – built compensator based on the induced errors of the electrode-to-bath voltage measurement, examination of the mutual inductance relationships in a three-conductor system as shown in *Fig. C.4.*

The ECM module measures two terms of the electrode-to-bath voltage that include the correct voltage, E_{AE} and an error term, E_{DE}, which is proportional to the currents flowing in the circuit. The mathematical model of the ECM is expressed by ***Bretthauer and Timm*** equations (C.8 and (C.9) [33]:

$$E_{M1} - E_{DE} = E_{AE} \quad (Electrode\ 1) \qquad (C.8)$$

$$E_{M2} - E_{DE} = E_{BE} \quad (Electrode\ 2) \qquad (C.9)$$

$$E_{M3} - E_{DE} = E_{CE} \quad (Electrode\ 3) \qquad (C.10)$$

Thus, $$E_{M1} - E_{DE} = \mu\,.\,b\,.\,f.\,log_e\,[1 = +(1+\frac{a}{r})]\,.\,I \qquad C.11)$$

Where; μ - *is the magnetic permeability of the medium.*

f - *alternating current frequency.*

E_{M1}, E_{M2}, E_{M3} - *measured electrode-to-bath voltages*

E_{AE}, E_{BE}, E_{CE} - *correct electrode-to-bath voltages*

E_{DE} - *error voltage signal.*

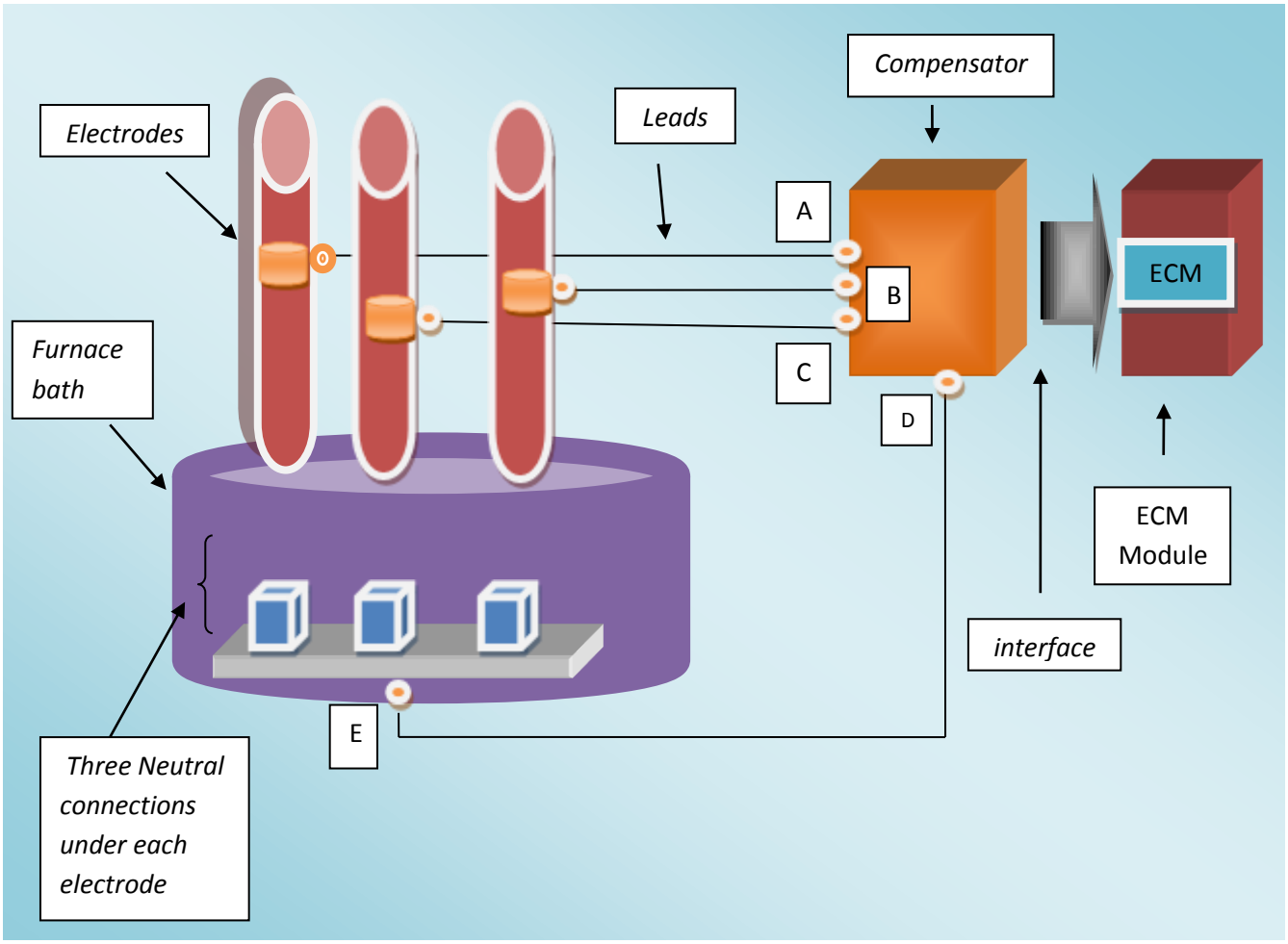

Figure C.4: Proposed ECM Measurement of electrode-to-bath voltages system diagram.

The measured values of the electrode-to-bath voltages are fed via a suitable compensator so as to convert the erroneous measurement of electrode-to-bath voltages to accurate values.

The analogue measured voltage signals are then fed to the ECM module via an interface for synthesis and display, as shown in *Fig C.4*. Neutral connections are provided under each electrode so as to provide less sensitive to changes in the position of the floating neutral connection, which affects the magnitudes of the inductances, L_1, L_2 and L_3. The proposed ECM measurement system is suitable for large ferrochromium furnaces, as it provides accurate measurements of the voltages.

C.5 Electrode Resistance and Impedance Calculation Module (ERICM)

The ERICM module (*Fig. C.5*) alleviate the problems of the on - line measurement of the electrode resistance by deriving the resistance measurement from beneath each electrode. It also controls each of these resistances by manipulating their corresponding electrode hoist, in order to balance the furnace operation. The ERICM module measures impedance between two nodes of a linear circuit as a function of frequency. It consists of a current source, (I_z) connected between inputs *1* and *2* of the module and voltage measurement V_z, connected across the current source.

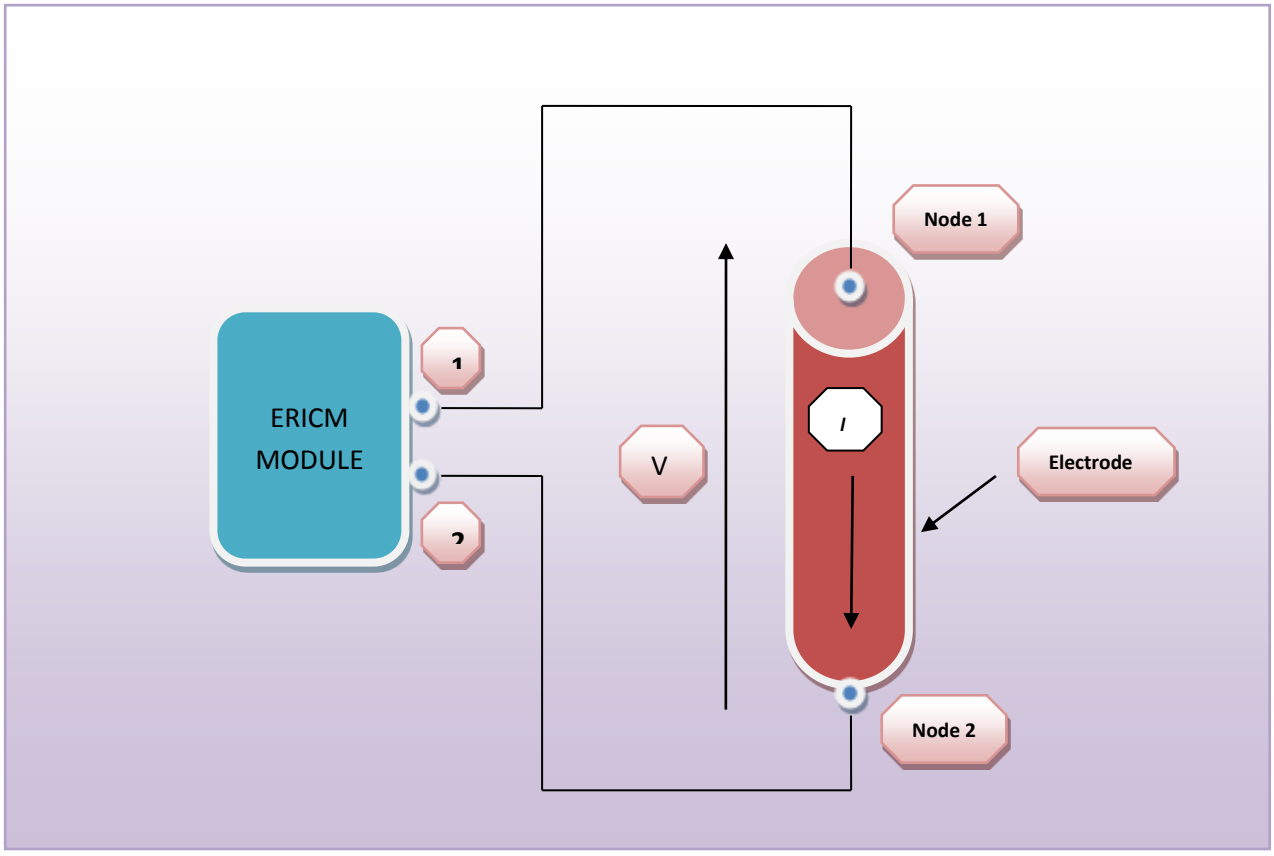

Figure C.5: Proposed ER1CM module for the measurement of electrode impedance.

The SAF electrode system impedance is determined as a transfer function $H_{(s)}$ from the equation:

$$H_{(s)} = \frac{V_{z\,(s)}}{I_{z\,(s)}} \qquad (C.12)$$

where: $V_{z(s)}$ - *voltage across the electrode*

$I_{z(s)}$ - *current flowing through the electrode.*

The Waveform Calculation Module (WCM) provides detailed waveform calculations that include harmonics, flicker, and voltage dip classification. This module consists of flexible harmonic calculation outputting facility that allows firstly the storage of discrete harmonic components and secondly, allows a magnitude of the continuous frequency spectrum. The module also has a provision to configure the outputs to limit the data storage to that outside user-defined thresholds. The WCM module consists of the harmonic calculation block (HCB) and the flicker calculation block (FCB).

C.6 Waveform Calculation Module (WCM)

A multiplication factor of 3 is applied since the impedance is measured between the ground or neutral and the electrode. The resistance of the electrode R_e , is derived from the CVCM module, $V_{phase\ to\ ground}$ measurements of the voltages and currents and is expressed as follows:

$$R_e = \frac{V_{ph}}{I_{ph}} \qquad (C.13)$$

where: R_e - *resistance of the electrode*

V_{ph} - phase - to - ground voltage

I_{ph} - phase current

BIBLIOGRAPHY

[1] Westly, J (1974), "Resistance and Heat distribution in submerged – arc furnace", INFACON 74, Proceedings of the 1st International ferro-alloys congress, pp. 121 – 127.

[2] A.S. Hauksdottir and H.Thingason, "On the system Identification of a ferrosilium Submerged Arc Furnace Supply to arc furnaces," 1991 American Control Conference, Boston, pp.1061 – 1062, 1991.

[3] Kennedy, J.; Eberhart, R. (1995). "Particle Swarm Optimization". Proceedings of IEEE International Conference on Neural Networks. IV. pp. 1942–1948. doi:10.1109/ICNN. 1995.488968.

[4] Rennie, M.S. The Operation, Control and Design of Submerged-arc Ferroalloy Furnaces, Proceedings of Mintek 50: International Conference on Mineral Science and Technology, Sandton, South Africa, March, 1984.

[5] X.Xiu. X.H.Shi, "Realizing Nueral Networks Control with Lab VIEW". Measurement & Control Technology, Vol.24, No 4, 2005:4.

[6] Roberts, Carol. M, "A practical and Comprehensive guide to planning, writing and defending your dissertation, Sage Publications Ltd, California 91320.

[7] Rumelhart, Hinton and Williams, "Learning internal representations by error propagation". International Journal of Computer Theory and Engineering, Vol. 2, No. 4, Nonember, 2007.

[8] Lindgvist, C, "ASEA furnace transformers". Seminar on Electrical Equipment for reduction furnaces, Johannesburg, 9 to 10 December , 1977.

[9] A.B. Stewart, "An Analysis of the electrical circuit of Submerged Arc Furnaces", Feb. 1980.

[10] Reddy, A.K.N, "The theory and design of electric smelting furnaces". J. of electrochemical society, India, vol. 22, no. 4, 1973, pp. 275-289.

[11] Lindgvist, C, "ASEA furnace transformers". "Seminar on Electrical Equipment for reduction Furnaces", Johannesburg, 9 to 10,1977.

[12] W.M.Kelly, "Calcul et Construction du Four a Arc Submerge", Journal du Four Electric, Vol. 2 No.1, 1956.

[13] Gu Derun, Zhao Yangji, Zhang Longlai, Development of the Monitoring System for Thermal Load of BF Cooling Plate [J], Bao Steel Technology, Vol. 2, 0-7803-2768-3/95, pp. 35-40, March 1998.

[14] A. Bermúdez de Castro, J. Bullón and F. Pena, "A finite element method for the Thermo electrical modelling of electrodes", Communications in Numerical Methods in Engineering, no. 14, 1998, pp. 581-593.

[15] Jose Farina, Juan Rodriguez Andina, "Measurement and Analysis of the Impedance of Electrodes in Arc Furnaces for Silicon Production, MIT Press, Cambridge, MA, 2003.

[16] Riley, M, "Processing Training Topics on Submerged Arc Furnaces", Sandton, South Africa, March, 2003.

[17] Modern Power Quality Measurements Techniques, Prentice-Hall Inc., Englewood Cliff, N.J.,1960, pp. 305-345.

[18] M.B. Stout, Basic electrical measurements, Prentice-Hall Inc., Englewood Cliff, N.J.,1960, pp. 321-356.

[19] Lassi Toivoneni, "Method for measuring the electric quantities of an AC Electric Furnce", Feb. 1996.

[20] Darling, Charles R, "Pyrometry. A Practical Treatise on the Measurement of High Temperatures." Published by E.&F.N. Spon Ltd. London. 1911.

[21] J. Farina, J.J. Rodriguez-Andina, J.Bullion and A. Lorenzo, "Measurement of temperature profiles in electrodes of arc furnaces for silicon metal production", in Proc. 39th Ann. Meeting of the IEEE Industry Applications Society, IAS'2004, Seattle, 2004, pp. 195-199.

[22] Phiphat Laohasongkram, Jakkrit Junsiri, and Jakkrit Oupayaso, "Application of Thermal Detector by Infrared for Electrical Arch Furnaces Transformer", International Conference on Control, Automation and Systems 2007 Oct. 17-20, 2007 in COEX, Seoul, Korea.

[23] John Merchant, "Infrared Temperature Measurement Theory and Application, Mikron Instrument Company Inc. Publication.

[24] R. Bergeron, Power Quality Measurement Protocol, CEA Guide To Performing Power Quality Surveys, CEA 220 D 711, May 1996.

[25] M.B. Stout, Basic electrical measurement, Prentice Hal Inc, Englewood Cliff, NJ. (1960).

[26] IEC 61000-4-30 "Testing and measurement techniques – power quality measurements methods".

[27] Riccardo Poli, James Kennedy, Tim Blackwell, "Particle swarm optimization, Swarm Intelligence", Vol. 1, 33-57 (2007)

[28] Esprit, I.F.Croall, J.P.Mason, " Industrial Applications of Neural Networks" (research reports).

[29] D.E Rumelhart, G.E. Hinton, and R.J. Williams, "Learning internal representations by error propagation," D.E. Rumelhart and J. McClelland, editors, *Parallel Data Processing*, Vol.1, Chapter 8, The M.I.T. Press, Cambridge, MA, 1986, pp. 318-362.

[30] Mark Hudson Beale, Martin T. Hagan, Howard B. Demuth, 'Neural Network Toolbox™ User's Guide R2011b.

[31] Mendes, R. (2004). Population Topologies and Their Influence in Particle Swarm Performance (PhD thesis). Universidade do Minho.

[32] Kennedy, J.; Eberhart, R. (1995). "Particle Swarm Optimization". Proceedings of IEEE International Conference on Neural Networks. IV. pp. 1942–1948. doi:10.1109/ICNN. 1995.488968. http://www.engr.iupui.edu/~shi/Coference/psopap4.html.

[33] A B Shi, Y.; Eberhart, R.C. (1998). "A modified particle swarm optimizer". Proceedings of IEEE International Conference on Evolutionary Computation. pp. 69–73. Intelligence", 1(1): 33-57 (2007).

[34] Kennedy, J. (1997). "The particle swarm: social adaptation of knowledge". Proceedings of IEEE International Conference on Evolutionary Computation. pp. 303–308.

[35] Miranda, V., Keko, H. and Duque, Á. J. (2008). Stochastic Star Communication Topology in Evolutionary Particle Swarms (EPSO). International Journal of Computational Intelligence Research (IJCIR), Volume 4, Number 2, pp. 105-116.

[36] Clerc, M. (2006). Particle Swarm Optimization. ISTE (International Scientific and Technical Encyclopedia), 2006.

[37] Yin, P., Glover, F., Laguna, M., & Zhu, J. (2011). A Complementary Cyber Swarm Algorithm. International Journal of Swarm Intelligence Research (IJSIR), 2(2), 22-41.

[38] De-Xian Huang, "Improved particle swarm optimization combined with chaos", chaos, solutions and Fractuals 25 (2005) 1261-1271.

[39] Russel Eberhart, James Kennedy, "A new optimizer using particle swarm theory", 6th International Symposium on micro machine and Human Science, 0-7803-2676-8/95, p. 39 -43.